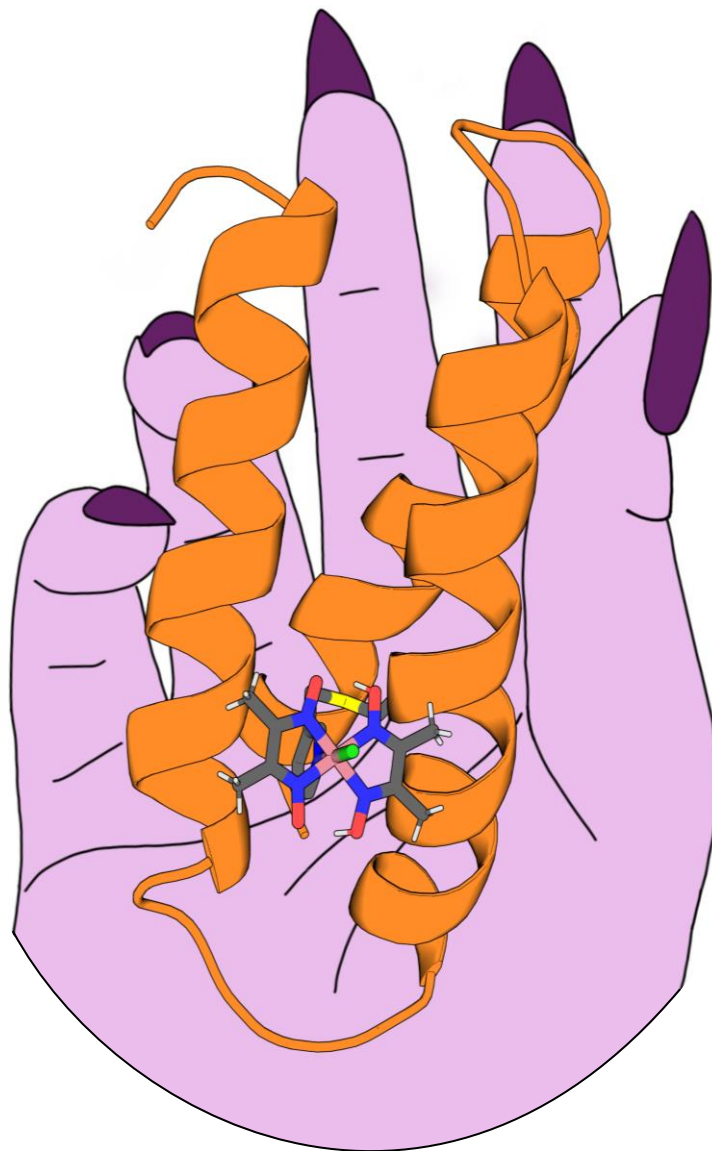


A de novo metalloenzyme for hydrogen evolution

Enzyme design in human hands

Licentiate thesis



Sigrid Berglund



UPPSALA
UNIVERSITET

Licentiate dissertation presented at Uppsala University to be publicly examined in Room 4003, Ångströmlaboratoriet, Uppsala, Friday 31 October 2025 at 09:15. The examination will be conducted in English. Opponent: Prof. Martin Högbom (Department of Biochemistry and Biophysics, Stockholm University).

Abstract

Berglund, S. 2025. A *de novo* metalloenzyme for hydrogen evolution 63 pp. Uppsala University

The climate is changing and we need new, sustainable energy systems to stymie the release of CO₂-equivalents in the atmosphere which cause global warming which is the root of it all. Sustainable energy sources are abundant, including wind and solar, and we are adept at using them. They are however transient, and storage for times when there is no wind or sun is required. Batteries are commonly used, but it is not always a practical solution, especially not for upscaled energy storage. Producing fuels from sustainable electricity is a crucial puzzle piece in the energy systems of the future, and one such fuel is hydrogen gas (H₂). The current production of H₂ is unsustainable, leading to massive release of CO₂. This thesis aims to provide insight into a sustainable method for H₂ production using biomimetic compounds to create a *de novo* metalloenzyme for hydrogen evolution. The cobalamin-mimicking catalyst cobaloxime has been combined with the *de novo* protein α_3C , forming the *de novo* metalloenzyme Co-MePy- α_3C . Cobaloxime is a thoroughly studied catalyst, and it has previously been applied to make artificial metalloenzymes for hydrogen evolution by combining it with natural protein scaffolds. The protein α_3C is a fully *de novo* protein and was designed to be structurally robust and redox-inert at biologically relevant conditions.

By circular dichroism (CD) spectroscopy it was found that the protein portion of Co-MePy- α_3C is structurally distinct from α_3C . By electron paramagnetic resonance (EPR) spectroscopy the cobaloxime in Co-MePy- α_3C was confirmed to coordinate to the protein scaffold. The hydrogen evolution reaction (HER) by cobaloxime and Co-MePy- α_3C were characterised using two reduction strategies: by chemical reduction using [Eu(EGTA)]²⁻ and by photosensitisation using [Ru(bpy)₃]²⁺, ascorbate and light. The initial rate of hydrogen evolution and the turnover number (TON) of the hydrogen evolution reaction (HER) by the two complexes were calculated, and it was found that the TONs of Co-MePy- α_3C are mildly perturbed compared to that of cobaloxime (80-90% of the cobaloxime TON). The initial rates when using photosensitisation remain unchanged, but with chemical reduction it is reduced to less than half of that of cobaloxime (ca 40%). This lowering of rate is likely due to the insulating effect of the protein scaffold on the catalyst, slowing the rate of transfer of protons and electrons to it. The effect is not visible when using photosensitisation as the reducing equivalents are produced slowly over several hours, which slow the reaction down significantly for both cobaloxime and Co-MePy- α_3C , resulting in matched rates.

By cyclic voltammetry (CV) the mechanism of electrocatalytic HER by cobaloxime and Co-MePy- α_3C was investigated. A pH-dependence study was conducted to characterise the process taking place in a reducing peak that appear at ca -0.9 V vs normal hydrogen electrode (NHE) for both Co-MePy- α_3C and cobaloxime. The calculated pH-dependencies suggest that a 1 H⁺/1 e⁻ process is taking place at this potential. Comparing with previously suggested mechanisms it is likely the reduction of the cobaloxime Co(II) to Co(I), coupled with the protonation to Co(III)-H, but further studies are necessary to ascertain precisely the process giving rise to the reducing peak at -0.9 V vs NHE. Future studies on Co-MePy- α_3C include a foot of the wave analysis (FOWA) of the cyclic voltammograms to determine initial rates of electrocatalytic HER by Co-MePy- α_3C and cobaloxime.

To conclude, Co-MePy- α_3C has been shown to act as a *de novo* enzyme for hydrogen evolution, and the effect on the incorporation of a catalyst into a *de novo* protein scaffold has been characterised. Further studies to characterise the electrocatalytic HER by Co-MePy- α_3C are planned, but initial data suggests that it behaves similarly to cobaloxime, as evidenced by comparison with previously published data.

Keywords: Bioinorganic chemistry, artificial metalloenzyme, hydrogen evolution, *de novo* protein, cobaloxime

Sigrid Berglund, Department of Chemistry – Ångström laboratory, Uppsala University, SE-751 20, Uppsala, Sweden.

© Sigrid Berglund 2025

Till alla doktorander som kämpar

List of manuscripts

This licentiate thesis is based on the following paper:

Berglund, S, Bassy, C, Kaya, I, Andrén, PE, Shtender, V, Lasagna, M, Tommos, C, Magnuson, A, Glover, SD 2024. Hydrogen production by a fully *de novo* enzyme. *Dalton Transactions*. 53: 12905-12916

Contribution to paper: I expressed, purified, and chemically modified protein, and I developed the methodology for chemical modification. I synthesized inorganic catalysts. I performed cyclic voltammetry and hydrogen evolution studies using Clark microelectrode and [Eu(EGTA)]²⁻ driven reduction. I supervised C. Bassy in performing hydrogen evolution studies using gas chromatography. I performed MALDI-TOF MS in collaboration with I. Kaya. I performed ICP-OES in collaboration with V. Shtender. I took a major part in data analysis, interpretation, and writing.

The EPR-spectroscopy and analysis were performed by A. Magnuson. The protein denaturation study and analysis were performed by S. D. Glover.

The following paper is not included in this thesis:

Grinberg, I. R., Berglund, S., Hasan, M., Lundin, D., Ho, F. M., Magnuson, A., Logan, D. T., Sjöberg, B., Berggren, G. (2019) Class Id ribonucleotide reductase utilizes a Mn²(IV,III) cofactor and undergoes large conformational changes on metal loading. *Journal of Biological Inorganic Chemistry* 24:863-877

Contents

1	Introduction	7
1.1	Aims	8
1.2	Biomimetic chemistry	8
1.2.1	Hydrogenases and mimicking them.....	9
1.2.2	Cobalamin enzymes to cobaloxime: catalyst design inspired by Nature.....	9
1.2.3	Ligand modifications	11
1.3	Artificial metalloenzymes and their scaffolds.....	12
1.3.1	The α_3X <i>de novo</i> protein family.....	13
1.3.2	Functionalisation of protein scaffolds.....	14
1.4	Summary	17
2	Methods	18
2.1	Recombinant protein production.....	18
2.2	Colourimetry	19
2.2.1	Bradford assay	20
2.2.2	BCA assay	20
2.2.3	PAR assay.....	20
2.3	EPR spectroscopy	21
2.4	Circular dichroism spectroscopy.....	22
2.5	Cyclic Voltammetry	23
2.5.1	Voltammetric pH dependence	24
2.6	Clark-type microelectrode.....	25
2.7	Summary	26
3	Constructing and characterising the fully <i>de novo</i> artificial metalloenzyme Co-MePy- α_3C	27
3.1	Production and characterisation of Co-MePy- α_3C	27
3.1.1	Functionalisation of α_3C	27
3.1.2	Functionalisation of MePy- α_3C	29
3.1.3	Protein and cobalt quantification	29
3.1.4	CD spectroscopy	31
3.1.5	Cyclic voltammograms of Co-MePy- α_3C and cobaloxime	32
3.2	Co-MePy- α_3C catalysis	34
3.2.1	Catalysis by photosensation.....	34
3.2.2	Catalysis by chemical reduction	36
3.2.3	Considerations when choosing a method for HER experiments.....	37
3.2.4	Discussion.....	38
3.3	Summary and conclusions	40
4	Electrocatalytic hydrogen evolution by Co-MePy- α_3C	41
4.1	Analysis of the electrocatalytic behaviour of Co-MePy- α_3C	44
4.2	Summary and outlook	49
5	Summary and outlook.....	50
	Populärvetenskaplig sammanfattning	52
	Popular scientific summary.....	53
	Acknowledgements.....	54
	References.....	55
	Appendix 1.....	60
	Appendix 2.....	62

Abbreviations

3-BrMe-Py: 3-bromomethyl-pyridine

3-MePy- α_3 C: 3-cysteinemethyl-pyridine- α_3 C

ArM: Artificial Metalloenzyme

BCA: Bicinchoninic acid

BF₂: Difluoroboryl

BSA: Bovine serum albumin

C: Cysteine

C: Chemical step in a catalytic mechanism

CD: Circular dichroism

Cobaloxime: [Co(dimethylglyoxime)₂L'L]

COF: Covalent organic framework

Co-MePy- α_3 C: [Co(dmgH)₂(3-MePy- α_3 C)L]

CV: Cyclic voltammogram

dmg: Dimethylglyoxime

E: Redox-step in a catalytic mechanism

ED: Sacrificial electron donor

EPR: Electron paramagnetic resonance

FOWA: Foot of the wave analysis

GC: Gas chromatography

Gdn-HCl: Guanidinium hydrochloride

HEC: Hydrogen evolution catalyst

HER: Hydrogen evolution reaction

ICP-OES: Induced coupled plasma optical emission spectroscopy

MALDI-TOF MS: Matrix assisted laser desorption ionization time of flight mass spectrometry

MOF: Metalorganic framework

NHE: Normal hydrogen electrode

PAR: 4-(2-pyridylazo)resorcinol

PS: Photosensitiser

PSII: Photosystem II

RP: Reverse phase

RPP: Recombinant protein production

SCE: Saturated calomel electrode

SDS-PAGE: sodium dodecyl sulphate polyacrylamide gel electrophoresis

SHE: Standard hydrogen electrode

TOF: Turnover frequency

TON: Turnover number

UV: Ultraviolet

W: Tryptophan

Y: Tyrosine

1 Introduction

Vanadium, chromium, manganese, iron, cobalt, nickel, copper, zinc, molybdenum, and tungsten—these are the transition metals that are known to be essential to life on Earth.(1) They give organisms the ability to perform complex chemistry at a very low energy cost, which has mesmerized chemists for decades. Biological entities form remarkably complex structures with transition metals such as the manganese tetrad in photosystem II, cobalamin cofactors, the nitrogenase iron molybdenum cofactor (FeMoco), the iron-sulphur clusters, tungstopterin and many, many more.(2–6) This thesis explores the design, production, and study of a *de novo* metalloenzyme—a fully artificial enzyme (ArM). Natural enzymes are masters of catalysis and accomplish this with relatively simple components. Constructing enzymes not occurring in nature gives insight into what kind of reactivity may be achievable with these simple components and expands the chemist’s toolbox for creating efficient catalysts.

One of the big challenges chemists are currently facing is to create new, more sustainable ways to make the fuels of the future. Sustainably produced hydrogen is an important component of the green power production infrastructure, because creating carbon neutral energy is commonplace today, but storing it is not straight forward.(7) Using batteries is currently the most common method but requires great amounts of materials and storage space. The other option is storing the excess energy in chemical bonds, for example in the H–H bond in hydrogen gas. When the energy is needed, the hydrogen can be consumed in a fuel cell, with the only waste product being water.(8)

Most H₂ on the market is today produced by the steam reformation of the fossil fuel methane, and the hydrogen which is not using fossil precursors is produced with platinum electrolyzers.(9,10) Methane steam reformation leads to release of CO₂, and platinum which is used in most standard electrolyzers is a metal with limited abundance in the Earth crust.(11) Chemists and engineers are working to find new ways to produce hydrogen sustainably. It is in principle a simple reaction (equation 1), but if not using highly efficient catalysts such as platinum metal, a lot of excess energy is required to drive it.



The excess energy required to drive the reaction compared to the potential at which the reaction in equation 1 is in equilibrium is known as overpotential.(12) Many catalysts have been developed in the pursuit of lowering the overpotential for the hydrogen evolution reaction (HER), which has given rise to a large body of knowledge regarding hydrogen evolution catalyst (HEC) design principles.(13) Chemical properties such as secondary coordination sphere effects, electron and proton channelling properties and solubility in water can be tuned by employing different types of framework strategies, and in this thesis a biological one has been used – a protein. Nature’s HECs are hydrogenases, which are highly efficient at making hydrogen, but simultaneously highly sensitive to ambient conditions. Additionally they are typically only suited for a narrow range of reaction conditions and with limited lifetimes.(14) Making artificial and *de novo* enzymes for hydrogen evolution which can overcome these limitations can be beneficial for the broadened understanding of natural enzyme catalysis, even if they at present do not reach the efficiency of natural hydrogenases.

1.1 Aims

In this thesis the fully *de novo* hydrogen evolving enzyme Co-MePy- α_3 C has been described. It is based on the HEC [Co(dimethylglyoxime)₂L'L] (cobaloxime (signified by Co)) and the *de novo* protein α_3 C through an *in vitro* modified methylpyridine amino acid (signified by MePy). The hypothesis was that with the use of a protein to mimic the solvation environment of an organic solvent (in which cobaloxime is more stable than in water) the HER catalysis will be improved by increasing longevity of the catalyst. This hypothesis has given rise to the following questions, which will be discussed in this thesis:

1. Will the resulting protein-catalyst conjugate be catalytically active? And if yes, how has the HER catalysis been altered by incorporation into the protein?
2. Does binding of the catalyst to the protein change the protein structure?
3. By what mechanism does the HER take place in the *de novo* metalloenzyme and does it differ from homogenous catalysis?
4. What role can a *de novo* protein scaffold play in the design of ArMs, and how is it different from using a natural protein? What are the advantages and limitations?

With this *de novo* metalloenzyme the possibility of using *de novo* proteins as frameworks and secondary coordination environments for molecular catalysts has been explored. Cobaloxime and α_3 C will be introduced in the following sections of Chapter 1, as well a general introduction to natural metalloenzymes, biomimetic chemistry and design strategies for artificial metalloenzymes. Chapter 2 introduces key methods, and Chapters 3 and 4 discuss the findings of the studies of Co-MePy- α_3 C.

In this thesis, unless otherwise specified, singular cobaloxime refer to the complex [Co(dimethylglyoxime)₂L'L] where L' is a pyridine and L is a chloride that can exchange for water or protons, or, when specified, [Co(dimethylglyoxime)₂L'L] where L' is the pyridine inside MePy- α_3 C. Unless otherwise specified, plural cobaloximes refer to cobaloximes in general which include cobaloximes with modified equatorial- and axial ligands.

1.2 Biomimetic chemistry

Enzymes are categorised into seven classes based on what kind of chemistry they perform: **1:** oxidoreductases (red-ox reactions, H or O transfer), **2:** transferases (transfer of a functional group), **3:** hydrolases (cleavage of substrate by hydrolysis), **4:** lyases (non-hydrolytic addition or subtraction of functional groups), **5:** isomerases (intramolecular rearrangement), **6:** ligases (C–O, C–S, C–N or C–C bond formation) and **7:** translocases (transfers molecules, usually across a membrane).(15) Metalloenzymes are represented in all seven classes, and remarkably Ni-dependent metalloenzymes, of which only nine are known in total, are represented in all except translocases.(16)

In this thesis the only transition metal that is of interest is cobalt, *via* the cobalamin mimic cobaloxime HEC that is used. Cobalt-dependent enzymes are often incorporating the cobalamin prosthetic group, the most well-known of them is vitamin B12. There are cobalt enzymes which do not incorporate cobalamins, but they are rare.(17)

This breadth of chemical functionality that is conferred by metalloproteins is remarkable and makes it clear that we can take inspiration from natural enzymes to construct catalysts for performing all kinds of chemistry. We can either adapt and improve existing natural enzymes, create biomimetic artificial complexes that take inspiration from nature, or create new ArMs that catalyse any reaction of interest, naturally occurring or not. The construction of ArMs is of interest because proteins can provide a platform to perform catalysis that, even if it is a reaction that occurs naturally, is improved in terms of which reaction conditions are tolerated, enantioselectivity when applicable and catalyst stability. An example which will be discussed further in this chapter is the enzyme hydrogenase. It can produce hydrogen at excellent turnover frequencies (TOFs) and turnover numbers (TONs) but is very sensitive to ambient oxygen levels.(18) Understanding the hydrogenase allows us to make use of its structural features which make it such an excellent catalyst, and to improve on them in a hydrogen evolving ArM.

Taking inspiration from nature's catalysts is an exciting possibility for a chemist. Unfortunately, simply copying the active site of an enzyme, and hoping it will perform just as well as the native enzyme is a path of disappointment, but taking inspiration from enzymes can give rise to new and interesting catalyst design. In the case of cobaloxime, it may even give rise to a catalyst that perform a completely different reaction from the original enzyme that inspired its design. A few examples of interest have been chosen, the first one being hydrogenase and the biomimics of hydrogenases, discussed in Section 1.2.1). The target reaction in the work done for this thesis has been proton reduction for hydrogen evolution, and so learning from nature's HER strategy is an important starting point. The complexes explored in this thesis have very little in common with hydrogenases, except for the fact that the target reaction is the same, but an insight into natural hydrogenases nonetheless will help us understand some important facets of biomimetic design. The second example is cobalamin-dependent enzymes, and its mimic complex cobaloxime. Cobaloxime is a HEC, but there are no reported natural cobalamin-dependent HER enzymes. Cobaloxime is the catalyst utilised in this thesis, and so it is an interesting example of how a biomimetic complex can end up performing completely different chemistry from the source of inspiration.

1.2.1 Hydrogenases and mimicking them

Nature's catalysts for hydrogen oxidation and proton reduction are hydrogenases (however nitrogenase does produce H₂ as a side product). In hydrogenases metal bearing prosthetic groups are present in the active site, composed of nickel and/or iron. There are three known classes of hydrogenases – NiFe, FeFe and Fe, where the active site contains one iron ion, two iron ions or one nickel and one iron ion, respectively.⁽¹⁸⁾ The active site of all variants is linked to the protein scaffold by a varying number of cysteines, but other non-protein ligands are also essential for the formation of the active site complex. The active sites are buried deep inside the protein scaffold and are provided with electrons from the surface by a relay-structure made of several FeS-clusters, while protons are provided via a chain of amino acid residues.^(19,20)

The active sites analogues have been synthesised before, and even incorporated into apo-hydrogenases for semi-artificial hydrogenases that are closely resembling the natural hydrogenases.⁽²¹⁾ The semi-artificial hydrogenases function like a natural hydrogenase, but active site analogues as molecular catalysts performs poorly and require outer-sphere functionalisation to maintain decent catalytic activity.⁽²²⁾ This makes it clear that the outer sphere coordination is critical for the functionality of the hydrogenase prosthetic groups, and that the native protein scaffold is necessary for optimal function. As the hydrogenase protein scaffold provides electrons and substrate protons through respective channelling functionalities, it is likely one of the reasons that the catalytic efficiency of the hydrogenase itself is so excellent. Without these channels the active site would be isolated by the protein scaffold. In a reaction solution, protons are provided either by freely diffusing protons or organic acids, and the electrons either by secondary reductants, or an electrode. The access to them should thus not be the limiting factor for the catalytic efficiency of a freely diffusing catalyst. The protein scaffold could also act as an enhancer for the catalyst: it could place the active site under a certain amount of strain to allow for a more labile catalytic centre, it could provide electrons faster than they could be transferred from an electrode or from diffusing reductants, or it could provide the substrate protons at the correct angle allowing for improved turnover, rather than if the isolated catalyst would freely diffuse and collide with substrate protons at any angle.

The lesson to be learned from the field of study of hydrogenases and the hydrogenase biomimics is that the active site of a metalloenzyme is not all that matters – a protein scaffold to provide the correct chemical environment and steric effects is essential. When designing a biomimetic catalyst or an ArM, understanding how the protein scaffold provides crucial functionalities to the catalyst is important. We can already hypothesise that placing an excellent catalyst deeply buried in a protein without any access to substrate will yield a poor ArM. But placing it in a protein cavity with proper channels for substrates may provide something beneficial to the catalyst, yielding a better ArM than in the previous example.

1.2.2 Cobalamin enzymes to cobaloxime: catalyst design inspired by Nature

Cobalamin dependent enzymes can be divided into three groups – isomerases (where carbon, nitrogen and oxygen atoms can be transferred), methyltransferases and dehalogenases. Cobalamins can perform this wide range of chemistry thanks to their unique structure.⁽²³⁾ They are octahedral complexes, where the equatorial bonds and one of the axial bonds are provided by the ligand corrin (Figure 1A). The second axial

ligand varies depending on which enzyme the cobalamin occupies, however typically involves a Co-C bond which is one of the key features in cobalamin that makes it so suitable for the chemistry it can perform.(23)

The importance of dietary cobalamin, although its molecular identity was not known, was identified in 1926.(24,25) It was not isolated until 1948, after which the first structure was proposed in 1955.(26,27) Because its importance was well understood, the total synthesis of cobalamin was pursued, and the over 70 step synthesis was not fully presented until 1972, after more than 10 years of work by a number of researchers.(28) Despite the total synthesis of cobalamin being known, still today industrial production of it remain biological using bacterial fermentation, highlighting how well-suited biological systems are for making very complex molecules with low human effort.(29)

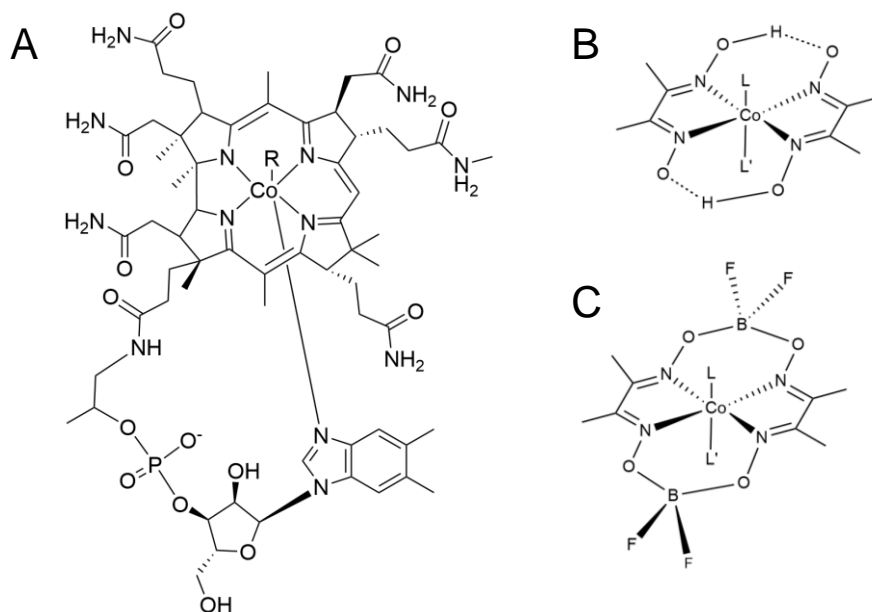


Figure 1: A: Structure of cobalamin, B: General cobaloxime and C: cobaloxime with difluoroboryl-substituted glyoximes.

R can be deoxyadenosine, methyl, OH, CN depending on the form of cobalamin.[23] L is typically a solvent molecule or chloride, L' is typically a solvent molecule, chloride or an organic base e.g., pyridine.

The discovery of the cobalamin structure and the complex synthesis required to produce it gave rise to the field of cobalamin mimics, one of them being cobaloxime. Two dimethylglyoximes (dmgs) coordinate the cobalt in a square planar fashion, with two axial ligands of varying identity – solvent molecules or chloride ions at its simplest (Figure 1B).(30) The reactivity scope of cobaloximes was explored, and they were eventually found to be HECs, and so the field of cobaloxime HER studies was started.(31) The case of cobaloxime highlights how the design of biomimetic catalysts can take surprising turns. A catalyst can be designed with a target reaction in mind but could still end up being better suited for a completely different purpose.(32)

The cobalamin ligand is unique and mimicking it has proven difficult. But in that challenging catalyst design, novelty lies, and unexpected reactivity arises. Cobaloxime became a HEC of wide interest, and many facets of its function have been investigated ever since it was found as a HEC. Understanding what previously have been found for cobaloxime was important when performing the studies presented in this thesis. To aid the discussion in the following chapters, this section summarises some of the areas that have been explored to improve the stability and function of cobaloxime to optimise their catalytic function.

Even though cobaloxime arose as a viable HEC in the 1960s, it wasn't until the 1990s that the literature in the field started to expand significantly (Figure 2). The investigations into cobaloxime hydrogen evolution have spanned from ligand modification to supramolecular strategies. A known issue with cobaloximes is their stability – the dimethylglyoxime ligand easily dissociate, especially in acidic media, and when they are lost, they will diffuse away and will not re-coordinate.(33,34) This section will go through some of the strategies used to improve cobaloxime catalysis in the last 30 years, to highlight some factors that were important in the work presented in this thesis.

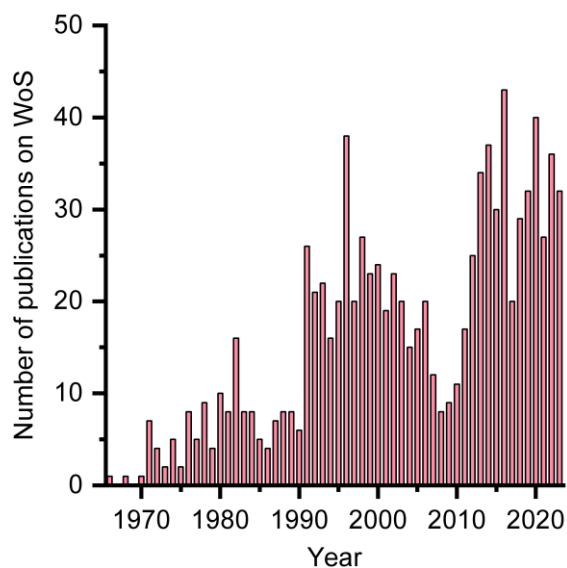


Figure 2: Number of publications per year with “cobaloxime” in any field on Web of Science.

1.2.3 Ligand modifications

The two glyoxime equatorial ligands are typically linked together by hydrogen bonding (Figure 1B), which leaves them susceptible to dissociation in solution. This hydrogen has been substituted with a difluoroboryl (BF_2 , Figure 1C), yielding a fully cyclised equatorial ligand, not only ensuring that the glyoxime ligands do not dissociate easily but also providing an electron withdrawing effect which gives the additional benefit of a lowered overpotential for the HER.^(31,33) A cobaloxime is typically only coordinating one organic axial ligand while the other is a chloride or solvent molecule.⁽³⁵⁾ This position coordinating the solvent or chloride can be protonated throughout the catalytic cycle.

The organic axial ligand has been thoroughly investigated, both to find which type of ligand yields the most effective catalyst, and to further modify them to improve catalysis, such as by adding proton relaying functionalisation.⁽³⁶⁾ Axial ligand screening with electrochemistry has been performed, as for example by Wakerley and Reisner, where cobaloximes with different axial ligands were formed *in situ*, and the voltammograms of the product cobaloximes were recorded.⁽³⁷⁾ They reported ten cobaloximes with varying axial ligands and how the voltammogram changes, both with peak positions, catalytic onset potentials and catalytic peak currents and therefore could show trends in axial ligand and catalytic behaviour. Wakerley and Reisner found that the identity of the axial ligand has a notable impact on the voltammetric response of the cobaloxime, where for example more electron withdrawing cyanopyridines yielded lower overpotentials but also lower catalytic current.

In another publication, Dolui et al. presented their work of using substituted pyridines as axial ligands. Several cobaloxime variants with peptide inspired proton-relaying moieties bound to the pyridine ligand were reported, and it was found that these modifications increased both the HER of the cobaloximes and the overall stability of the catalysts.⁽³⁶⁾ This study will be discussed more in Chapter 4.

1.2.3.1 Solvent effects on activity

The effects of solvent choice on cobaloxime have also been of interest. Although cobaloxime is active for hydrogen evolution in water, it is much more active in organic solvents. To perform sustainable chemistry, it is of interest to improve the activity in aqueous conditions, to be able to lower the volume of organic solvents that is required in industrial hydrogen production. This difference in catalytic activity has typically been attributed to the complex staying better coordinated in organic solvents than in aqueous solvents. Two examples of these studies are performed by Luo et al., and by Du et al. using a basic cobaloxime with an axially coordinating pyridine.^(34,38) Luo et al. found that in mixtures of water and acetonitrile the

cobaloxime activity increased with increasing acetonitrile concentration, and Du et al. found the same with their systems. By these findings it appears that cobaloxime is sensitive to its surroundings, and that a fully aqueous system is a disadvantage in terms of hydrogen production.

1.2.3.2 Artificial hydrogenases based on cobaloxime

From the example of the hydrogenase, we learn about the importance of the secondary coordination environment for catalysis. Except for the effects discussed above regarding hydrogenases, other effects of the protein scaffold can also have an effect on catalysis, such as the tuning of the polarity and dielectric constant of the near environment. Approaches such as modifying the ligands yield a more stable complex, and although these moieties on the ligands are not directly involved in coordination, this modification provides stabilization to the complex and still improves the functionality of the catalyst. Examples of how changing the secondary coordination sphere affects the cobaloximes have been investigated with, among others, proteins, metal-organic frameworks (MOFs), covalent organic frameworks (COFs) and polymers.(39–43) For the purposes of this thesis, the interactions between cobaloxime and proteins are of most interest.

Bacchi et al. were the first to report the incorporation of cobaloxime into a protein scaffold, myoglobin (Figure 3A) and haem oxidases (Figure 3B).(39,40) Their functionalisation strategy was to coordinate the cobaloxime to native histidine residues in the protein binding pockets. With circular dichroism (CD) spectroscopy it was found that upon cobaloxime functionalisation the myoglobin scaffold folds in a helical manner, however it was not reported if the degree of helicity changed. The resulting myoglobin-based ArM was characterised with a range of methods, among them cyclic voltammetry and a HER experiment, monitoring the hydrogen with a Clark type H₂ micro-sensor. They found small differences in the voltammograms of the protein-bound cobaloxime and the dissolved cobaloxime, and only a very small difference between them in their HER efficiency. By chemical reduction with [Eu(EGTA)]²⁻ they saw an increase in turn over number (TON) from 2.5 (no protein) to 3.2 (with protein). By photosensitisation they recorded a decrease in TON, with [Ru(bpy)₃]²⁺ from 7 (no protein) to 3 (with protein). These results highlight complexity of rational design of artificial enzymes above. Even with robust methodology and components, the outcome of a novel complex can be difficult to predict. In the design of the system explored in this thesis, inspiration was taken from the ArMs prepared by Bacchi et al.. (39,40)

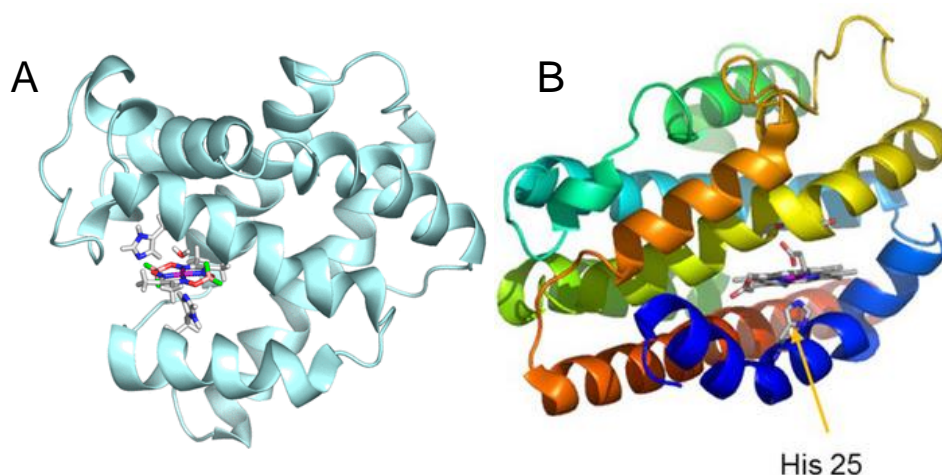


Figure 3: Artificial metalloenzymes based on cobaloxime and A: Myoglobin, B: Haem oxidase. A reprinted with permission from reference 39: Copyright 2014 American Chemical Society. B reprinted with permission from reference 40: Copyright 2016 John Wiley and Sons.

1.3 Artificial metalloenzymes and their scaffolds

Although there were some early reports of ArMs during the second half of the 1900s, with the invention of recombinant gene technology the field could truly start growing in the 2000s (Figure 4).

The last ten years the field has been growing, with advances in design, functionalisation methods, reaction scope and catalytic optimisation. ArMs have now been designed for a wide range of catalysis, among them a host of different organic reactions, reduction – and oxidation reactions, hydrogenation, and C-H activation. Natural enzymes are widely used in industrial chemical synthesis and in everyday products, and the widening of the scope of reactions that enzymes can perform will give chemists a bigger toolbox of highly specific and efficient catalysts. In this section, the protein scaffold for the *de novo* metalloenzyme presented in this thesis, α_3C , is introduced, followed by an introduction to the field of artificial metalloenzymes.

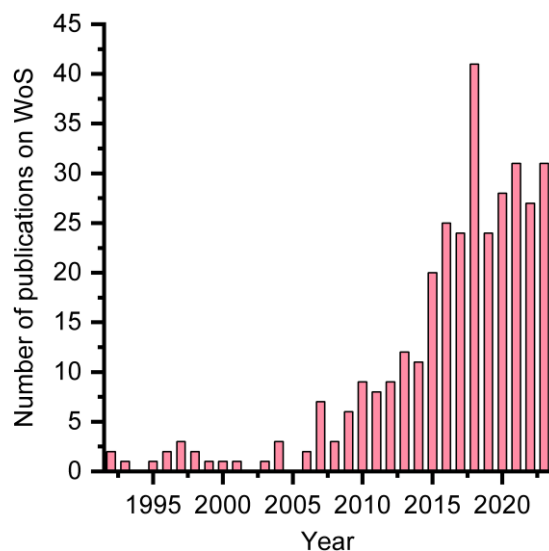


Figure 4: Number of publications per year with “artificial metalloenzyme” in any field on Web of Science.

1.3.1 The α_3X *de novo* protein family

In this thesis the *de novo* protein α_3C was used as the protein scaffold for the *de novo* metalloenzyme. It is one of several members of the α_3X family of proteins, which initially consisted of α_3Y and α_3W (Figure 5B), presented first in 1999 as model systems for tyrosine (Y) and tryptophan (W) radicals in natural enzymes.⁽⁴⁴⁾ Amino acid radicals can be found in many enzymes but studying them is challenging. In large proteins their behaviour is hard to isolate from other processes, and dissolving pure amino acids in solution removes them from their native shielded protein environment. There are two key examples of enzymes where Y and W radicals play an important role: ribonucleotide reductases (RNRs) and photosystem II (PSII). In RNRs, Ys and Ws are involved in a radical transport chain stretching over more than 32 Å, and in PSII, a Y is responsible for oxidising the active site manganese cluster, where a neutral Y radical is generated as a result.^(45,46) Both these cases illustrate important reasons to understand the intraprotein amino acid radical formation and decay dynamics, and so a protein-based model system is a helpful tool to reach this goal.

The α_3X protein is a 67 amino acid sequence, with the amino acid side chain of the central position being buried in the hydrophobic core of the protein. For α_3Y (Figure 5A) the central amino acid is a Y and in α_3W (Figure 5B) it is a W, and thus in α_3C which was used for the work described in this thesis it is a cysteine (C). The protein folds into three helices, giving rise to the first part of the name. The sequence contains no other residues that are redox active under biologically relevant conditions. Because of this, the activity of the Y or W could be isolated. The protein scaffold was also designed to be structurally robust over a wide pH-range to allow the study at several pH values without compromising on the protein structure. The structural robustness additionally comes with the advantage that α_3X can be denatured and re-folded completely, which is not typical for natural proteins.

The α_3X protein sequence was adapted from a previously reported coiled coil protein, which was designed as a biomimic of naturally occurring coiled coils, α -helices coiling together to form helix bundles.^(44,47,48) It is a common structural motif in Nature, and during the late 1900s they were a target of some interest.^(49–52) It was found that the α -helix can be reduced to a seven amino acid motif, which can

be adapted to the protein design questions of interest. In the case of the α_3X – proteins, it was adapted to be this robust amino acid radical model system.

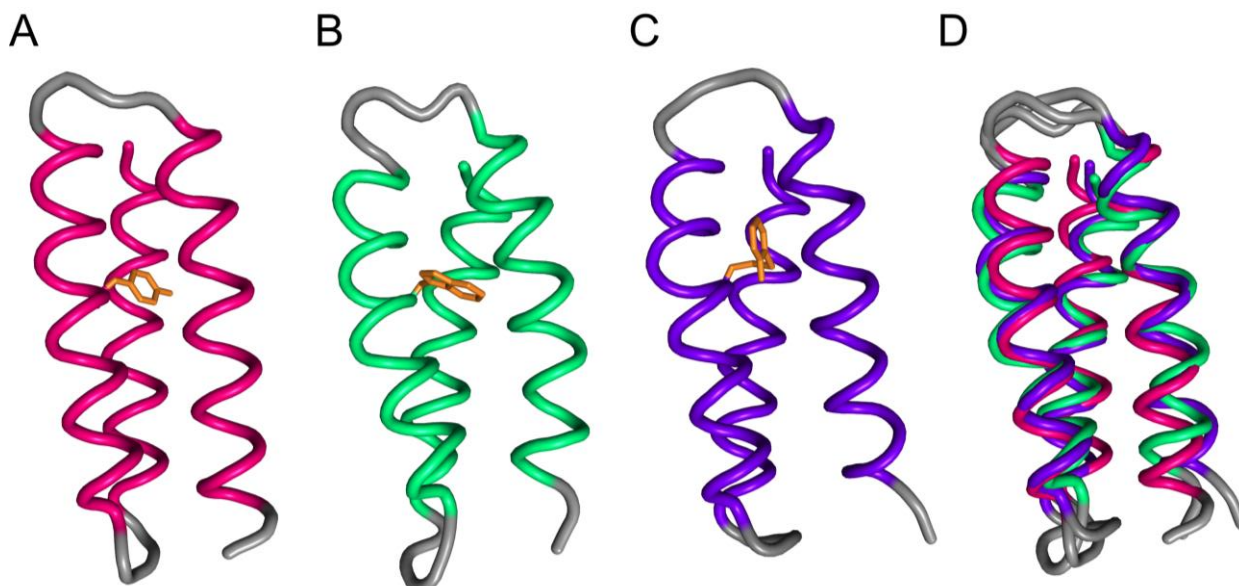


Figure 5: Solved NMR structures for the α_3X protein family. A: α_3Y (PDB: 2MI7). B: α_3W (PDB: 1LQ7). C: α_3C -2-mercaptophenol (PDB: 2LXY). D: Tertiary structure overlap of α_3Y , α_3W and α_3C -2-mercaptophenol.

The α_3X family was later expanded with the new member α_3C . (53) This variant has been used to create noncanonical phenol amino acids in the central position, most notably the 2-mercaptophenol variant of which an NMR structure has been solved (Figure 5C). The C was functionalised with a 2-mercaptophenol to create a variant of α_3Y where the alcohol is buried even deeper into the protein structure. When overlapping the three solved α_3X structures, their high structural similarity becomes very clear (Figure 5D) In this thesis, α_3C was functionalised with 3-methylpyridine, and so for all structural models the structure of α_3C -2-mercaptophenol was used as mercaptophenol is structurally similar to methylpyridine.

Although the α_3X proteins were not designed to be artificial enzymes, they still act as good examples of the strength of using rational design of biomimetic *de novo* proteins. With it, protein structures can be constructed that fulfil the chemical requirements to answer certain research questions or chemical needs. With the adaptation of α_3C shown in this thesis, the relevance of the α_3X proteins, and other *de novo* proteins, as biomimetic protein scaffolds for artificial metalloenzymes are highlighted.

1.3.2 Functionalisation of protein scaffolds

There are four main methods of protein functionalisation to form artificial metalloenzymes: i. direct coordination of a metal ion or complex by the introduction of coordinating non-native amino acids, ii. native metal substitution to either a native metal prosthetic group or native directly coordinated metal ion, iii. linkage of a high affinity enzyme prosthetic group or inhibitor to a metal complex for specific binding or iv. covalent binding between metal complex functional groups and protein scaffold.(54,55) In the work presented in this thesis, method iv was used, but all four methods will be described here along with relevant examples of ArMs.

i. Direct coordination of metal ion or complex to non-native amino acids

The introduction of non-native amino acids to a protein scaffold can be performed with essentially any protein. With modern bioinformatic tools a protein structure can be modelled and the impact of the amino acid substitutions can be investigated. Rational design of a metal binding site or catalyst coordination point can be performed. An example of this type of approach was reported by Drienovská et al., employing a codon suppression technology to introduce artificial amino acids *in vivo* for coordination into the Lactococcal multidrug resistance regulator.(56) They chose a bipyridine amino acid, which coordinated copper ions that then catalysed Friedel-Crafts alkylations (Figure 6). The benefit of using the direct coordination strategy is that in principle any suitable protein can be used, and with modern biochemistry methods the

introduction of non-native amino acids becomes an extra chemical tool to widen the coordination scope, either by *in vivo* or *in vitro* modification.

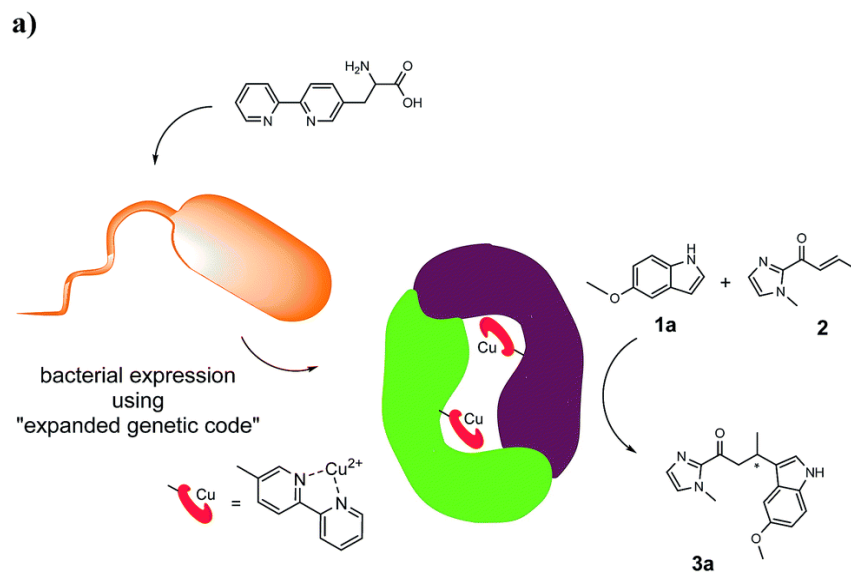


Figure 6: Bipyridine coordinated copper ions in artificial metalloenzyme for Friedel-Crafts alkylation. Reprinted under CC BY3.0 license from reference 56.

ii. Native metal substitution

In the case of ArMs, the metal that is substituted can be either a prosthetic metal ion (e.g., substituting a zinc with cobalt), the metal ion in a prosthetic group (e.g., substituting a haem iron for a copper), or a full prosthetic group (e.g., substituting a haem with a cobaloxime). Suitable examples for the latter is the work of Bacchi et al., where they substituted the native haem group in myoglobin and haem oxygenases with cobaloximes (Figure 3).^(39,40) The native histidines which act as the haem anchoring point instead becomes the axial ligand anchoring point of the cobaloxime. Myoglobins are oxygen carriers and so do not perform any native catalysis, but by introduction of the cobaloxime an artificial hydrogenase is made. Several examples employing haem proteins for ArMs exist in literature, highlighting one of the benefits of using a naturally occurring metalloprotein to give rise to novel activity. For haem proteins it is already known that the protein can accommodate a metal complex like the one of interest.^(39,40,57) When repurposing a non-metal binding protein for metal coordination as with method i., it is not certain that the protein will be able to adapt to a new prosthetic group. This is why using a protein that natively binds a metal may be beneficial—metal-coordinating amino acid geometries and cavities for prosthetic groups are already present.

iii. High affinity prosthetic group linkage

Many proteins bind inhibitors or prosthetic groups with high affinity. If the protein contains a suitably sized pocket around the binding site, this molecule can be modified with a catalyst. The most typical example of this methodology is the use of the biotin/streptavidin pair. Streptavidin is a smaller protein (52 kDa) that associate to biotin with one of the strongest non-covalent interactions in nature ($K_D=10^{-14}$ M).⁽⁵⁸⁾ This property has been used in the design of artificial metalloenzymes by functionalising metal complexes with a biotin, which then bind to the streptavidin enclosing the complex in the protein. The streptavidin scaffold can be mutated or applied to directed evolution around the active site pocket to improve the new catalytic efficiency. One of the earliest reports of an ArM is from 1978 by Wilson and Whitesides, making use of this convenient property.⁽⁵⁹⁾ A diphosphinerhodium catalyst was functionalised with a biotin unit and subsequently it was joined to avidin. The free catalyst could perform the target hydrogenation reaction but with no notable enantiomeric selectivity, but when introduced to the avidin however, an enantiomeric selectivity was observed. It was noted that the catalytic function is neither improved nor deteriorated upon introduction to the protein scaffold, but attribute the novel enantioselectivity to the active site cavity surrounding the catalyst.

Since the study by Wilson and Whitesides was published the biotin/avidin strategy has been used by many researchers, a suitable example is that it has been employed with a cobalt pentapyridyl HEC by Keller et

al. (Figure 7).(60) Keller et al. investigate the role of close-lying amino acids for proton relays. As discussed above (Section 1.2.1) proton relays are an essential function existing in natural hydrogenases and is likely one of the structural functions that make it such a highly efficient catalyst.

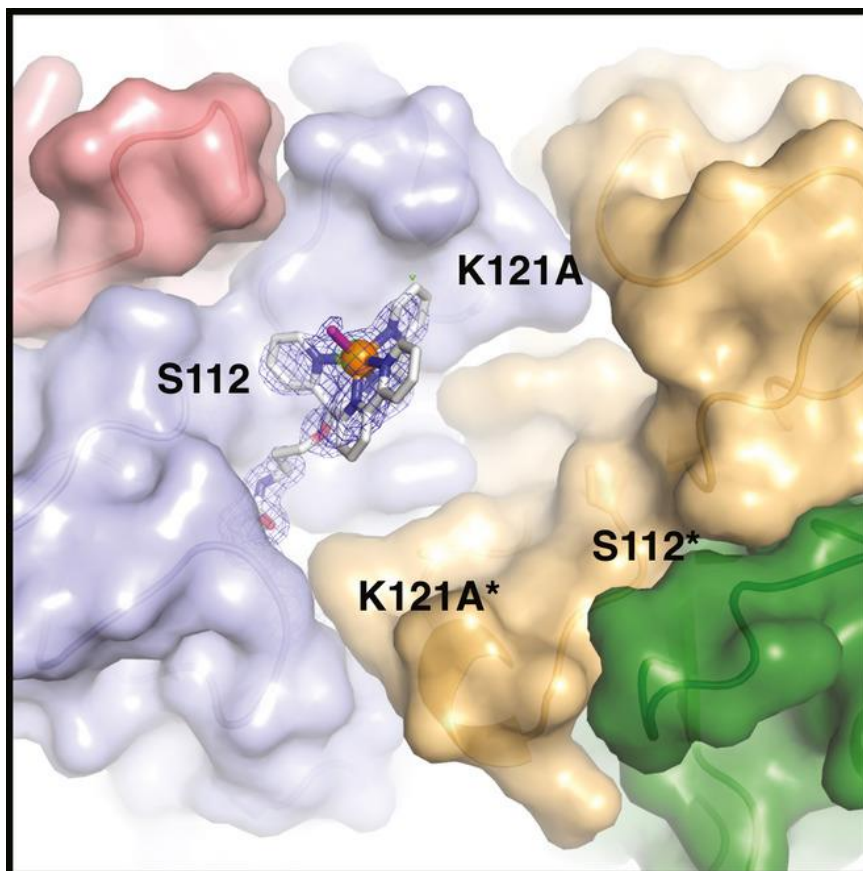


Figure 7: Close up of the active site in the cobalt-pentapyridyl-avidin artificial hydrogenase. Reprinted with permission from reference 60: Copyright 2018 John Wiley and Sons.

Another example of this functionalisation method was shown by Monnard et al., who used a natively zinc-bearing carbonic anhydrase.(61) The protein was prepared with its native zinc ion, to which a *para*-substituted aryl-sulfonamide coordinated with high affinity. An iridium transfer hydrogenation catalyst functionalised with this type of sulfonamide was prepared and then conjugated to the carbonic anhydrase zinc ion. Incorporation of the catalyst to the carbonic anhydrase transformed the carbonic anhydrase into a transfer hydrogenase with both catalytic activity and enantioselectivity improved compared to the free catalyst.

iv. Covalent binding between protein and catalyst

Covalent linkage of a catalyst to a protein will yield an ArM with a firmly attached catalyst, prohibiting any potential dissociation.

Srivastava et al. introduced the unnatural amino acid azidophenylalanine to a prolyl oligopeptidase using stop codon suppression technology.(62) The mutation site was chosen to disrupt the native enzymatic function, and so that the catalyst would instead occupy the active site cavity in the centre of the protein. The azidophenylalanine was then used as the covalent anchoring partner to the dirhodium catalyst. The catalyst was functionalised with an alkyne which can react with the azide of the unnatural amino acid through strain-promoted azide-alkyne cycloaddition. Several mutations of the host prolyl oligopeptidase were prepared, and increases in both the target olefin cyclopropanation yield and enantioselectivity were noted.

Another example of the covalent linkage of a catalyst is that of Davies and Distefano, who employed chemical modification of an amino acid to build the catalyst inside the protein scaffold.(63) A phenanthroline was covalently bound to a C in the adipocyte lipid binding protein. A copper ion was coordinated by the phenanthroline-modified protein, catalysing ester hydrolysis of a variety of substrates.

The approach of Davies and Distefano to chemical modification of the protein scaffold to build up the catalyst in the protein interior is similar to the one employed here. The protein scaffold $\alpha_3\text{C}$ was modified with a pyridine to coordinate the cobaloxime. The procedure of modifying $\alpha_3\text{C}$ will be described further in Chapter 3.1.

1.4 Summary

In our climate changing world, we need to find new ways to sustain our need for energy and hydrogen as fuel is a promising component in the future energy landscape. Making hydrogen gas is a simple reaction, yet only unsustainable methods for upscaled production are widely available, which demand a lot of energy and release a large amount of CO_2 .

In this thesis, a fully artificial metalloenzyme has been constructed and studied for its hydrogen-evolving properties, consisting of the *de novo* protein $\alpha_3\text{C}$ and the catalyst cobaloxime. Cobaloxime is a biomimetic complex, originally studied as a cobalamin analogue, but has been found to be a HEC. Cobaloxime is prone to dissociation, but many methods have been used to stabilise it and improve its hydrogen-evolving function, among others by incorporation into natural proteins. Here, it was incorporated into $\alpha_3\text{C}$, a *de novo* protein, forming a *de novo* metalloenzyme—a fully artificial metalloenzyme. Initially, $\alpha_3\text{C}$ was designed to study the formation and degradation of amino acid radicals and was made to be structurally robust over a range of pH-conditions, a useful property to understand potential changes in the cobaloxime behaviour upon introduction to the protein.

This thesis aims to address the research questions that arose upon formulation of the hypothesis that the *de novo* enzyme would have improved HER compared to free cobaloxime. The questions revolve around the elucidation of any effects the two components have on each other, if their structures and functions are changed and why these changes might arise. To lay the foundation for the remainder of this thesis, this chapter has introduced the relevant concepts of natural hydrogen-producing enzymes, cobaloxime as a biomimic of cobalamin, the various methods used previously to immobilise and modify cobaloxime and production methods for artificial metalloenzymes. In Chapter 2 the methods used for the project are introduced, and Chapter 3 and 4 focus on the construction and characterisation of the *de novo* metalloenzyme Co-MePy- $\alpha_3\text{C}$.

2 Methods

Several methods have been used in the work presented in this thesis. A selection of them will be described in this chapter to aid in the discussion in the remainder of the thesis. Recombinant protein production will be briefly described, as well as the different colourimetric assays used, and the different types of spectroscopies and electrochemistry that were used to characterise the *de novo* metalloenzyme Co-MePy- α_3 C.

2.1 Recombinant protein production

The protein used in this thesis, α_3 C, was produced by recombinant protein production (RPP). RPP is the production of a protein in a non-native organism, for example producing a human protein in yeast. This is done to enhance the yield, as extraction from the native organism typically is difficult, labour intensive, and perhaps unethical (like in the case of the study of a human protein). The general, simplified process of RPP is as follows:

1. *Identify the gene of interest* and copy it. With modern biotechnology it is cheap and easy to synthesise custom DNA sequences on demand.
2. *Insert the isolated DNA-sequence* either directly into the genome of the host organism, or more typically, into a plasmid. A plasmid is a small, circular DNA molecule which bacteria and yeasts may transcribe.
3. *Transform the host organism*. This is the process of introducing the plasmid to the host, which can be performed with several methods, most commonly heat-shock. The bacteria are kept in ice and then heat-shocked at 42°C which makes the cell membrane temporarily porous allowing the plasmid to enter.
4. *Grow the host organism* which now contain DNA that encodes for the gene of interest and will produce it.
5. *Harvest and lyse the cells*. After some hours, typically at least 24, the host organism is harvested by centrifugation. This removes the liquid media, leaving only the cells containing the target protein. The cells are then broken, lysed, to gain access to it. Lysis can be performed with several methods, in the work presented here it has been performed by freeze-thawing cycles, where the cells are frozen in liquid nitrogen, then thawed in warm water several times. The resulting sample is called a lysate.
6. *Remove the insoluble components*. The lysate contains everything that the bacteria were made up of, but now in a mixture rather than organised cell components. All insoluble components like membranes and large pieces of DNA need to be removed before further processing takes place. The lysate is ultracentrifuged, pelleting the insoluble cell debris, and the liquid supernatant is collected. The supernatant contains only soluble cell components, the target protein included (unless it is a membrane protein, in which the insoluble pellet is reserved rather than the supernatant, a case not applicable for this thesis).

As α_3 C is a *de novo* protein, there is no host organism to copy the DNA from. When the α_3 -protein initially was conceived the protein was fully synthesised by solid phase peptide synthesis.(64) Upon finding the final sequence, a custom α_3 W-transcribing DNA-sequence was inserted into a plasmid, which was used for the subsequent steps of the protein production.(65) The α_3 -proteins are expressed as a thioredoxin fusion protein, where it is attached to the larger thioredoxin protein, aiding in the expression and purification.

The many steps of recombinant protein expression are far more detailed than outlined above, and so for the purposes of this thesis, and so only the purification of the protein will be described in more detail. After lysis-subsequent centrifugation, the lysate supernatant is reserved, and in the case of α_3 C-purification three

chromatography steps were performed to remove other soluble proteins as well as the thioredoxin fusion protein, which is enzymatically cleaved off:

1. *Ni-affinity chromatography*. The thioredoxin fusion protein has a His-tag—a tail of six histidines. These amino acid residues coordinated with high affinity to Ni^{2+} bound to the chromatography resin, which allowed the specific exclusion of the target $\alpha_3\text{C}$ -fusion protein from the solution.
2. *Cleavage of the fusion protein*. In the peptide sequence a specific thrombin cleavage sequence has been included in between the $\alpha_3\text{C}$ -section and the thioredoxin-section. The eluted fusion protein was treated with the protease thrombin for several hours, allowing for complete digestion.
3. *Ni-affinity chromatography*. Again, the His-tag of the thioredoxin coordinated to the Ni^{2+} in the chromatography resin, but in this step the non-bound protein was the target. The $\alpha_3\text{C}$ -section could not coordinate to the column and is immediately eluted and collected.
4. *Reverse phase chromatography (RP chromatography)*. This is the final step to remove any lingering non-target proteins, salts and other remaining impurities. RP chromatography was performed in a mixture of acetonitrile and water and operates on the principle of that the polarity of the proteins shifts as the ratios of solvents shift. The column material was C18–hydrocarbon chains with 18 carbon atoms. The protein was immobilised in the column matrix, and as the concentration of acetonitrile increased, its polarity shifts allowing it to dissociate at a specific point. This is how $\alpha_3\text{C}$ was separated from any remaining unwanted proteins and organic impurities.

Each step was controlled by sodium dodecyl sulphate polyacrylamide gel electrophoresis (SDS-PAGE) where protein components in a sample can be distinguished by their mass. This is especially of interest after the cleavage, where the $\alpha_3\text{C}$ and the thioredoxin appear as two bands of lower mass, rather than one band of higher mass. After the final RP-chromatography all fractions were lyophilized to remove all solvent, allowing the identification of protein-containing fractions. Small samples from these fractions were collected and analysed by matrix assisted laser desorption ionization time of flight mass spectrometry (MALDI-TOF MS) which with high precision and sensitivity determined the mass and purity of the sample protein.

2.2 Colourimetry

Colourimetry is an assay type where the analyte can be identified or quantified by a change of colour, as measured by an ultraviolet (UV)-visible spectrometer. Colourimetric assays are convenient because a standard UV-visible spectrometer is all that is needed in addition to general lab equipment and they can be performed by anyone with some laboratory experience. Procedures for performing certain colourimetric assays using a mobile phone camera has even been presented as an accurate alternative for teaching in schools or universities that do not have resources to purchase spectrometers highlighting its availability.(66)

In this thesis three colourimetry assays have been used and will be outlined in this section: Bradford assay and bicinchoninic acid (BCA) assay for the determination of protein concentration and 4-(2-pyridylazo)resorcinol (PAR)-assay for the determination of cobalt concentration. Protein concentrations are often determined by the absorbance of the sample at 280 nm, where the aromatic amino acids tryptophan and tyrosine absorb. These are not present in $\alpha_3\text{C}$ and so the colourimetric assays were necessary to determine the protein concentration.

For a colourimetric assay a standard curve must be made each time the experiment is performed. In a standard curve a known quantity of a standard compound is plotted against the resulting absorbance, yielding a linear equation which can be used to calculate the concentrations in the unknown samples. For the protein assays the standard protein bovine serum albumin (BSA) was used. For the PAR-assay, CoCl_2 and dichlorocobaloxime $[\text{Co}(\text{dmg}_2)\text{Cl}_2]$ were used. The standard curve samples and the unknown samples were prepared the same way, by mixing the samples with the reaction solution, and subsequent recording of their absorbances. The standard curve was then plotted, forming a line, and the resulting linear equation was used to calculate the concentrations of the unknown samples, rather than relying on previously published extinction coefficients.

2.2.1 Bradford assay

The Bradford assay was invented by Marion Bradford in 1976 and the measured colour change arises from the interaction between the protein and the pigment Coomassie brilliant blue G250.(67) The unbound Coomassie is cationic, and red. It binds to the protein through interactions with the anionic amino acids, which shifts Coomassie to the anionic form, which is blue, with an absorbance maximum at 595 nm.

The Bradford assay is very sensitive to low concentrations of protein, and relatively insensitive to non-protein contaminants. Because the chemical interaction taking place in the Bradford assay is largely ionic, the amino acid profile of the target protein will affect the interactions of the assay. In a protein with a number of anionic amino acids lower than that of BSA, the Bradford assay may underestimate the protein concentration. For the *de novo* metalloenzyme Co-MePy- α_3 C presented in this thesis it was found that the Bradford assay was completely unusable. The hypothesis for this is that the cobaloxime is a relatively large, cationic species bound to a relatively small protein, giving rise to repelling of the cationic Coomassie molecules, which prevents the protein-Coomassie interaction from taking place. Therefore, for Co-MePy- α_3 C the BCA assay was used instead. The Bradford assay was useable for determining concentrations of α_3 C and MePy- α_3 C, and because it is faster to perform than the BCA assay it was used in these cases.

2.2.2 BCA assay

The BCA assay was invented by Paul Smith at the Pierce Chemical Company, now part of ThermoFischer, and was patented by them in 1989.(68) The assay quantifies the bonds and is thus not depending on the identities of the side chains of the protein. The components of the assay are CuSO_4 (green), in which the copper is Cu^{2+} , and BCA. BCA specifically coordinates Cu^{1+} which forms upon the reduction of Cu^{2+} by the peptide bonds, which are cleaved in the process. Therefore, the concentration of Cu^{1+} is proportionate to the concentration of peptide bonds. The $(\text{BCA}_2[\text{Cu}^{1+}])$ complex is vividly purple, with an absorbance maximum at 562 nm. I was found compatible with Co-MePy- α_3 C, and it was therefore used to quantify the protein portion of the *de novo* metalloenzyme. For the most precise determinations, α_3 W was been used as the reference protein for the standard curve rather than BSA, where the concentration of α_3 W was first determined by absorbance at 280 nm.

The BCA assay is precise, but requires incubation for 30 minutes at 60°C. Thus, all samples must be prepared simultaneously, because they must all be incubated precisely the same duration or the quantification will not be precise. When performing protein quantifying assays the protein concentration is often completely unknown, and so performing a Bradford assay where the unknown sample can be diluted and measured immediately without incubation is practical.

For quantifying completely unknown protein concentrations by BCA assay a wide range of dilutions must be prepared, which may still be too high or low with regard to the standard curve, and is a waste of precious protein sample. For Co-MePy- α_3 C samples the order of magnitude of protein was already known, and so only a small number of dilutions was required to find a sample with absorbance within the standard curve.

2.2.3 PAR assay

PAR is a bright orange coordinating agent with an absorbance maximum of 410 nm, which shifts to around 500 nm upon coordination of various transition metal ions: for $[\text{PAR}_2(\text{Co}^{2+})]$ the absorbance maximum is 514 nm. In the work presented in this thesis the absorbance at 510 nm was used, as it was the apparent maximum in the collected spectra. The use of the PAR assay for determination of the concentrations of a range of metal ions has been described several times in literature, and was here used as an initial method to determine concentrations of cobalt in Co-MePy- α_3 C. (69–71)

Because the cobalt in Co-MePy- α_3 C is likely partially buried, the protein solutions were prepared with the addition of the denaturant guanidinium hydrochloride (Gdn-HCl), and so the standard curve was prepared in the same way. The denaturant was added to unfold the protein, exposing the cobaloxime inside to the solution. It was found that the PAR assay underestimates the concentration of cobalt in Co-MePy- α_3 C, most likely because the cobalt in addition to being buried in the protein also is coordinated by the two equatorial glyoxime ligands. This shifts the coordination equilibrium as the cobalt ions must initially dissociate from the glyoxime before coordinating the PAR. This will be discussed further in Chapter 3.

2.3 EPR spectroscopy

Electron paramagnetic resonance (EPR) spectroscopy was used in the work discussed in this thesis to verify the oxidation state of the cobalt ion in the *de novo* enzyme Co-MePy- α_3 C, and to verify its coordination to the protein scaffold. The mode of EPR spectroscopy used here probes an odd number, unpaired electrons, for example an unpaired d-electron in a cobalt ion, such as that in cobaloxime or Co-MePy- α_3 C. The electron spin quantum number is $s = 1/2$, and because it has a magnetic moment, the magnetic spin quantum number $m_s = \pm 1/2$ is degenerate in the absence of an external magnetic field.⁽⁷²⁾ When an external field is applied, as in EPR spectroscopy, the two split and form a high and low energy state. This phenomenon is known as the Zeeman effect and is described by equation 2:

$$\Delta E = g \times \mu_B \times B_0 \quad (2)$$

The energy difference (ΔE) between the lower energy state ($m_s = -1/2, \beta$) and the higher energy state ($m_s = +1/2, \alpha$) is governed by the variable Landé factor, or g -factor, the constant Bohr magneton $\mu_B (e\hbar/2m_e, e = \text{elementary charge}, \hbar = \text{reduced Planck constant}, m_e = \text{electron mass})$ and the variable external magnetic field B_0 (Figure 8).

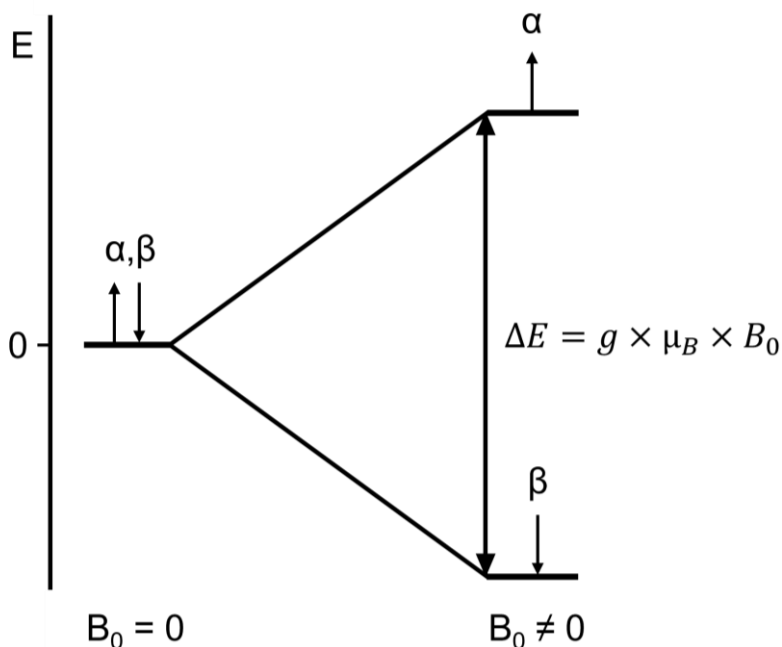


Figure 8: The Zeeman effect.

The low energy population β can be promoted to the high energy state by the input of energy ($h\nu$). The energy required varies based on the local magnetic field of the unpaired electron, such as its orbital, nearby nuclei and other nearby unpaired electrons. This affects the g -factor which describes the coupling between the electron magnetic moment and its angular momentum, making ΔE unique for each species. In EPR spectroscopy this energy is what is probed.

Experimentally, a set frequency of electromagnetic radiation ($h\nu$) is applied to the sample, and the magnetic field is swept. Different frequencies of electromagnetic radiation can be used, the most common, and the one used in this thesis, is X-band at with a frequency of ca 10 GHz. Others may also be used, mostly seen in literature other than X-band is Q-band at ca 35 GHz. The naming convention of the bands are the same ones used for radiocommunication and radar, as standardised by the Institute of Electrical and Electronics Engineers.⁽⁷³⁾ When the field strength reaches the point where $h\nu = \Delta E$ (equation 2) a signal in the spectrum appears, from which the unique g -factor can be calculated. As follows by equation 2, with an increasing frequency (or higher energy) the field strength must also increase, and so it is impractical to assign transitions to a certain frequency or field strength, rather its g -value is used. Because the g -factor is sensitive to subtle changes in the local magnetic field of the probed unpaired electron, it is unique and

constant for each species. Therefore, changes or differences in the local environment of the electron can be probed by seeing shifts in g -values for certain spectral features. In the work presented in this thesis it was used to verify that the cobaloxime of Co-MePy- α_3C is inside α_3C , as the exposure to the solvent changes and so the local magnetic field changes.

Only species with an odd number of unpaired electrons are EPR-active, which is how the resting oxidation state of the cobalt ion could be determined. The most likely resting oxidation states for the cobalt in cobaloxime are Co^{2+} , with an electron configuration of $[Ar]3d^7$, and Co^{3+} , with an electron configuration of $[Ar]3d^6$. Because Co^{2+} has an odd number of valence electrons it has an odd number of unpaired electrons, making it EPR-active, yielding an EPR-spectrum. Co^{3+} does not have an odd number of unpaired electrons, and so is not detectable with the mode of EPR used in this thesis. Because of this, it can be distinguished if the cobalt in cobaloxime is Co^{3+} or Co^{2+} in the resting state. If no signal appears with the untreated sample of cobaloxime or Co-MePy- α_3C , and a signal appears after a one-electron reduction, the cobalt is Co^{3+} in the resting state.

2.4 Circular dichroism spectroscopy

To investigate of how the α_3C protein folding was affected by the chemical modifications CD spectroscopy was used. It is a variant of UV-vis absorption spectroscopy, where the light is circularly polarised, and it probes for chiral centres. The sample is irradiated by right- and left-hand polarised light, and the signal is a difference spectrum of the two. Achiral centres will absorb the right – and left-hand polarised lights equally (difference = 0), there is no signal in the CD spectrum (but a signal in a normal UV-vis absorption spectrum). Chiral centres will absorb the lights differently (difference $\neq 0$), and so there is a signal in the CD-spectrum, as well as in the UV-vis absorption spectrum.

Proteins are chains of amino acids, which are chiral (Figure 9A). When proteins fold into their secondary structures (α -helices, β -sheets) or remain unstructured, different UV-vis absorption processes will dominate, which gives rise to different shapes in the CD spectra (Figure 9B).^(74,75) Most proteins fold with a mix of secondary structures, and then the CD spectrum will be a linear combination of the three signals. The protein used in this thesis, α_3C , is almost completely helical, and so its spectrum appears very close to that of a text-book α -helix spectrum. Because of this, CD spectroscopy was used to determine if the helicity of α_3C is disrupted by introducing the pyridine and cobaloxime. The helical signal decrease when the helicity is decreased, and it turns into the signal of unstructured protein. This effect can be quantified by the CD spectral changes at 222 nm, at which helical folding give rise to a signal, but unstructured folding does not (Figure 9B).

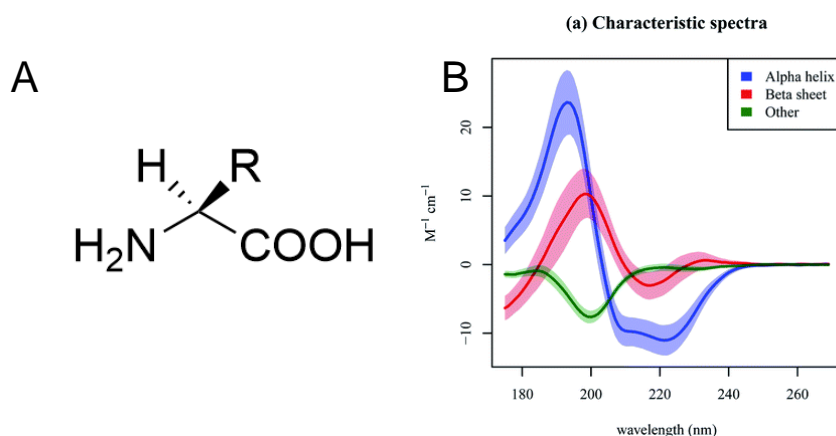


Figure 9: A: An L-amino acid, R = the sidechain. B: Reference CD-spectra of α -helix, β -sheet and unstructured peptide. B reprinted under CCBY3.0 license from reference 74.

The signal recorded by the instrument is in ellipticity (θ_{obs} , millidegrees) and can be converted to mean residue molar ellipticity $[\theta]$ ($deg \times cm^2 \times dmol^{-1}$):

$$[\theta] = \frac{\theta_{obs} \times 10^6}{C \times l \times n} \quad (3)$$

Where C is the concentration of protein (μM), l is the pathlength (mm) and n is the number of amino acids. In the case of α_3C , it is known that it is primarily helical, and so the signal will be that of α -helix. As described above, to understand if the helix was disrupted when introducing the chemical modifications, the spectral changes were monitored. To understand if the protein structure was less stable upon modification, the energy of unfolding was calculated by a denaturation study. This is performed by titration of a denaturant (for example urea which was used here), and subsequent collection of CD spectra at each concentration. The $[\theta]$ at a certain wavelength can then be related to the concentration of denaturant to yield the ΔG for unfolding.(76)

2.5 Cyclic Voltammetry

In voltammetry the potential at which a current pass from electrode to an analyte is measured by creating a circuit between a working electrode (where the reduction or oxidation of the analyte takes place) and a counter electrode, which is oxidised/reduced by solution which connect the two. The solution contains the analyte and an electrolyte, to make it conductive to be able to close the circuit.(77) A third electrode is often used, the reference electrode, which maintains a constant potential through the experiment and act as the reference to the potential at the working electrode.(77)

In cyclic voltammetry which is the method that was used here, the potential is swept linearly from the start value to the end value, where it then sweeps back to the start again (Figure 10A). At certain potentials reductions or oxidations may occur, which appears as peaks in the cyclic voltammogram (CV), here illustrated with the reduction and re-oxidation of ferrocene, known to be an electrochemically reversible process (Figure 10B).(78)

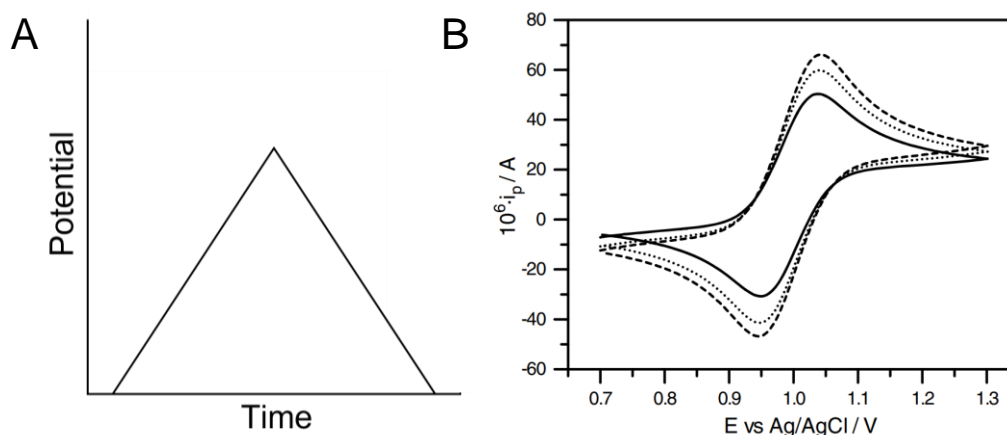


Figure 10:A: Waveform of a cyclic voltammogram. B: Example cyclic voltammogram of ferrocene reprinted from reference 78: Copyright 2007 Springer Nature.

The peak of the waveform in Figure 10A represents the turning point of the voltammogram, in the example CV at 0.7 V vs Ag/AgCl (Figure 10B). The benefit of cyclic voltammetry specifically is that it is simple to observe both the reductions and oxidations taking place in one measurement, which is especially interesting as some oxidations may only arise because of a reduced species having been formed first. This type of process is referred to as electrochemically reversible, where the reduced species readily is re-oxidised ($X + e^- \leftrightarrow X^-$), also known as a Nernstian reaction where the relation of X and X^- at a set potential is governed by the Nernst equation (equation 4, see the following section). A reversible wave is typically characterised

by the cathodic and anodic peaks being separated by ca 59 mV, and that the current density of the two peaks is equal because the formed concentration of X^- is the same concentration that is being re-oxidised.

The peak in a voltammogram forms because the reducible or oxidisable species in the diffusion layer, the layer closest to the electrode surface (or as is applicable in this thesis, in the adsorbed layer on the electrode surface) is consumed. When doing cyclic voltammetry with an electrocatalyst, eventually the potential at which catalytic turnover takes place will be reached. A catalyst is defined by the ability of being able to be regenerated, the implication of which in cyclic voltammetry is that the reducible (or oxidisable) species is regenerated in the diffusion layer, and so a peak does not form in the same way because the reducible species is continuously regenerated. This gives rise to a feature in the CV called a catalytic current or catalytic wave, exemplified by a CV of the *de novo* metalloenzyme produced and studied in this thesis (Figure 11).

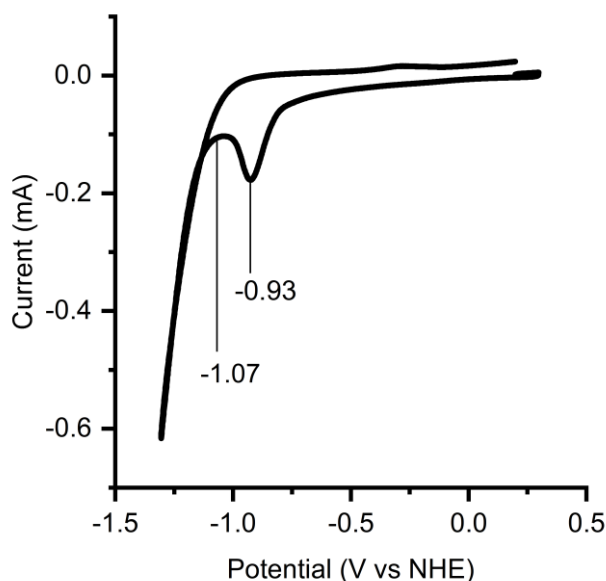


Figure 11: Example CV of the cobaloxime-based *de novo* metalloenzyme used in this thesis, demonstrating an irreversible reduction (peak: -0.93 V vs NHE) and a catalytic current (onset: -1.07 V vs NHE).

The features of the CVs of cobaloxime and the *de novo* metalloenzyme will be discussed more in depth in later chapters, exploring what processes take place at what potentials. In the example CV the catalytic wave can be seen with an onset at -1.07 V vs NHE. Because it does not have a peak, the onset potential is instead referenced. In contrast with the reversible reduction of ferrocene in Figure 10B, in this CV an irreversible peak can be seen at -0.93 V vs NHE. This indicates that by the time the anodic sweep takes place, a different species than the one being reduced has formed, which cannot be oxidised at a matching potential.

In Figure 10 and Figure 11 the potential has been given versus Ag/AgCl and normal hydrogen electrode (NHE). These are reference electrodes against which the potential is measured. Practically, the reference electrode used is Ag/AgCl, and so the raw data is in V vs Ag/AgCl. It can be re-calculated to other reference electrode depending on the needs. For HER it is common to use NHE, which is why it is used here as well to allow for simpler comparison with other published CVs. NHE is 0.197 V vs Ag/AgCl, which is added to all raw potentials to give the potential vs NHE.(79)

2.5.1 Voltammetric pH dependence

In HER not only reduction is necessary for the turnover to take place, also two protonations must occur. Because the experiments in this thesis are all performed in water, a pH-dependence study can be performed to gain insight into when reduction (or oxidation) and protonation may be coupled, it will give rise to a shifting peak potential as the pH is changed. Protonation of a reduced species may be why an irreversible peak is formed, like in the CV in Figure 11 (-0.93 V vs NHE), and so investigating if the reductive peak is

pH-dependent may give insight into what process is taking place during that reduction. The pH-dependence of the potential is a linear relationship (equation 4) derived (see Appendix 1) from the Nernst equation (equation 5).

$$E = E_0 - 0.0591 \text{ pH} \quad (4)$$

$$E = E_0 - \frac{RT}{nF} \ln \left(\frac{[X^-]}{[X]} \right) \quad (5)$$

The Nernst equation relates the concentrations of a reduced ($[X^-]$) and oxidised ($[X]$) species with the potential (E) and the standard equilibrium potential (E_0) for the electrochemically reversible process X^-/X . R is the universal gas constant ($8.3145 \text{ J K}^{-1} \text{ mol}^{-1}$), T is the temperature in $^\circ\text{K}$, n is the number of electrons passed in the process and F is the Faraday constant ($96\,485 \text{ C/mol}$).⁽⁷⁹⁾

The pH-dependence of the reduction peak of cobaloxime (ca -0.9 V vs NHE) and the *de novo* metalloenzyme showed in this thesis is of interest to elucidate which mechanism is plausibly the dominant one under the experimental conditions used. In Section 2.5 above it was described that this peak is electrochemically irreversible. It is important to note that just because the process appears irreversible under these conditions doesn't mean that the reduction is not behaving in a Nernstian fashion. Because the reduced species forming at this reduction is likely becoming protonated, a chemical step follows the reduction, which means that the reduction itself is not what is yielding the product which cannot be re-oxidised. To illustrate this a CV of a cobaloxime with increasing concentrations of proton donors is shown (Figure 12). The electrochemically reversible wave turns into an irreversible wave upon addition of acid. The reduced species is chemically modified, yielding a species unlike the one formed during reduction.⁽⁸⁰⁾ Therefore, the Nernst equation is still valid for analysis of the reductive peak, even though it does not visually appear to be reversible, as in water it is impossible to remove the proton source completely.

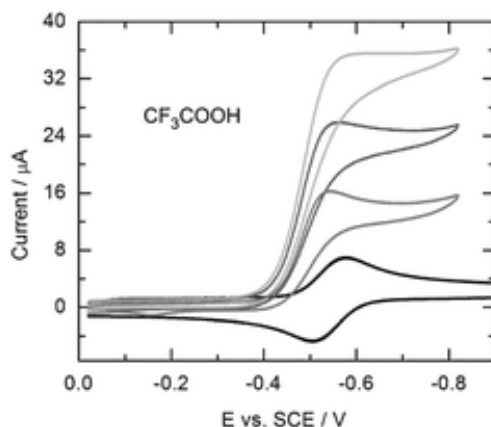


Figure 12: Example CVs of a cobaloxime in organic solvent, lacking a proton source (black), and with increasing concentrations of a proton source added (grey). Reprinted with permission from reference [80]: Copyright 2005 Royal Society of Chemistry (Great Britain).

In the example CV in Figure 12 both axes are turned around compared to how they are showed in this thesis. The potential is showed being more cathodic on the right side, and the current has been inverted to show the reductive current as positive, this is the US convention of plotting CVs. In this thesis, the cathodic potential is shown on the left and the reductive current shown as negative in the CVs, this is the IUPAC convention.⁽⁸¹⁾ This is just a choice of how to show the data, and not a difference in the actual voltammetric response in the experiment.

2.6 Clark-type microelectrode

A typical Clark electrode detects oxygen, by reducing it to water. The electrode itself, a cathode, is made of platinum, and is placed in an electrolyte. The sample is separated from the electrolyte by an oxygen-permeable membrane, which allows the generated oxygen to diffuse over and be reduced by the electrode.

A Clark type H_2 microelectrode is constructed in a similar way, where the platinum anode is submerged in an electrolyte inside of a tip together with a reference electrode, which is then sealed by a hydrogen permeable membrane. (Figure 13A). The hydrogen is quantified by its consumption at the anode and compared to a previously measured standard curve of known concentrations of hydrogen, yielding raw data measuring the $\mu\text{M H}_2$ over time. The raw data were corrected for by dividing by catalyst concentration, to give a more precise comparison between each data point (Figure 13B).

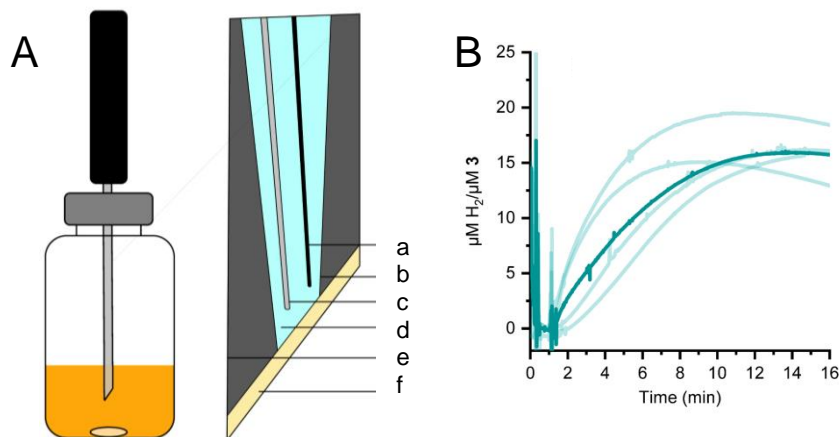


Figure 13: A: Schematic over experimental setup of Clark type needle sensor submerged in a HER-sample inside a septum-sealed microwave vial, and a zoomed in schematic of the sensor tip and its parts. a: Counter electrode, b: Sensor casing, c: Platinum anode, d: Electrolyte, e: Casing, e: Semi-permeable membrane. B: Sample data collected with Clark-type microelectrode, corrected for the catalyst (Co-MePy- $\alpha_3\text{C}$ (**3**)) concentration (reprinted from paper I (83)).

Because the measurement appears because of the consumption of H_2 , the plateau appearance does not mean that the HER has stopped, it means that the H_2 is being produced as fast as it is being consumed. When the line dips, which can be seen in one of the lines in the example data above, that means the HER is slowing down.

Gases like hydrogen can also be quantified by gas chromatography (GC), and this was done in the work presented here too. However, using a Clark-type microelectrode for quantification allows for the direct measurement of the H_2 in solution, rather than wait for gas to accumulate in the headspace, which is necessary for GC. An issue with especially H_2 is that it is prone to escape even tightly sealed vials, and so headspace concentrations may not be accurate, especially after several hours, which is the timescale necessary for GC here. But with a microelectrode, measuring immediately upon formation directly in solution gives no chance for the gas to escape, which additionally allows the measuring of the initial phase before the plateau is reached. Additionally, microelectrodes are very sensitive, down to $0.3 \mu\text{M H}_2$ in water, making them very useful for dilute catalyst samples.(82)

2.7 Summary

The protein scaffold $\alpha_3\text{C}$ was produced by recombinant protein expression, and the product Co-MePy- $\alpha_3\text{C}$ was characterised with a range of methods, some key methods described in this chapter. Colourimetric methods were used to quantify protein and cobalt in samples of Co-MePy- $\alpha_3\text{C}$. EPR spectroscopy was used to verify the coordination of the catalyst to $\alpha_3\text{C}$, and CD spectroscopy was used to quantify any changes in $\alpha_3\text{C}$ folding upon this coordination. CV was used to understand the impact of coordination upon the voltammetric and electrocatalytic behaviour of the mechanism. The HER was measured using a Clark-type microelectrode, quantifying the produced H_2 in solution. Additional methods were used but were not described here, and all experimental details can be found in paper I.

3 Constructing and characterising the fully *de novo* artificial metalloenzyme Co-MePy- α_3 C

This chapter is based on the paper “Hydrogen production by a fully *de novo* enzyme” from 2024. (83) In this paper, the *de novo* metalloenzyme Co-MePy- α_3 C was first published. Co-MePy- α_3 C is made up of the HEC cobaloxime and the *de novo* protein α_3 C, forming a fully artificial – *de novo* – enzyme. In this chapter the design, production, characterization and HER catalysis of Co-MePy- α_3 C is discussed, and in Chapter 4 the electrocatalytic behaviour of Co-MePy- α_3 C is discussed.

When constructing an artificial metalloenzyme, the effect of the catalyst on the protein and vice versa is of interest. Performing catalytic studies allows the investigation of if anything has changed for the catalyst—is its catalytic function improved or not by the presence of the protein, and how? Conversely, it is also of interest to understand if the protein is affected by the catalyst as it could help guide further modifications of the protein as well as understanding of catalytically important factors such as solvent access. Is the protein folding altered upon catalyst incorporation, and is it easier to unfold?

Here, catalytic studies were performed with two different methods, and structural studies were based on CD spectroscopy. The CD spectroscopy study indicated that the stability of the protein scaffold of Co-MePy- α_3 C is identical to that of unmodified α_3 C, but that the folding is less helical. That suggests that the cobaloxime interrupts the hydrogen bonding in the secondary structure leading to partial unfolding. The findings of the catalytic studies reveal that the TONs of HER by Co-MePy- α_3 C was approximately 80% of that of cobaloxime, and the TOFs of HER by Co-MePy- α_3 C was approximately 40% of that of cobaloxime. Some experiments do however indicate improved longevity of Co-MePy- α_3 C, which would allow for increased hydrogen production simply because of it being available to catalyse for a longer period. The implications of the findings presented in the paper will be discussed in this chapter and highlights the need of further studies into artificial enzyme design.

3.1 Production and characterisation of Co-MePy- α_3 C

The components of the *de novo* metalloenzyme Co-MePy- α_3 C were introduced in Chapter 1 (1.2.2 and 1.3.1). For the protein scaffold α_3 C was found suitable because it is highly stable under a wide range of conditions, contains no amino acid side chains that may be reduced at applicable potentials and has a single suitable modifiable amino acid (the central C).

The HEC cobaloxime was chosen as a suitable model catalyst for making a *de novo* HER enzyme, because it has been very thoroughly studied and the related literature is extensive. That allows for convenient comparison of Co-MePy- α_3 C as a proof of concept for *de novo* metalloenzymes with existing literature. The procedure for producing the cobaloximes used in this thesis has been previously published, and the preparation of α_3 C was discussed in Chapter 2.1. (84,85)

The α_3 C was modified in two steps, with dialysis in between to remove excess reactants (Figure 14). The formation of the intermediate MePy- α_3 C was verified with MALDI-TOF MS, and the coordination of the cobaloxime to MePy- α_3 C to form Co-MePy- α_3 C was verified by EPR-spectroscopy. In Sections 3.1.1 and 3.1.2 these two functionalisation steps and the quantification of protein and cobalt in the product will be discussed.

3.1.1 Functionalisation of α_3 C

The α_3 C was prepared by biological protein expression and purified from the *Escherichia coli*. The protein α_3 C contains a single C, the sulphur side chain of which was functionalised with 3-bromomethyl-pyridine

(3-BrMe-py) under alkaline and denaturing conditions (Figure 14). The sulphur substituted the bromide 3-BrMe-py, yielding 3-cysteinemethyl-pyridine α_3 C (3-MePy- α_3 C). Because no other groups were available in the protein to react with 3-BrMe-py, the C was specifically functionalised. The pH of the reaction mixture was at least 8.5, as the pK_a of cysteine is ca 8.3, ensuring that a large portion of the Cs were deprotonated and in the S^- form. S^- is a better nucleophile than SH, allowing for a more efficient nucleophilic attack on the carbon.(86)

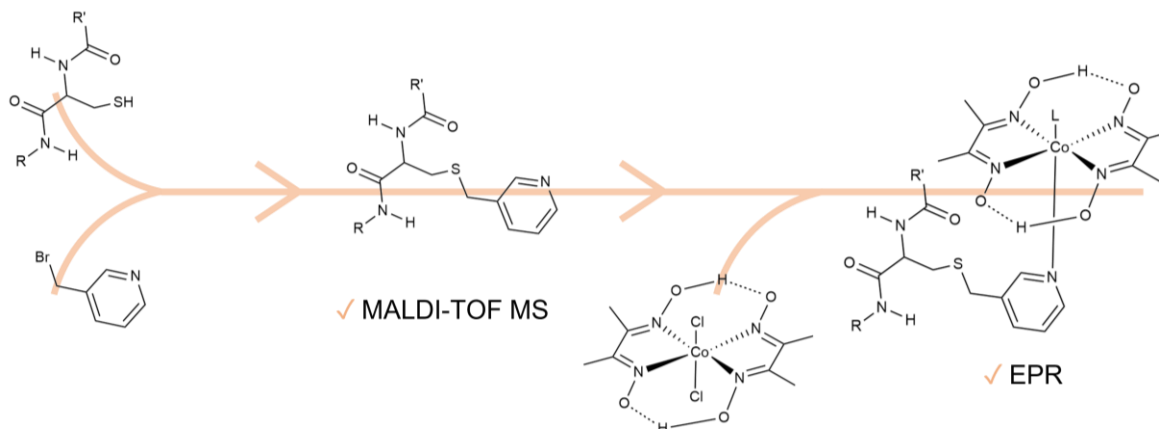


Figure 14: Overview reaction of the functionalisation of α_3 C to form Co-MePy- α_3 C. 3-Br-MePy reacts with C34 in α_3 C ($R = \alpha_3$ C N-terminal sequence from cysteine 34, $R' = \alpha_3$ C C-terminal sequence from cysteine 34) to form MePy- α_3 C, which in turn reacts with the dichlorocobaloxime to form Co-MePy- α_3 C (where L is a chloride which likely was substituted with a water during the modification). MePy- α_3 C formation was verified with MALDI-TOF and Co-MePy- α_3 C formation was verified with EPR-spectroscopy.

In α_3 C the solvent access of C is limited, and so denaturing conditions were required so that C is exposed to the bulk solution. This was achieved by the addition of the chaotropic salt Gdn-HCl which disrupts the secondary structure of proteins by interfering with the hydrogen bonding with the bulk water. As the reaction mixture was left to stir or shake for several hours, up to overnight, it yielded a yellow product due to the released bromine. The excess 3-BrMe-py was removed by 3.5 kDa cut-off dialysis, which ensured that only large molecules such as the functionalised protein (7.5 kDa) was remaining inside the membrane.

MALDI

MALDI-TOF MS was used to confirm the formation of 3-MePy- α_3 C. The mass of the sample was compared to that of untreated α_3 C as well as the reference protein α_3 Y, and it was found that 3-MePy- α_3 C form with no detectable remnants of unmodified α_3 C (Figure 15). The peak marked α_3 C in Figure 15 was a measurement of unmodified α_3 C, and no extra peak at the mass of α_3 C appeared in the MALDI-TOF MS of 3-MePy- α_3 C.

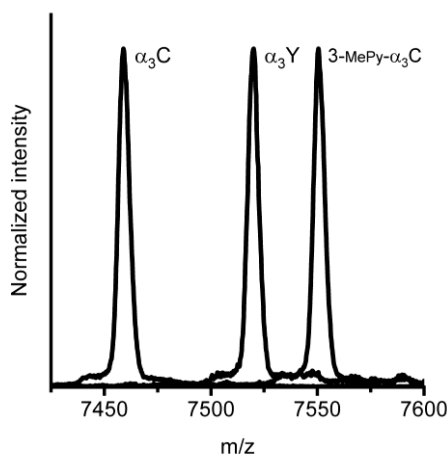


Figure 15: MALDI-TOF MS of α_3 C, α_3 Y and 3-MePy- α_3 C. The peak intensities were normalised to be 1 to allow for closer comparison. Reprinted under CCBY3.0 license from paper I.(83)

3.1.2 Functionalisation of MePy- α_3 C

After formation of 3-MePy- α_3 C, the pyridine acted as an axial ligand for the cobaloxime. A cobaloxime variant without an axial pyridine ligand ($[\text{Co}(\text{dmgH})_2\text{Cl}_2]$) was mixed with 3-MePy- α_3 C under anoxic, denaturing conditions. To this mixture the oxidant triethylamine (TEA) was added to ensure that the cobaloxime was dechlorinated to allow for coordination to the protein-bound pyridine, forming the product $[\text{Co}(\text{dmgH})_2(3\text{-MePy-}\alpha_3\text{C})\text{L}]$ (Co-MePy- α_3 C).

EPR

X-band EPR-spectroscopy is a method which can detect paramagnetic species, for example the odd numbered, unpaired d-electron in the $[\text{Ar}]3d^7 \text{Co}^{2+}$. EPR-spectra were collected of samples of the free cobaloxime and Co-MePy- α_3 C, both showing no EPR signal which suggests that they were in the typically undetectable Co^{3+} ($[\text{Ar}]3d^6$) oxidation state. To verify this hypothesis, a one electron reduction of the samples was performed with the reductant $[\text{Eu}(\text{EGTA})]^{2-}$ yielding the EPR-detectable Co^{2+} (Figure 16), confirming the prepared redox state of the cobalt ion in cobaloxime and Co-MePy- α_3 C to be Co^{3+} .

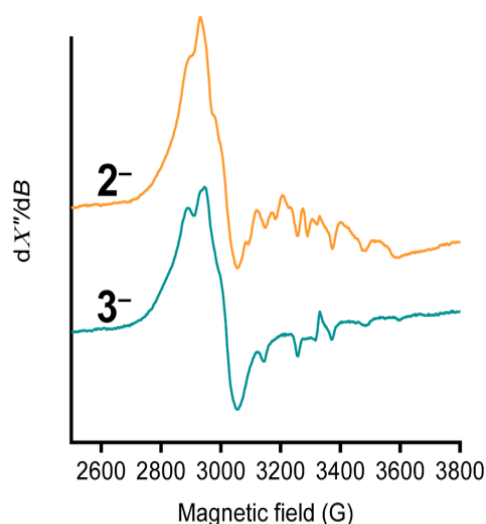


Figure 16: EPR spectra of reduced cobaloxime (2^-) and Co-MePy- α_3 C (3^-). Reprinted under CCBY3.0 license from paper I.(83)

X-band EPR-spectroscopy was also used to determine if the cobaloxime was coordinated to α_3 C in the *de novo* metalloenzyme (Figure 16). In X-band EPR spectroscopy it is typically not possible to resolve the spectral fine structure, and definitive analysis to minor ligand field changes can be difficult. With comparison with previously published EPR spectral characterisations of cobaloximes some conclusions can be drawn. Making these comparisons with literature, the spectra shown here for reduced cobaloxime and Co-MePy- α_3 C was determined to be consistent with one axial pyridine coordination, as expected. Other spectral differences were subtle, but they suggested a difference in the coordination environment of the cobalt in both catalysts. Because the non-pyridine axial ligand of the cobaloxime in Co-MePy- α_3 C is likely a solvent molecule, changing the solvent access can give rise to weak changes in the ligand field of the cobalt. In comparing the spectra of cobaloxime and Co-MePy- α_3 C this can be seen by the subtle changes in the spectral fine structure around 3000 G.

3.1.3 Protein and cobalt quantification

In Section 2.2, the various colourimetric methods for quantification were described. For quantification of the protein in the final Co-MePy- α_3 C samples, the BCA-assay was used. For the cobalt quantification a mix of the PAR-assay and induced coupled plasma optical emission spectroscopy (ICP-OES) was used. Initially, the PAR-assay was used because it was a suitable option to perform without setting up external collaborations. The standard curves were first prepared with a range of concentrations of CoCl_2 , but it was

found that the concentration ratios of cobalt to protein were inconsistent (data not shown). To understand if there were any potential issues with the PAR-assay, the dichloro-cobaloxime ($[\text{Co}(\text{dmg})_2\text{Cl}_2]$) replaced CoCl_2 as the cobalt standard in the calibration curve, and found approximately a two-fold difference between the two (Figure 17).

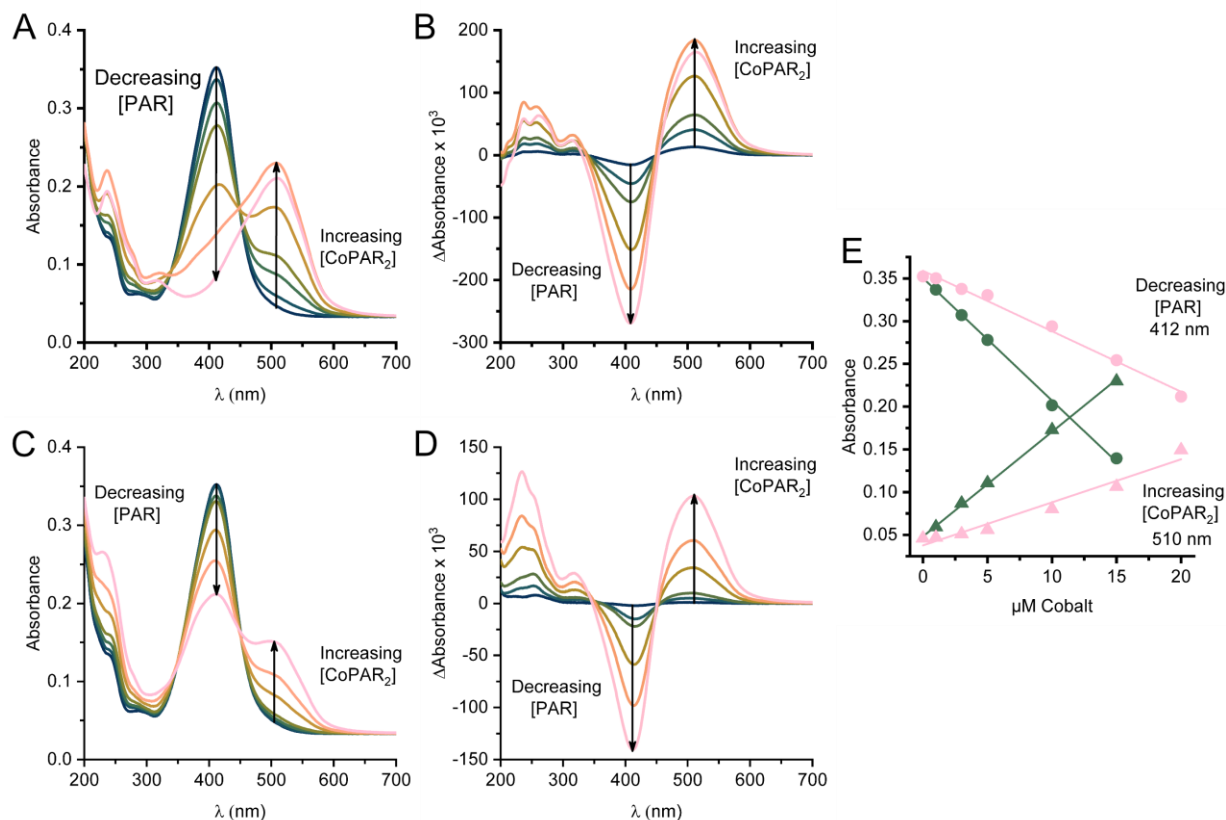


Figure 17: Spectra and difference spectra of PAR with Co from A, B: CoCl_2 and C, D: cobaloxime $[\text{Co}(\text{dmg})_2\text{Cl}_2]$. E: Absorbance at 412 (circles) and 510 (triangles) nm as a function of the concentrations of CoCl_2 (green) and $[\text{Co}(\text{dmg})_2\text{Cl}_2]$ (pink). Reprinted under CCBY3.0 license from paper I.(83)

To verify the concentrations already determined, the PAR-assay was compared with ICP-OES, and it was found that the PAR-assay (using CoCl_2) underestimated the cobalt concentration by 3.5-fold. Some data had already been collected with the affected batch, and so the used concentrations were corrected by this factor, the data affected was the photocatalysis-assays (Section 3.2.1).

Ideally, both the protein- and cobalt concentrations should have been determined by the same method, and several attempts at using ICP-OES to quantify the sulphur content (only one sulphur per protein molecule in $\alpha_3\text{C}$) in the samples were made. Due to the low sensitivity to sulphur by ICP-OES, it was never successful. Because the cobalt is the key component in the assay, it was determined that the most important things to consider when quantifying the protein and cobalt was finding a reliable cobalt concentration and estimating if there was an excess of protein or cobalt in the samples. Thus, it was decided that using ICP-OES for quantifying the cobalt together with the colourimetric BCA-assay for the protein concentration was suitable.

An excess of protein was desirable, because an excess of cobalt would indicate the presence of free cobaloxime not bound to the protein, which would affect the HER assay performed following the quantification. Therefore, using both colourimetry, for the protein concentration, and ICP-OES, for the cobalt concentration, was deemed acceptable, and the concentrations were determined for each batch of prepared $\text{Co-MePy-}\alpha_3\text{C}$ (Table 1). It was found that the coordination of cobaloxime to $\alpha_3\text{C}$ never formed 100% $\text{Co-MePy-}\alpha_3\text{C}$, and there was always some presence of excess 3-MePy- $\alpha_3\text{C}$.

In addition to the determination of the concentrations of each batch of $\text{Co-MePy-}\alpha_3\text{C}$ that was prepared, the concentrations of each individual HER assay sample was determined for the largest set of data produced for the paper was that using $[\text{Eu}(\text{EGTA})]^{2-}$ as a reductant (Section 3.2.2) (see table S2 in the SI of paper I), and the concentrations of evolved hydrogen was corrected by this concentration.

Table 1: Determined concentrations and cobalt:protein ratios for three batches of Co-MePy- α_3 C the ratio between them. Concentrations of cobalt was determined with ICP-OES (relative standard deviation, RSD, given) and the concentration of protein was determined by BCA-assay (R^2 value given). Adapted from paper I.(83)

Sample	[Co] (M)	[Co] RSD (%)	[3-MePy- α_3 C] (M)	Standard curve R^2	Co: α_3 C ratio
A	$3.53 \cdot 10^{-5}$	0.4	$5.31 \cdot 10^{-5}$	0.9999	1:1.50
B	$1.45 \cdot 10^{-4}$	0.9	$3.88 \cdot 10^{-4}$	0.9999	1:2.68
C	$5.76 \cdot 10^{-4}$	0.4	$6.89 \cdot 10^{-4}$	0.9999	1:1.20

3.1.4 CD spectroscopy

Co-MePy- α_3 C was further characterised by CD spectroscopy, where potential functionalisation-induced protein folding changes were measured. The α_3 – proteins are a family of *de novo* proteins with near-identical sequence, only differing in the central amino acid, which has been substituted to fulfil the needs of the various studies performed. The structure of α_3 W has been determined by NMR and has been found to be almost entirely helical (Figure 5 in Section 1.2.4). The CD spectra of α_3 C and α_3 W being nearly identical (Figure 18) and consistent with an α -helical structure (Figure 9B, Section 2.4) indicated that the helical content of α_3 C was identical to that of α_3 W. Further it suggested that the tertiary structure of α_3 C likely mimicked that of the other α_3 -proteins. By comparing the CD spectra of α_3 C and α_3 W with that of Co-MePy- α_3 C, a decrease in the features that are typically connected with helicity was detected for Co-MePy- α_3 C.

The CD spectra were normalised by both path length and concentration of chiral centres (equation 3), so the decrease in signal for Co-MePy- α_3 C relative to that of α_3 C cannot be attributed to a lower concentration of chiral centres. This drop in signal can only be attributed to an unfolding of circa 50% of the backbone for Co-MePy- α_3 C relative to α_3 W and α_3 C.

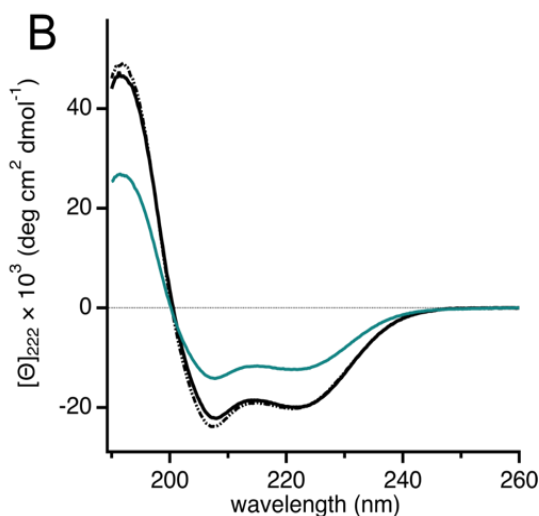


Figure 18: CD spectra of α_3 W (black dot-dash), α_3 C (solid black), and Co-MePy- α_3 C (teal). Reprinted under CCBY3.0 license from paper I.(83)

To gain more insight into this apparent folding difference, a denaturation study to find the free energy of unfolding for the respective peptides was performed. The denaturant urea was titrated into the protein sample, and the concentration of it was related to the spectral intensity at 222 nm, an α – helix fingerprint wavelength. As the helical folding decreases, the CD intensity at 222 nm is expected to decrease proportionally. This decrease was used to calculate the free energy of unfolding (Figure 19).

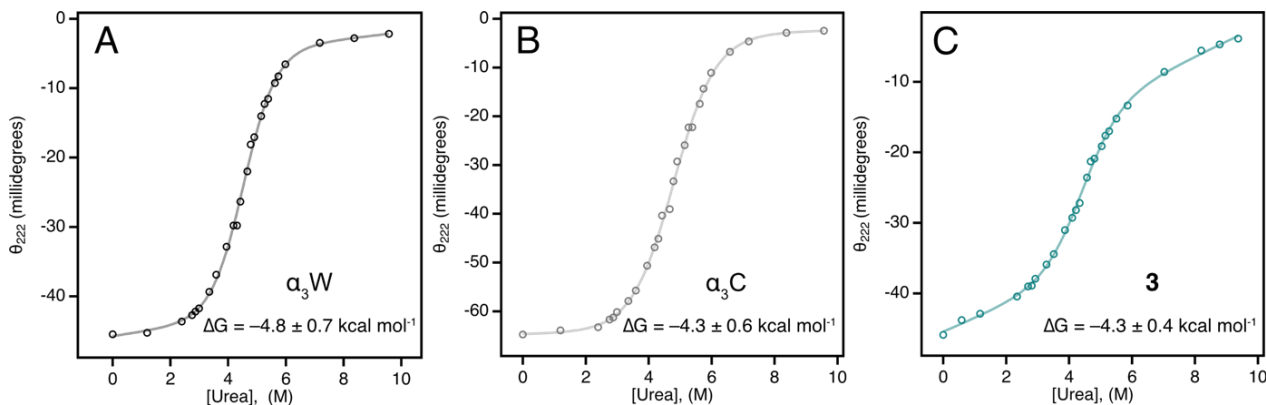


Figure 19: Urea titration graphs and calculated ΔG s of unfolding of A: α_3W , B: α_3C , C: Co-MePy- α_3C . Reprinted under CCBY3.0 license from paper I.(83)

The shape of the denaturation data took on a sigmoidal shape, indicating a transition from fully folded (has a CD-intensity at 222 nm) to unfolded (has no CD-intensity at 222 nm). The curves were very similar in shape for the control proteins α_3W and α_3C , but somewhat different for Co-MePy- α_3C . Already at the very lowest concentrations of urea Co-MePy- α_3C the signal at 222 nm decreased, indicating a partial unfolding of the protein, compared to α_3W and α_3C requiring urea concentrations above 2 M to start unfolding. This is consistent with the observations of the spectral differences between α_3C and Co-MePy- α_3C seen in Figure 18 above.

The sigmoidal fit for each curve yields the free energy (ΔG) of unfolding for the three complexes, which is nearly identical ($-4.8 \text{ kcal mol}^{-1}$ (α_3W) and $-4.3 \text{ kcal mol}^{-1}$ (α_3C and Co-MePy- α_3C)). This suggests that although the protein scaffold is partially unfolded in Co-MePy- α_3C , the helical portion is just as stable as that of α_3W and α_3C .

From what was found using CD – and EPR spectroscopy, it appeared that the protein scaffold partially unfolded to accommodate the cobaloxime, and that the cobaloxime was partially buried in the protein. A structural model of Co-MePy- α_3C was prepared using PyMOL by attaching a 3D molecular model of cobaloxime to the NMR-structure of α_3C -2-mercaptophenol (PDB: 2LXY). It showed the burial of the cobaloxime by the protein scaffold, where the cobaloxime slightly protrudes between helix 1 and 2 (Figure 20).

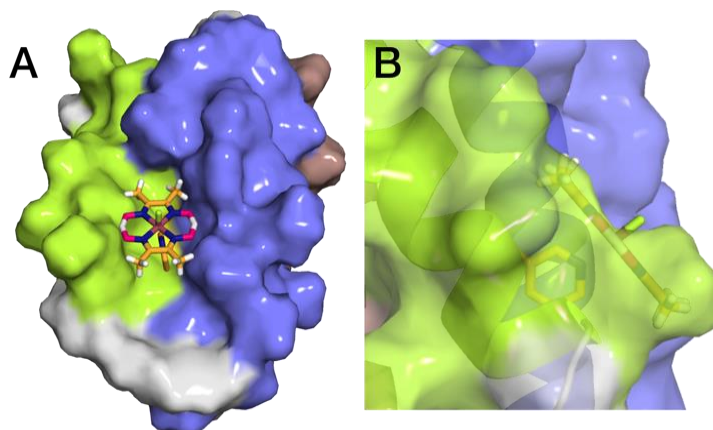


Figure 20: Surface model of Co-MePy- α_3C showing A: The face-on view of the cobaloxime situated between helix 1 (green) and helix 2 (blue), and B: A side view of the transparent surface model showing the depth of the cobaloxime inside the protein. Reprinted under CCBY3.0 license from paper I.(83)

3.1.5 Cyclic voltammograms of Co-MePy- α_3C and cobaloxime

CVs of Co-MePy- α_3C were collected using protein films adsorbed to a pyrolytic graphite edge working electrode surface which was prepared by sandpapering it to increase the available surface area. The film was then made by either dipping the electrode in the protein solution for 30-60 seconds, or by placing a

droplet on the surface of the electrode and allowing it to dry. CVs of cobaloxime were instead collected using solutions of cobaloxime (Figure 21).

When scanning in the cathodic direction (from 0.1 V vs NHE to -1.4 V vs NHE) both Co-MePy- α_3 C and cobaloxime gave rise to a reducing wave with a peak current at ca -0.9 V vs NHE and a catalytic wave with onset at ca -1 V vs NHE. For cobaloxime, the ca -0.9 V vs NHE peak presented with two small shoulders, however from preliminary experimentation it appears that it is not necessary that the shoulders are. The presence of them seems to be related to concentrations of anions which may be coordinated by the cobaloxime (data not shown here). When scanning back in the anodic direction both Co-MePy- α_3 C and cobaloxime gave rise to an oxidation peak (-0.3 V vs NHE for Co-MePy- α_3 C and -0.2 V vs NHE for cobaloxime). This general appearance is comparable to previously published CVs of cobaloximes in water, which further supports the formation of the one-pyridine axially ligated cobaloxime in the centre of Co-MePy- α_3 C.(36)

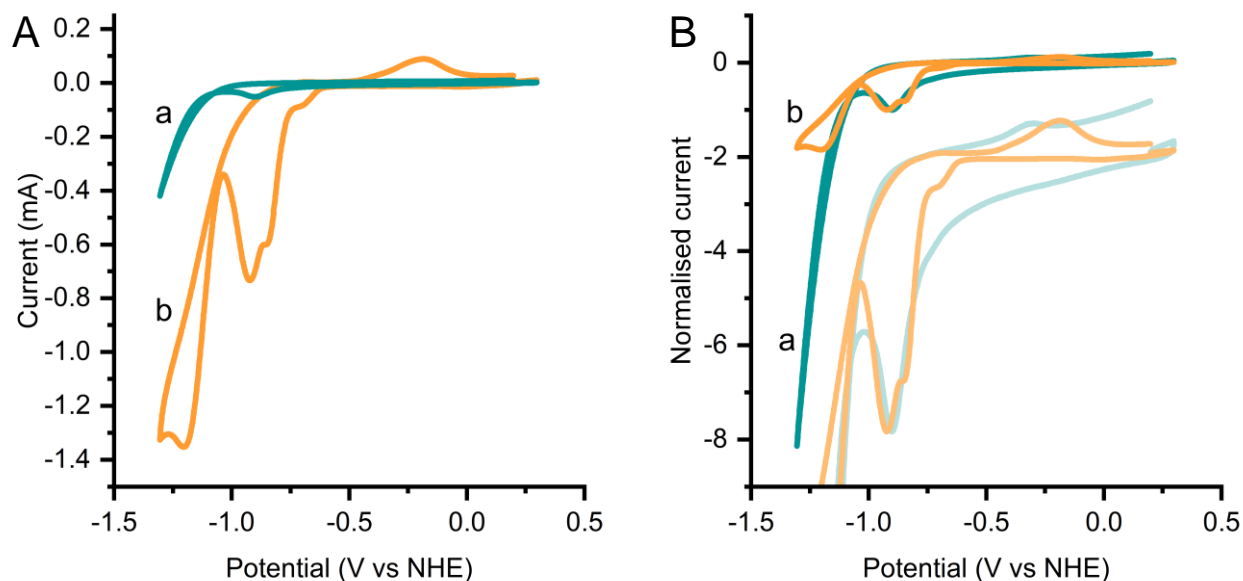


Figure 21: A: Example voltammograms of Co-MePy- α_3 C (a, teal) and cobaloxime (b, orange). B: Normalised voltammograms of Co-MePy- α_3 C (a, teal) and cobaloxime (b, orange). The fainter CVs are zoomed in on the normalised CVs a and b in this figure to emphasise the reducing and oxidising peak.

To account for the concentration differences between Co-MePy- α_3 C and cobaloxime to be able to compare the relative intensities of the voltammetric features, the CVs were normalised at the peak at ca -0.9 V vs NHE (Figure 21B). The normalisation was performed by dividing the CV with the absolute current at the peak potential, setting the ca -0.9 V vs NHE-peak to ca -1.

This normalisation revealed two things – that Co-MePy- α_3 C gave rise to a relatively larger catalytic current than cobaloxime, and a relatively smaller oxidation peak. However, because the CVs of the two were collected on different types of samples (protein film vs cobaloxime solution), it was not straightforward to compare the two directly. Co-MePy- α_3 C was adsorbed to the surface of the electrode, and cobaloxime was diffusing in solution. When diffusing, the catalyst molecules may collide with each other and react differently than when adsorbed to a surface, for example by different HER mechanisms or through degradation through aggregation into cobalt nanoparticles, which is a known degradation pathway for cobaloxime.(87)

A further discussion on the electrocatalytic behaviour of Co-MePy- α_3 C and cobaloxime can be found in Chapter 4, where preliminary analysis of the pH-dependence of the ca -0.9 V vs NHE-peak is discussed. For the purpose of the discussion in this chapter, these CVs have been used to aid in the characterisation of Co-MePy- α_3 C.

3.2 Co-MePy- α_3 C catalysis

The key interest in Co-MePy- α_3 C has been to understand if the catalytic function of the catalyst was impacted by the *de novo* protein framework, and if it was different from how it interplays with a natural protein. Previous work on cobaloxime-based ArMs showed at best approximately a doubling of TON using haem oxygenases as scaffolds, and at worst an almost halving of TON using myoglobin as a scaffold. (40) In those studies, the native haem was replaced by cobaloximes through histidine coordination. These proteins naturally bind a metal complex and hence may accommodate the catalyst more readily than the α_3 C. The studies of the haem proteins as cobaloxime-based ArMs did however not involve structural characterisation to reveal if the native protein structure was disrupted by cobaloxime binding. Additionally, histidine as an axial cobaloxime ligand is known to be detrimental to catalysis, whereas pyridines similar to the one used here is known to be beneficial for catalysis. (37) Using the *de novo* protein α_3 C allowed for the specific inclusion of a pyridine ligand for the cobaloxime, which may be beneficial for HER catalysis by the *de novo* metalloenzyme.

In the study discussed in this chapter, the hydrogen evolution was driven by two methods (photocatalysis and chemical reduction by $[\text{Eu}(\text{EGTA})]^{2-}$) and the produced hydrogen was probed with two methods.

In the *ex situ* quantification of H_2 , measured by gas chromatography, a set volume of headspace gas was taken out by Hamilton syringe from the reaction vial, and was injected into the gas chromatographer which quantify the amount of H_2 . The amount of H_2 was recalculated with a standard curve and corrected for the total headspace volume and the concentration of catalyst (resulting unit is $\mu\text{mol H}_2/\mu\text{mol catalyst}$). The reaction was left for several hours, after which the headspace H_2 was measured for an end-point assay.

In the *in situ* quantification of H_2 , measured by Clark-type microelectrode, the H_2 was measured continuously directly in the solution. The software automatically re-calculated the measured current to $\mu\text{M H}_2$, based on the collected standard curve of H_2 -concentration. The dissolved concentration of H_2 was corrected for the dissolved concentration of catalyst (resulting unit is $\mu\text{M H}_2/\mu\text{M catalyst}$). The experiment was left to run until a plateau was reached. The stagnation of catalysis may be for the following reasons – degradation of catalyst or depletion or degradation of the external reduction components (photosensitiser, electron donor or chemical reductant).

3.2.1 Catalysis by photosensation

Using a photocatalytic approach when studying a HEC is interesting for two reasons: (i) the potential required to reduce the catalyst can be reached, and (ii) it shows that photocatalysis is possible with the system in question, which poises it in the field as a candidate for future upscale photocatalytic systems for fuel production. Photocatalysis requires a photosensitiser (PS), a sacrificial electron donor (ED), and photons ($h\nu$), where the PS is used to convert the incoming light energy to an electron to reduce the catalyst. Upon illumination the PS is excited to PS^* , and this excited state can be reduced by an ED. The PS^- then collides with the catalyst, reducing it, and the catalyst can in turn reduce protons to form H_2 (Figure 22).

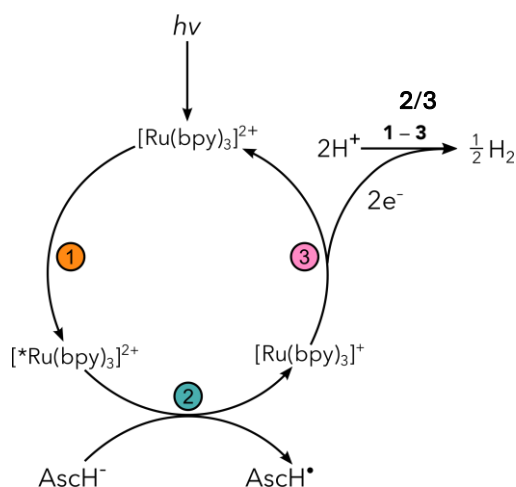


Figure 22: Photocatalytic reaction scheme of the PS $[\text{Ru}(\text{bpy})_3]^{2+}$, ED ascorbate (AscH^-) and Co-MePy- α_3 C (2) or cobaloxime (3). Reprinted from paper 1.(83)

Through this process, the ED cannot be regenerated, which is why it is referred to as sacrificial. It is important to note that a sacrificial ED may be a limiting component in a photocatalysis experiment such as this, as it can be depleted throughout the experiment. Here, the PS $[\text{Ru}(\text{bpy})_3]^{2+}$ and the ED ascorbic acid was used.

The PS is a light-sensitive molecule, which is the key property making it suitable to act as a PS. This might also make it sensitive to photodegradation, which can be lessened by filtering out higher energy wavelengths. For $[\text{Ru}(\text{bpy})_3]^{2+}$, filtering the light below 420 nm is suitable to hinder the photodegradation, as it has an absorbance peak at 450 nm allowing for excitation to $[\text{*Ru}(\text{bpy})_3]^{2+}$. An additional important consideration with this PS is that $[\text{*Ru}(\text{bpy})_3]^{2+}$ can be quenched by oxygen, hindering the generation of reducing equivalents available to the catalysts. Additionally, ascorbic acid can be oxidised by oxygen rendering it incapable of reducing the *PS. Therefore, all samples were prepared for photocatalysis by sparging with argon to remove dissolved oxygen. To ensure as consistent photon flux as possible, the distance between lamp and sample was measured with a ruler, and the light intensity at the sample was measured with a power sensor to be as close as possible each time.

The HER measured *in situ* with the Clark type electrode was used to calculate the TON and the hydrogen evolution rates at pH 6 (Figure 23A, Table 2). The initial HER-rate was essentially unchanged for cobaloxime and Co-MePy- $\alpha_3\text{C}$, whereas the TON was somewhat deteriorated for Co-MePy- $\alpha_3\text{C}$ relative to that of cobaloxime.

The *ex situ* quantification of H_2 (Figure 23 B) was measured by gas chromatography as an end-point assay. This was performed at several pH-values to find both the catalytic maxima and compare the catalytic function. The maxima for both cobaloxime and Co-MePy- $\alpha_3\text{C}$ were found to be pH 6.2.

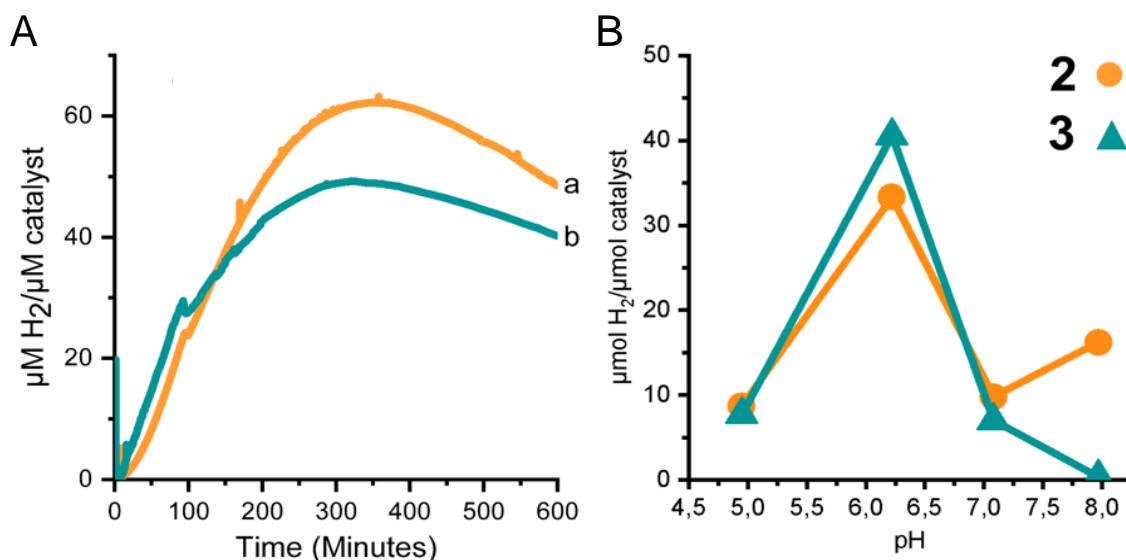


Figure 23: Hydrogen evolution by photosensitisation for cobaloxime (a/2) and Co-MePy- $\alpha_3\text{C}$ (b/3). A: Hydrogen measured by Clark-type electrode or B: Gas chromatography. Reprinted under CCBY3.0 license from paper I.(83)

Table 2: Turnover numbers (TON) and time passed in minutes (min) at the calculation point, and hydrogen evolution rates in $\mu\text{mol H}_2/\mu\text{mol catalyst}/\text{min}$ for cobaloxime and Co-MePy- $\alpha_3\text{C}$ calculated from *in situ* measurements of HER by photocatalysis. Adapted from paper I.(83)

TON (min) Cobaloxime	HER-rate Cobaloxime	TON (min) Co-MePy- $\alpha_3\text{C}$	HER-rate Co-MePy- $\alpha_3\text{C}$
62 (354)	0.32	49 (320)	0.35

3.2.2 Catalysis by chemical reduction

The reductant $[\text{Eu}(\text{EGTA})]^{2-}$ ($E^0_{[\text{Eu}(\text{EGTA})]^{2-}/[\text{Eu}(\text{EGTA})]^{1-}} = 0 \text{ V}$ vs standard hydrogen electrode (SHE) at pH 8) was used to provide reducing equivalents to cobaloxime and Co-MePy- $\alpha_3\text{C}$.(88) All HER-measurements with $[\text{Eu}(\text{EGTA})]^{2-}$ were performed with the Clark-type microelectrode. $[\text{Eu}(\text{EGTA})]^{2-}$ is sensitive to oxygen, so the preparations of both the reductant and the catalyst samples were done inside of a glovebox. Individual solutions of EuCl_2 and EGTA were prepared, and mixed stoichiometrically to form $[\text{Eu}(\text{EGTA})]^{2-}$ immediately before each measurement. Because $[\text{Eu}(\text{EGTA})]^{2-}$ quickly degrade preparing it fresh for each measurement is the simplest way to ensure that each sample is provided as similar concentrations of reductant as possible.

Quadruplicate measurements were performed for each condition: pH 7 and 8 for both cobaloxime and Co-MePy- $\alpha_3\text{C}$ (Figure 24), as it was not possible to form $[\text{Eu}(\text{EGTA})]^{2-}$ at pH 6 due to EGTA being insoluble at acidic pH. At least three measurements for each condition were used to calculate an average turnover number and rate for each (Figure 24, Table 3). The TON of Co-MePy- $\alpha_3\text{C}$ was mildly deteriorated in comparison with that of cobaloxime (ca 85% on average) whereas the HER-rate of Co-MePy- $\alpha_3\text{C}$ was only ca 41% of that of cobaloxime.

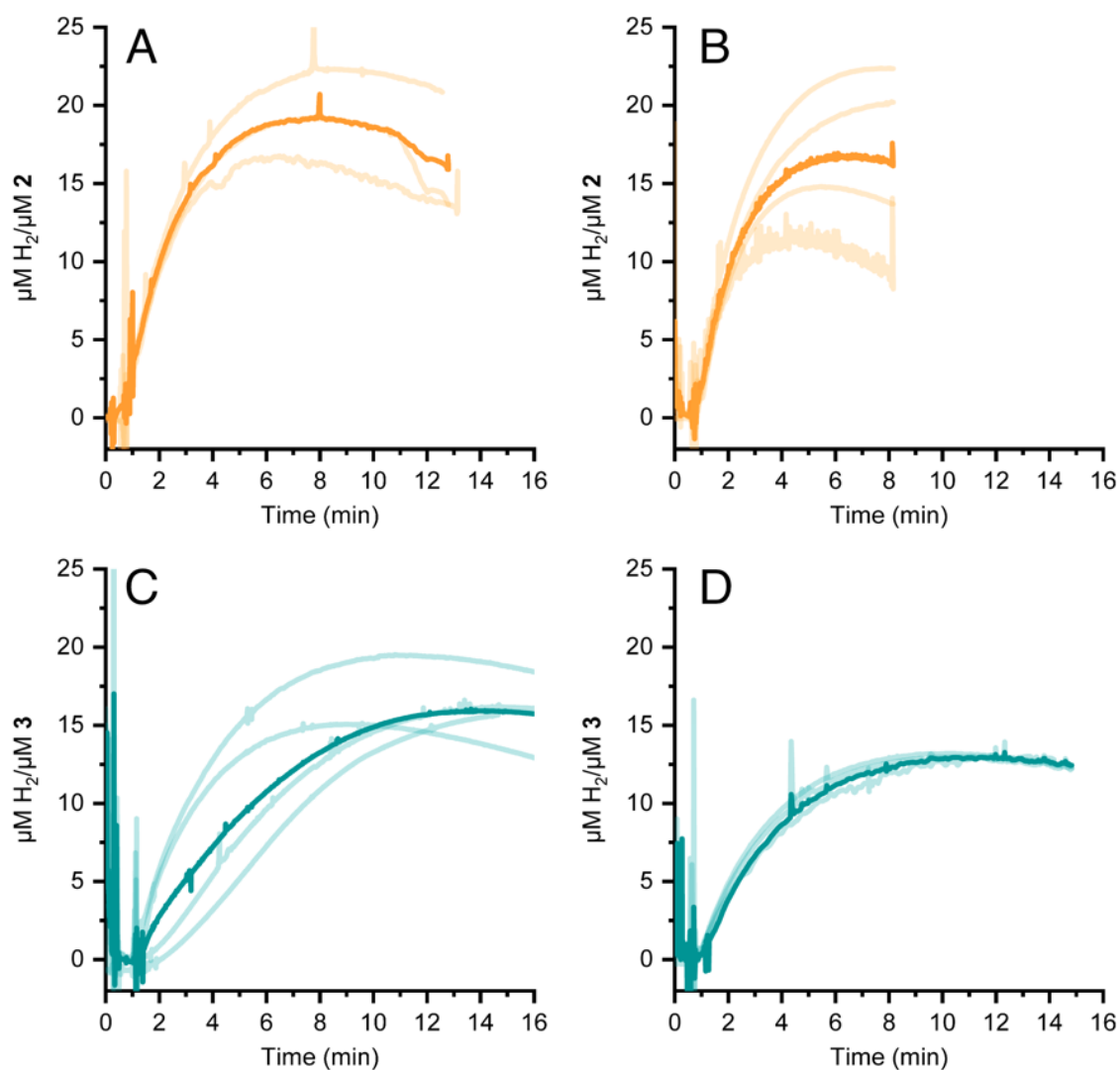


Figure 24: Hydrogen evolution by $[\text{Eu}(\text{EGTA})]^{2-}$ reduction from cobaloxime (2, A and B) and Co-MePy- $\alpha_3\text{C}$ (3, C and D) measured by Clark-type electrode at pH 7 (A, C) and 8 (B, D). The light traces are individual measurements, and the bold traces are the average of the light traces in each panel. Reprinted under CCBY3.0 license from paper I.(83)

Table 3: Turnover numbers (TON) (and time passed in minutes at the calculation point) and HER-rates for cobaloxime and Co-MePy- α_3 C at pH 7 and 8, when reducing equivalents were provided by [Eu(EGTA)]²⁻. Adapted from paper I.(83)

pH	TON (min) Cobaloxime	HER-rate Cobaloxime	TON (min) Co-MePy- α_3 C	HER-rate Co-MePy- α_3 C
7	18 \pm 3 (8)	6.0 \pm 0.5	16 \pm 2 (13)	2.5 \pm 0.5
8	16 \pm 5 (5)	7.8 \pm 0.9	13 \pm 0.2 (10)	3.2 \pm 0.3

3.2.3 Considerations when choosing a method for HER experiments

The two methods described in this thesis to generate reducing equivalents is the photoactivated PS-ED system and by using a strong chemical reducing agent. Both have their advantages and drawbacks, them and their effects on the experiments described in this chapter will be discussed in this section.

With a PS-ED strategy several components must act together to form the final reductant (PS⁻): the PS, the ED, and the photons. Perturbations in any of them can cause experimental difference which may make the interpretation of the results difficult, as an issue with reproducing the data may arise from several different sources of errors, it might not simply be due to the catalyst. The system may be affected by photo- and oxidative degradation. The photodegradation may be alleviate with a longpass-filter and the oxidative degradation may be alleviated by making the samples anoxic, as was done in this project.

The third component is the photons. Ideally, each sample should experience the same light level each time, but this can be complicated for several reasons. Physically positioning the light source and the samples identically each time can be challenging, but specially manufactured holders for constraining samples and holders can simplify this.

Additionally, a balance must be struck between a high enough concentration of PS to generate sufficient PS⁻ but avoiding significant inner filter effect. This effect refers to the removal of photons as they are absorbed by the PS, so that the whole sample does not experience the same light level. This can be somewhat alleviated by stirring and using reaction vessels with a low path length, but it is not always practical. Here, a moderate concentration of PS was used along with using a septum-sealed cuvette as the reaction vessel, for the experiments where the HER was measured *in situ*.

When the HER was quantified by GC it was done by hand-injecting a set volume of the headspace gas into the chromatographer. Removing headspace gas both changes the pressure, and risk affecting the gas composition by introducing air, in which the O₂ quench PS*. This risk is further amplified when performing repeated draws. Additionally, the vial must also be replaced in the light with the same precision as described above, to ensure a consistent photon flux. Therefore, all measurements of HER over time that were included here were performed with the Clark microelectrode, where the sample and the light is fixed and minimal contamination of the headspace is introduced. The drawback with this strategy is that only one measurement can be recorded at a time, whereas with the GC, several samples can be illuminated in parallel making the time to collect all repeats using Clark electrode very long.

Chemical reduction has its own issues, such as high sensitivity to atmospheric O₂, rapid degradation and low solubility at acidic pH. A mildly acidic pH was determined to be optimal for both Co-MePy- α_3 C and cobaloxime (Figure 23 B), and in contrast the PS-ED system described above is suitable down to pH 4.5. Comparing the results achieved with chemical reduction and with photosensitisation, the first apparent difference is the timescale. The reactions driven with [Eu(EGTA)]²⁻ level off after a few minutes, whereas with PS-ED, it takes five hours for the reaction to level off. This is most likely due to the degradation or consumption of [Eu(EGTA)]²⁻, as hydrogen can be produced with cobaloxime and Co-MePy- α_3 C for several hours, such as with photosensitisation. Using photosensitisation is therefore the useful option for investigating the longevity of the catalyst itself, however even there the ED is eventually consumed and must be replenished.

A final method which was not used here is bulk electrolysis, where the reducing equivalents are provided by an electrode rather than external reducing agents. An electrode is placed inside the sample, and a set potential (where catalysis is known to take place) is applied while stirring. The reaction proceeds until the substrate is consumed or the catalyst is degraded. In the case of proton reduction, the pH could potentially

be measured before and after to determine the consumption of substrate but necessitates a GC to relate to the change of pH and the resulting current. Bulk electrolysis was never employed here, as it requires a too high concentration of Co-MePy- α_3 C. This is also why all the voltammetry performed was using protein films, as only a small quantity of protein was required to produce them.

To conclude, both methods used here are useful for different reasons. Photosensitisation has many components which must be precisely prepared and performed to be reproducible, and it can be challenging to find which component is problematic if poor reproducibility is found. It however offers information regarding the catalyst longevity and is functional over a wider pH-range than the chemical reductant [Eu(EGTA)]²⁻. Using the chemical reductant instead gives shorter experimental times with fewer components which may degrade, allowing for simpler troubleshooting, if necessary, making it a practical strategy with a large sample volume. It however necessitates the use of a glovebox to exclude oxygen, and is only suitable at pH 7 or higher, but if this is accessible and acceptable, using [Eu(EGTA)]²⁻ to generate reducing equivalents is suitable and practical.

3.2.4 Discussion

The hydrogen evolution rates and TONs calculated for Co-MePy- α_3 C at pH 6, 7 and 8 were lower than for cobaloxime (Table 2 and Table 3). From the characterisation of Co-MePy- α_3 C it was found that the catalyst was likely partially enveloped by the protein scaffold, limiting access to substrate protons and collision with reductants. The cobaloxime in the reference samples were not sterically hindered, and had free access to substrate protonated water and collision with the reductants.

The α_3 X proteins were designed to be redox inert (see 1.3.1), and have previously been shown to have limited exposure to the bulk solvent.(89) This could limit both the electron transfer from reductants and proton transfer from the solvent to the cobaloxime buried in α_3 C. Introducing select mutations to allow for improved rates of electron- and proton transfer could be an interesting strategy to improve TOFs and TONs by Co-MePy- α_3 C. As discussed in Chapter 1, rational design of proteins is complex, but because it is well understood what amino acid residues may facilitate transfer of protons and/or electrons, performing that kind of modification may be a viable strategy to iterate on Co-MePy- α_3 C.

Previously three comparable cobaloxime-based artificial metalloenzymes have been published, by Bacchi et al.(40) Their ArMs were based on haem-binding proteins haem oxygenase (one mammalian from rat (Co-HOm) and one bacterial from *Corynebacterium diphtheriae* (Co-HOb)) and myoglobin (mammalian, from sperm whale (Co-MG)). Haem oxygenase is an enzyme which degrade haem through a process including both protonations and reductions. Substrate haem binds to the enzyme by histidine coordination to the central iron-ion. Myoglobin is not an enzyme, it is an oxygen carrier *via* its haem prosthetic group, coordinating to a histidine just as in haem oxygenase. For all three variants the natively haem coordinating histidine was used to coordinate cobaloxime, to form the artificial metalloenzymes. All three proteins used by Bacchi et al. natively contain pockets that can accommodate a metal complex in the size of haem, such as cobaloxime. Just as in the work presented in this thesis, Bacchi et al. used both photosensitisation and chemical reduction to characterise the HER by their artificial metalloenzymes. They observed that by photosensitisation the calculated TONs of the ArMs were mildly degraded (60-76% of that of cobaloxime), and in one case approximately doubled (184% of cobaloxime) and with chemical reduction they observed mildly improved TONs (128-248% with regard to cobaloxime) (Table 4). The improving effect on TON appears larger for the Co-HOs compared to the Co-MG. Comparing the TONs, it appears that Co-MePy- α_3 C is barely affected, with 80-90% of the TONs of cobaloxime.

Bacchi et al. do not present initial rates for their ArMs, so they cannot be compared with the ones calculated for Co-MePy- α_3 C, but a discussion of how TOFs compare between Co-MePy- α_3 C and cobaloxime is relevant because it can aid our understanding of how the catalyst is affected by the inclusion into a *de novo* protein. The rate of hydrogen evolution by Co-MePy- α_3 C (with chemical reduction) is only approximately 40% of the ones calculated for cobaloxime (Table 4). It is a notable decrease in rate upon introduction of the protein scaffold, the TONs were close to unchanged, whereas the rates were more than halved. Interestingly, when using photosensitisation, the relative TON was similar to when using chemical reduction (ca 80%), but the relative rate was nearly 100%.

Table 4: Table summarising TONs and TOFs from measurements with photocatalysis (PS) and chemical reduction (CR) for cobaloxime and Co-MePy- α_3 C presented in this thesis,(83) compared with TONs from measurements with PS and CR for cobaloxime and cobaloxime-based artificial metalloenzymes made with mammalian haem oxygenase (Co-HO-m), bacterial haem oxygenase (Co-HO-b) and myoglobin (Co-MG) published by Bacchi et al..(39,40) The relative TONs and TOFs for the *de novo* and artificial metalloenzymes are calculating by dividing the TONs/TOFs from the enzyme by the TON/TOF for the cobaloxime.

	Photosensitised			Chemically reduced		
	TON	TOF	Rel. TON/(TOF)	TON	TOF	Rel. TON/(TOF)
Berglund	pH 6			pH 7/8		
Cobaloxime	62	0.32		18/16	6.0/7.8	
Co-MePy- α_3 C	49	0.35	79%/(109%)	16/13	2.5/3.2	89%/81%/(42%/41%)
Bacchi	pH 7			pH 7		
Cobaloxime	8.3			2.5		
Co-HOm	6.3		76%/(-)	6.2		248%/(-)
Co-HOb	15.3		184%/(-)	5		200%/(-)
Co-MG	5		60%/(-)	3.2		128%/(-)

Both haem oxygenases and myoglobin must have channels to allow diffusion of solutes, like substrate, products and O₂. The substrate for a cobaloxime-based ArM is likely protonated water which is similar in size to an oxygen molecule and could potentially diffuse to the active site by the same channel that O₂ use (in the case of myoglobin). The haem oxygenases natively have a large substrate (haem) and product (biliverdin) which could explain why Co-HOm and Co-Hob were found to produce more H₂ than Co-MG.

In the first crystal structure of a native haem oxygenase several waters were co-crystallised in the active site, suggesting that water normally diffuses in and out of the active site. Haem oxygenase requires electron transfer to the active site, indicating that it harbours electron transferring functionalities, which may be why the haem oxygenase-based ArMs display the most improved HER for all the ArMs discussed here.(90)

In comparison, the *de novo* Co-MePy α_3 C does not contain any specifically designed structural features to accommodate a prosthetic group or efficient transport of electrons or substrate protons. The lack of proton- and electron channelling functionalities, and limited access to the bulk solvent in the core of the α_3 C scaffold is likely the reason why especially the rates of HER by Co-MePy- α_3 C are decrease compared to cobaloxime. This only was true for when chemical reduction was used, indicating that when photosensitisation was used the insulation of the cobaloxime active site in Co-MePy- α_3 C had a weaker effect on the HER than the rate of generation of PS⁻. The HER-rate was unchanged between cobaloxime and Co-MePy- α_3 C when it was photosensitised.

When chemical reduction was used, all reducing equivalents were provided immediately and do not need to be continuously generated as with photosensitisation, which as discussed in the previous section is affected by several factors. The only limiting factor was the concentration of reductant (here provided in excess with regard to catalysts) and the rate of diffusional collision between reductant and catalyst. This suggests that the rate of HER by Co-MePy- α_3 C with chemical reduction was limited by the presence of the protein scaffold, which do not provide any assistance in electron transfer to the active site.

Because limitation of hydrogen evolution in a cobaloxime-based ArM is not a general principle, as seen when comparing Co-MePy- α_3 C with the haem protein-based ArMs, it can be concluded that the lack of substrate access (both protons and electrons) is the key limiting factor. For Co-MePy- α_3 C both were limited. For Co-MG access to electrons was limited. For the Co-HOs neither were limited but rather assisted. From the TONs (by chemical reduction) by all the ArMs the trend can be followed, somewhat lowered for Co-MePy- α_3 C, somewhat increased for Co-MG and greatly increased for the Co-HOs.

The TONs and TOFs of HER by Co-MePy- α_3 C was shown to be decreased compared to those of cobaloxime, but observations in some of the experiments point toward that Co-MePy- α_3 C had improved catalyst longevity. In the end-point assay of the pH-maxima of Co-MePy- α_3 C and cobaloxime (Figure 23B), at pH 6, Co-MePy- α_3 C produced slightly more H₂ than cobaloxime. In the *in situ* photocatalytic hydrogen evolution experiment (Figure 23A) it appears that the slope-off of HER by Co-MePy- α_3 C after the peak hydrogen concentration was somewhat less steep than that of cobaloxime. In the chemical reduction experiments (Figure 24), it appears that Co-MePy- α_3 C HER remains plateaued for a longer time than that of cobaloxime, which slope off earlier. The longevity of the two catalysts has not been compared in depth, but

initial speculation on it indicates that binding to the protein might somewhat improve the stability, and hence longevity of cobaloxime.

3.3 Summary and conclusions

The artificial metalloenzyme Co-MePy- α_3 C joins together the protein α_3 C and the catalyst cobaloxime to investigate the role of proteins as the secondary coordination environment. The protein portion of Co-MePy- α_3 C has been found to be structurally distinct from the starting protein but maintain its structural robustness.

The initial rate of HER by Co-MePy- α_3 C compared to cobaloxime was found to be approximately 40% of that of cobaloxime (using chemical reduction). It can likely be explained by that the protein scaffold limited the access to the bulk solvent, slowing the rate of protonation of the active site. The protein may also have acted as an insulator, slowing the rate of electron transfer from reductants to the active site.

At present, the structural effect on α_3 C by the chemical modification with 3-MePy and cobaloxime is only partially understood. A structural NMR study of Co-MePy- α_3 C could give insight into precisely what parts of the protein scaffold was unfolded in comparison with unmodified α_3 C. Cobalt however may be problematic – paramagnetic species make interpretation of NMR data complex because they give rise to spectral shifts and decreased relaxation times(91). The unique NMR-features arising due to the presence of a paramagnetic species may also facilitate certain types of analyses, but complete structural analysis may not be possible.

Co²⁺ is paramagnetic, and Co³⁺ may be paramagnetic, if in the high-spin state, or diamagnetic in the low-spin state. At cryo-temperatures it is in the low spin state, as demonstrated here by EPR-spectroscopy, but it does not necessitate it being low spin at room temperature. If the Co³⁺ in Co-MePy- α_3 C is shown to be in the paramagnetic high spin state, complicating NMR-analysis, it could potentially be replaced with a non-paramagnetic metal such as Zn²⁺. A structural NMR study could be a possible next step for further characterising Co-MePy- α_3 C.

In comparing the different methods used for determination of hydrogen evolution, there is no universal choice when deciding how to study a HEC. Using a PS-ED system involves many variable components that may have a large effect on the outcome of the experiment. Using a chemical reductant, while less components hinges on the stability of the reductant, is sensitive to O₂ contamination and degrades rapidly and thus need to be prepared fresh for each separate measurement. In addition, the reductant used here was only suitable at neutral and above pH, making it unsuitable for use at the pH-maxima (6.2) for Co-MePy- α_3 C and cobaloxime. Both these methods also must employ strong enough reductants to reduce the catalyst efficiently. Using both methods and complimentary reductants to piece together the puzzle, like shown here, may at present be the most suitable method.

The fully *de novo* ArM Co-MePy- α_3 C shows that a completely human-designed ArM for hydrogen evolution is possible, but the lack of designated catalysis environment and adjacent proton- and electron channelling functions yield a decreased HER compared to cobaloxime. The study described in this chapter showcases the challenges of performing rational enzyme design. With the use of a redox-inert scaffold such as α_3 C opens the stage for future work in improving the catalytic function of ArMs such as Co-MePy- α_3 C with point mutations that can act as proton – and electron relays. In conclusion, the work presented in paper I and that has been discussed in this chapter has addressed question 1, 2 and 4 outlined in Section 1.1 Aims.

4 Electrocatalytic hydrogen evolution by Co-MePy- α_3 C

In Chapter 3 of this thesis the CVs of cobaloxime and Co-MePy- α_3 C were presented. There they were used as a tool for characterisation of Co-MePy- α_3 C to make a comparison of the redox properties between it and cobaloxime. In this chapter, the CVs of Co-MePy- α_3 C and cobaloxime will be used for a preliminary discussion on the following questions:

- What is the electrocatalytic behaviour of Co-MePy- α_3 C and is it different from that of cobaloxime? Is it consistent with what has been previously reported?
- What is the rate constant for electrocatalytic HER by Co-MePy- α_3 C and is it different from that of cobaloxime?

To understand the electrocatalytic behaviour of Co-MePy- α_3 C and how it compares with that of cobaloxime will assist in understanding how the catalyst is affected by binding to the protein. Several mechanisms for electrocatalytic HER by cobaloxime have been previously suggested, and they can be used as a starting point for the discussion regarding the electrocatalytic behaviour of Co-MePy- α_3 C. It is relevant to understand which mechanism is probable to be dominating under the experimental conditions, as it can help guide future experiments and analysis, particularly the calculations of TOFs by foot of the wave analysis (FOWA). FOWA is the analysis of the foot of the catalytic wave to calculate the TOF, and it is done because at this early part of the electrocatalysis the interfering effect on the catalytic current from catalyst degradation and substrate depletion is minimised.⁽⁹²⁾ The interpretation of the FOWA can be different depending on the dominant mechanism giving rise to the voltammetric wave that is being studied.⁽⁹³⁾

The mechanism of electrocatalysis of HER by cobaloximes have not been widely studied in aqueous systems, and so it is of interest to understand if the previous conclusions regarding it based on studies in non-aqueous systems remain applicable. Additionally, it is interesting to understand if the protein scaffold affects the dominant mechanism of HER by cobaloxime, as it may help guide future *de novo* enzyme design.

The TOFs of HER by Co-MePy- α_3 C were calculated from experiments where secondary reductants ($[\text{Ru}(\text{bpy})_3]^{2+}$ and $[\text{Eu}(\text{EGTA})]^{2-}$) were used to supply reducing equivalents. The analysis of the TOFs calculated using photosensitisation suggest that they may be limited by the rate of formation of $[\text{Ru}(\text{bpy})_3]^{1+}$, the form of the PS which reduces the cobaloxime. It is possible that the rate of electron transfer from $[\text{Eu}(\text{EGTA})]^{2-}$ may also affect the TOF for HER by Co-MePy- α_3 C. Calculating the TOF from CVs using FOWA excludes these effects, and may better reflect the effect of the protein scaffold on the catalytic behaviour of cobaloxime.

The discussion in this chapter is based on the analysis of CVs of Co-MePy- α_3 C and cobaloxime. All CVs discussed here are collected with a three-electrode setup using a sandpapered pyrolytic graphite edge working electrode, a platinum rod counter electrode and a Ag/AgCl reference electrode. Unless otherwise stated, the CVs were collected in 100 mM 2-(N-morpholino)ethanesulfonic acid (MES), 100 mM 3-(N-morpholino)propanesulfonic acid (MOPS), 75 mM KCl, with the pH titrated using HCl and KOH. CVs of cobaloxime were collected on solutions of 0.99 mM cobaloxime, and the CVs of Co-MePy- α_3 C were collected of protein films. The films were prepared by submerging the freshly sandpapered and subsequently rinsed working electrode into a 75 μM solution of Co-MePy- α_3 C for at least 30 seconds. This is followed by wiping off droplets of samples solution from the electrode casing and subsequent drying the surface with a flow of $\text{N}_{2(\text{g})}$.

The voltammograms show three major features, and to support the discussion in the chapter the peaks will be named as follows: the reductive wave, E_{red} (ca -0.9 V vs NHE in the cathodic direction), the catalytic wave, E_{cat} (onset at ca -1 V vs NHE in the cathodic direction) and the oxidative wave, E_{ox} (ca -0.3 V vs NHE in the anodic direction) (Figure 25A).

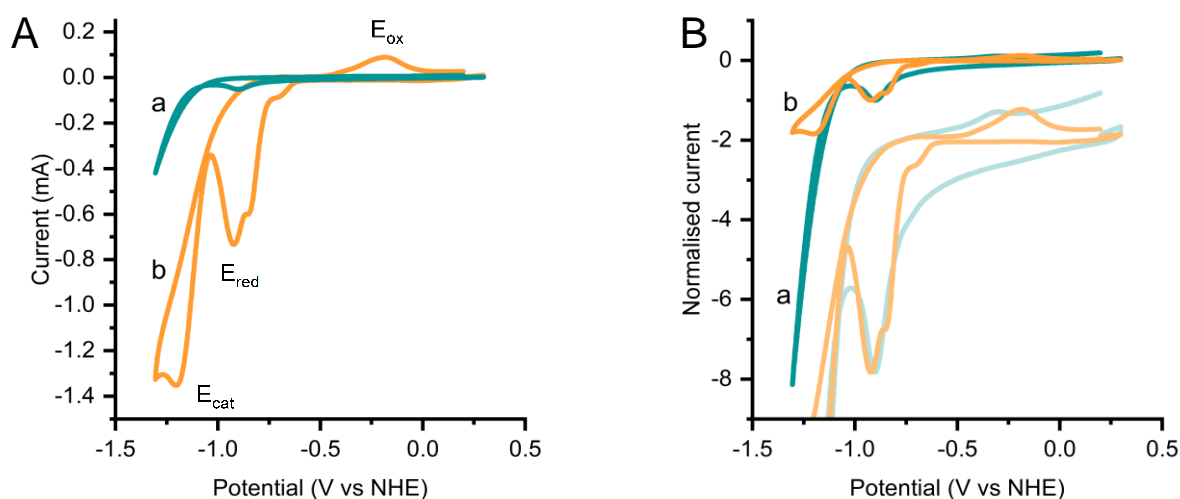


Figure 25: A: Example voltammograms of Co-MePy- α_3 C (a, teal) and cobaloxime (b, orange). B: Normalised voltammograms of Co-MePy- α_3 C (a, teal) and cobaloxime (b, orange). The fainter CVs are zoomed in on the normalised CVs a and b in this figure to emphasise E_{red} and E_{ox} .

To compare the two CVs more closely, they were normalised by setting the current at $E_{\text{red}} = -1$ (Figure 25B). Because E_{red} likely arise due to the one electron reduction of Co(II) to Co(I) (see Section 4.1), normalising the current at this peak potential to -1 allows for the comparison of the magnitude of current at E_{cat} and E_{ox} despite the concentration differences of Co-MePy- α_3 C and cobaloxime. The normalised CVs show that the peak- and onset potentials of E_{red} are near coincident for cobaloxime and Co-MePy- α_3 C. The onset of E_{cat} is also near coincident for both catalysts, but the relative current at E_{cat} appears larger for Co-MePy- α_3 C than for cobaloxime. The normalised CV also show that the current and peak potential of E_{ox} is different between cobaloxime and Co-MePy- α_3 C, the current is smaller and the peak is shifted ca 100 mV more cathodic for Co-MePy- α_3 C relative to that of cobaloxime.

The behaviour of E_{red} is what will be the focus of this chapter, as it is with the existing data the voltametric feature that can give most insight into the electrocatalytic mechanism for HER by Co-MePy- α_3 C. It is of interest to investigate if the electrocatalytic behaviour of Co-MePy- α_3 C is consistent with that previously suggested for cobaloximes. Two main types of mechanisms have been suggested for cobaloximes: monometallic (or heterolytic) mechanisms where the full mechanism takes place on one cobaloxime molecule, and bimetallic (or homolytic) mechanism where two cobaloximes react together to eliminate an H_2 . The bimetallic mechanisms are unlikely for Co-MePy- α_3 C for because the cobaloxime in Co-MePy- α_3 C is buried in the protein and will likely not be able to directly react with another Co-MePy- α_3 C. Additionally, in the voltammetric studies Co-MePy- α_3 C was adsorbed to the surface of the electrode disabling it from diffusing and colliding with another Co-MePy- α_3 C.

Many intermediates have been suggested for monometallic HER mechanisms by cobaloximes, and a consensus mechanism has not been identified. To simplify the discussion about these intermediates the cobaloxime structure has been simplified to $[\text{Co}(a)(\text{L})]^b$, where Co is the cobalt ion, L represents the equatorial ligand (dimethylglyoximes, or in one literature case, diamine-dioxime, which will be described below), a is the oxidation state of the cobalt ion and b is the overall charge of the complex. Although the cobaloxime resting state is typically $[\text{Co}(\text{III})(\text{L})]$, the $[\text{Co}(\text{II})(\text{L})]$ -state is most often considered the starting point in the proposed mechanisms, and will therefore be considered the same here, except for when otherwise stated.

The intermediates can be divided into cobalt hydride-intermediates ($[\text{Co}(a)\text{-H}(\text{L})]$) and protonated ligand intermediates ($[\text{Co}(a)(\text{LH})]$). The intermediates can also be cobalt hydrides with protonated ligands ($[\text{Co}(a)\text{-H}(\text{LH})]$). Most of the studies on the cobaloxime mechanisms have been performed in organic solvents, both experimentally and by calculation, some of them will be discussed here to provide a framework to analyse the data in this chapter along with a recent study performed using water.

As the result of an experimental study on cobaloxime electrocatalysis by Rountree et al. (2016) it was proposed that cobaloxime performs HER by an *ECEC* mechanism – a reduction (*E*) followed by a protonation (*C*, for chemical step) followed by another reduction and protonation (Figure 26A).(94) This

mechanism was proposed following the measurement of the rate constants for the two *C*-steps in the electrocatalytic HER.

The *ECEC* mechanism suggested by Rountree et al. had been suggested previously by Baffert et al. (2007), when using an intermediately strong acid as the proton source.(95) In addition Baffert et al. also suggested two other mechanisms, depending on which acid strength that was used: with a weaker acid an *EECC* mechanism (Figure 26B), and with a stronger acid an *ECC(E)* (Figure 26C) mechanism. In the *ECC(E)* mechanism the (*E*) is not a step in the HER, but necessary to regenerate the starting catalyst.

A computational analysis of cobalt(diimine-dioxime) catalysts was presented by Bhattacharjee et al. (2013) which is structurally very close to cobaloxime (Figure 27).(96) It was explored which mechanistic steps were energetically favourable in organic media with three differently strong acids and found the *ECEC* mechanism favourable even with the strongest acid. In the same study the possibility of the involvement of protonation of the dioxime was also explored, proposing an *ECCE* mechanism with ligand protonated intermediates to be energetically favourable (Figure 26D), with two possible ways for H₂-elimination to occur.

A	Baffert et al. (2007) (Intermediate acid) Bhattacharjee et al. (2013) (Co-H mechanism) Rountree et al. (2016)	$[\text{Co(II)}(\text{L})] + e^- \xrightarrow{\text{E}} [\text{Co(I)}(\text{L})]^- + \text{H}^+ \xrightarrow{\text{C}} [\text{Co(III)}-\text{H}(\text{L})] + e^- \xrightarrow{\text{E}} [\text{Co(II)}-\text{H}(\text{L})]^- + \text{H}^+ \xrightarrow{\text{C}} [\text{Co(II)}(\text{L})] + \text{H}_2$
B	Baffert et al. (2007) (Weak acid)	$[\text{Co(II)}(\text{L})] + e^- \xrightarrow{\text{E}} [\text{Co(I)}(\text{L})]^- + e^- \xrightarrow{\text{E}} [\text{Co(L)}]^{2-} + \text{H}^+ \xrightarrow{\text{C}} [\text{Co(I)}-\text{H}(\text{L})]^- + \text{H}^+ \xrightarrow{\text{C}} [\text{Co(II)}(\text{L})] + \text{H}_2$
C	Baffert et al. (2007) (Strong acid)	$[\text{Co(II)}(\text{L})] + e^- \xrightarrow{\text{E}} [\text{Co(I)}(\text{L})]^- + \text{H}^+ \xrightarrow{\text{C}} [\text{Co(III)}-\text{H}(\text{L})] + e^- \xrightarrow{\text{E}} [\text{Co(III)}-\text{H}(\text{L})]^+ + \text{H}^+ \xrightarrow{\text{C}} [\text{Co(II)}(\text{L})] + \text{H}_2$
D	Bhattacharjee et al. (2013) (Protonated ligand mech.)	$[\text{Co(II)}(\text{L})] + e^- \xrightarrow{\text{E}} [\text{Co(I)}(\text{L})]^- + \text{H}^+ \xrightarrow{\text{C}} [\text{Co(I)}(\text{LH})] + \text{H}^+ \xrightarrow{\text{C}} [\text{Co(III)}-\text{H}(\text{LH})]^+ + e^- \xrightarrow{\text{E}} [\text{Co(II)}-\text{H}(\text{LH})] \begin{cases} \xrightarrow{\text{H}^+} [\text{Co(II)}-\text{H}_2(\text{L})] \rightarrow [\text{Co(II)}(\text{L})] + \text{H}_2 \\ \rightarrow [\text{Co(II)}(\text{LH})]^- + \text{H}_2 \rightarrow [\text{Co(II)}(\text{L})] + \text{H}^+ \end{cases}$

Figure 26: Overview of mechanisms for electrocatalytic HER by cobaloxime proposed by Rountree et al. (A), Baffert et al. (A-C) and Bhattacharjee et al. (A, D).

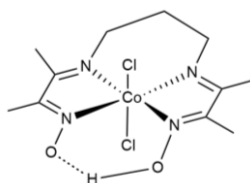


Figure 27: Structure of Co(diimine-dioxime)

These studies by Rountree et al., Baffert et al. and Bhattacharjee et al. were performed in non-aqueous solvents, with organic acids of different strengths as proton sources, whereas in this thesis water was used as a solvent. It cannot be assumed that the catalytic properties of cobaloximes are the same in aqueous and non-aqueous solvents, and acid strength has less of a meaning in a buffered aqueous system where the proton donor is a protonated water rather than the acid itself. These studies are still important to consider because the literature on electrocatalytic mechanisms for HER by cobaloxime is limited.

A recent study of the mechanism of electrocatalytic HER by some cobaloximes in water was presented by Dolui et al. (2019), in which the axial pyridine of the cobaloximes they study was modified to include proton relaying functionalities.(36) The CVs observed are similar to those presented here, with waves with shapes similar to E_{red} and E_{cat} . The manner in which CVs were scanned does not however reveal if a peak similar to E_{ox} was present.

Dolui et al. proposed that two different mechanisms of electrocatalytic HER occurred in their experiments(at neutral pH). At E_{red} a *CEC+E* mechanism (Figure 28E) and at E_{cat} a *CCEE* mechanism (Figure 28F), both involving glyoxime-protonated intermediates.

E	Dolui et al. (2019) (Co ^{II} -centric mechanism)	$\begin{array}{c} \downarrow \\ \text{[Co(II)(L)]} + \text{H}^+ \xrightarrow{\text{C}} \text{[Co(II)(LH)]}^+ + \text{e}^- \xrightarrow{\text{E}} \text{[Co(I)(LH)]} + \text{H}^+ + \text{e}^- \xrightarrow{\text{C+E}} \text{[Co(II)-H(LH)]} \rightarrow \text{[Co(II)(L)]} + \text{H}_2 \end{array}$
F	Dolui et al. (2019) (Co ^I -centric mechanism)	$\begin{array}{c} \downarrow \\ \text{[Co(I)(L)]}^- + \text{H}^+ \xrightarrow{\text{C}} \text{[Co(I)(LH)]} + \text{H}^+ \xrightarrow{\text{C}} \text{[Co(III)-H(LH)]}^+ + 2\text{e}^- \xrightarrow{\text{EE}} \text{[Co(I)(L)]}^- + \text{H}_2 \end{array}$

Figure 28: The two mechanisms for electrocatalytic HER proposed by Dolui et al. E: The Co[II]-centric mechanisms proposed to take place at E_{red} . F: The Co[I]-centric mechanism proposed to take place at E_{cat} .

It was reported that hydrogen evolved with 62-100% current efficiency in bulk electrolysis at E_{red} , hence they argue that a separate HER-process is taking place at this potential. Because the axial ligands in the systems used in their study were modified to provide a proton-channelling effect, it is likely that a ligand protonated intermediate was present during the catalytic turnover. One of the steps in the CCEE-mechanism proposed by Dolui et al. is the protonation of $[\text{Co(I)(LH)}]$ to $[\text{Co(I)-H(LH)}]^+$, which was calculated to be energetically disfavoured by Baffert et al. (in organic solvent), possibly except for when using the strongest acid (resulting in a free energy of -0.1 kcal/mol at best). Again, the concept of acid strength is less relevant in buffered water, instead the concentration of protons must be considered as that is what affects the equilibrium of protonation of intermediates. At pH 7 the concentration of H_3O^+ is 10^{-7} M, meaning that the concentration of protons is lower than typical experimental conditions (in this thesis the lowest used concentrations were in the order of magnitude of 10^{-6} M, meaning at least a 10-fold excess of catalyst to protonated water. This shifts the equilibrium to be less protonated catalyst, and with a process having been, computationally, shown to be energetically unfavoured, possibly makes the formation of the $[\text{Co(III)-H(LH)}]^+$ suggested in mechanism F questionable.

One of the main arguments by Dolui et al. that the mechanism taking place in E_{cat} does not involve a Co(II)-intermediate, for example like mechanism A (Figure 26), is that during bulk electrolysis no Co(II) can be observed spectroscopically. However, the intermediates during catalysis should not accumulate, and so the absence of Co(II) cannot rule out that it is not present during turnover. The spectroscopic signal of Co(II) was however observed to remain at E_{red} , which is inconsistent with a reduction of Co(II). Coupled with the observed hydrogen evolution at E_{red} lead to the proposal of a Co(II)-centred HER-mechanism taking place at this potential. In mechanism E (Figure 28) all intermediates except one is a Co(II) intermediate, making it more plausible that a spectroscopically detectable concentration of Co(II)-species was present at E_{red} .

Mechanism A, proposed by Baffert et al., Bhattacharjee et al. and Rountree et al. will be used. It has been suggested on both experimental and computational basis, and has wide precedence in literature. No experiments have been performed to rule out mechanisms E and F (Figure 28) suggested by Dolui et al., but what that may look like will be discussed briefly below.

4.1 Analysis of the electrocatalytic behaviour of Co-MePy- $\alpha_3\text{C}$

As the HER process is the reduction of two protons to form hydrogen, examining if the peak potential of E_{red} is pH-dependent can give insight into which mechanistic step corresponds to the process that gives rise to current at E_{red} , and if it involves one or more protons. As was described in Chapter 2, the voltammetric pH-dependence is found by calculating the slope (k) of the linear equation ($y = kx + m$) between the pH (x) and the peak potential (y). A redox-event with a pH-dependence of ca. -59 mV/pH correspond to a one proton per one electron process, ca -29.5 mV/pH to a one proton per two electrons process and ca -118 mV/pH to a two protons per one electron process. If the process does not involve a protonation, the slope is expected to be 0 mV/pH. Additionally, only mechanistic steps that involve a reduction or oxidation are visible in the CV, so a mechanistic step that involves a protonation without a reduction cannot be observed by voltammetry. Finally, reductions that yield the catalytically active form of the catalyst result in a catalytic wave in the presence of substrate.

The pH-dependence of the peak potential at E_{red} for Co-MePy- $\alpha_3\text{C}$ and cobaloxime was -57.9 mV/pH and -60.7 mV/pH, respectively (Figure 29, CVs are zoomed in to emphasise E_{red} , full CVs are shown in appendix 2). For Co-MePy- $\alpha_3\text{C}$ two measurements were collected for pH 5.5, 6 and 7.9, and one for pH 7 (Figure 29A for zoomed in CVs, Figure for full CVs), for cobaloxime three measurements were collected for all pH-values (Figure 29B for zoomed in CVs, FigureA2 for full CVs). For Co-MePy- $\alpha_3\text{C}$ both peak potential values were plotted, but the displayed line is calculated on the average of the two (Figure 29C). For cobaloxime the average peak potentials at E_{red} were plotted, and the line was fit to those averages (Figure 29D).

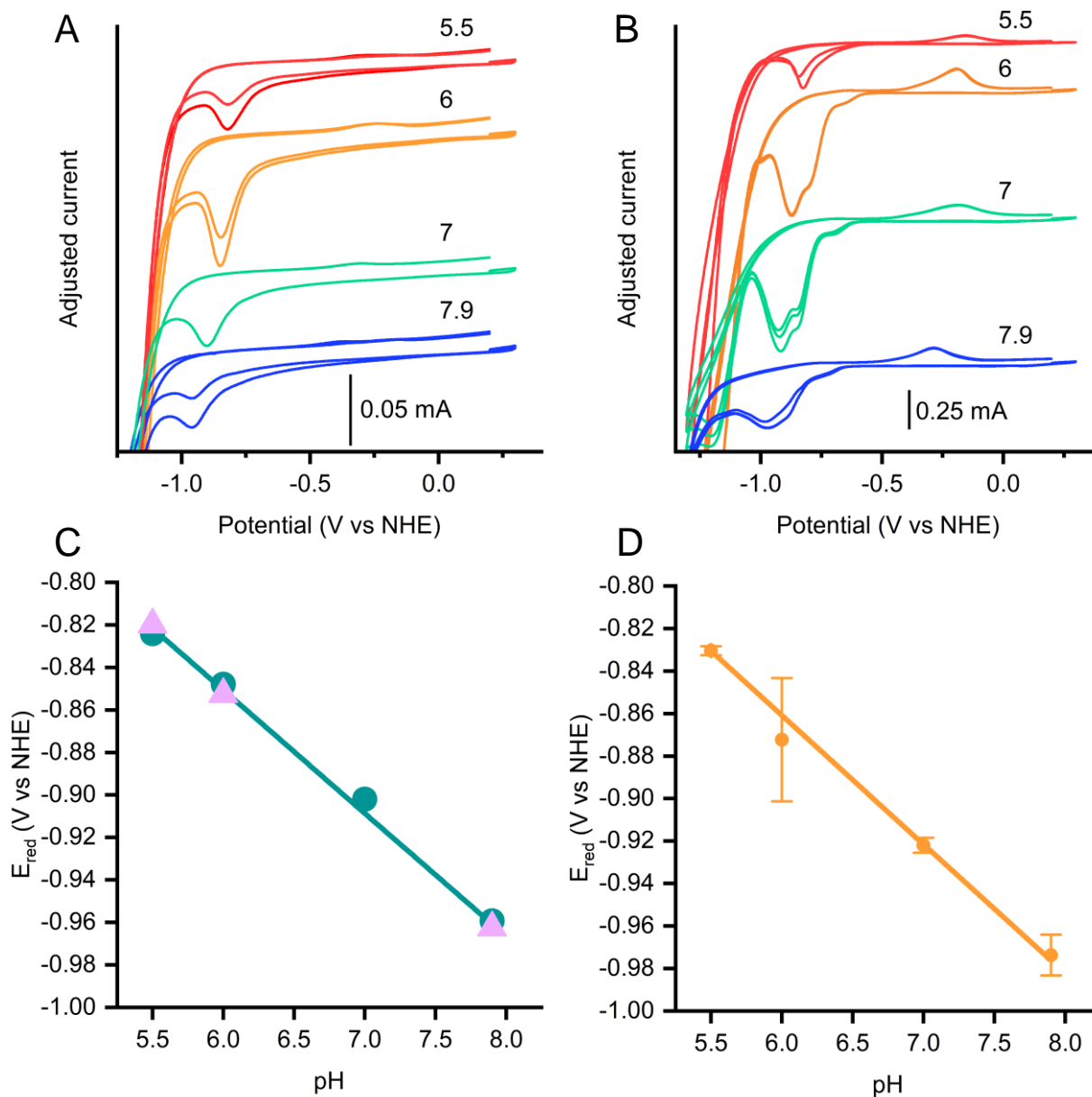


Figure 29: Zoomed in CVs of E_{red} at pH 5.5-7.9 for Co-MePy- $\alpha_3\text{C}$ (A, two individual scans for pH 5.5, 6 and 7.9, one for 7) and cobaloxime (B, three individual scans for each pH), and the pH dependence of E_{red} of Co-MePy- $\alpha_3\text{C}$ (C) and cobaloxime (D).

The pH-dependencies being consistent with a one proton per one electron process suggests that the current at E_{red} arises from an *EC*-process. Because it is known from EPR-experiments (Chapter 3) that the resting redox state of the cobalt ion in Co-MePy- $\alpha_3\text{C}$ and cobaloxime is $[\text{Co(III)}(\text{L})]$, it is tempting to assume that this reduction corresponds to the $[\text{Co(III)}(\text{L})]/[\text{Co(II)}(\text{L})]$ reduction coupled to a protonation of the reduced catalyst. This process is however known from previous studies on the electrocatalytic behaviour of cobaloxime to occur close to 0 V vs NHE, where it has been reported as a broad wave.⁽³⁶⁾ A similar broad wave has been observed for cobaloxime, consistent with what has been shown previously (Figure A3 in Appendix 2). The reduction from $[\text{Co(III)}(\text{L})]$ to $[\text{Co(II)}(\text{L})]$ does not involve a protonation and so would

not be pH-dependent. That, coupled with the elevated potential of E_{red} relative to what has been previously observed for $[\text{Co(III)(L)}]/[\text{Co(II)(L)}]$ make it unlikely to arise because of this reduction, but rather $[\text{Co(II)(L)}]/[\text{Co(I)(L)}]$ coupled to a protonation of the cobalt ion forming either $[\text{Co(III)-H(L)}]$ (consistent with the first *CE*-step in mechanism A (Figure 26)) or $[\text{Co(I)(LH)}]$ (consistent with mechanism D (Figure 26)).

As discussed previously it was suggested by Dolui et al. that an E_{red} -like voltammetry peak of cobaloximes arose because of a separate HER process taking place at this potential. Based on the calculated pH-dependence of the E_{red} peak potential of Co-MePy- $\alpha_3\text{C}$ and cobaloxime it is not possible to exclude that possibility here. $2\text{H}^+ + 2\text{e}^- \rightarrow \text{H}_2$ is also a one proton per one electron process and would give rise to the same pH-dependence. To verify whether Co-MePy- $\alpha_3\text{C}$ and cobaloxime can perform electrocatalytic HER at E_{red} or not, a future bulk electrolysis experiment at E_{red} where the headspace H_2 -concentration is monitored may be suitable. However, as mentioned in Section 3.2.3, bulk electrolysis may be challenging with an ArM, because an elevated concentration of catalyst is required. Conclusions drawn from a bulk electrolysis experiment using cobaloxime could possibly be applied to Co-MePy- $\alpha_3\text{C}$ as well, because their respective E_{red} appear at identical potentials with identical pH-dependencies, suggesting they arise from the same process. In Chapter 3 it was shown that HER by Co-MePy- $\alpha_3\text{C}$ and cobaloxime was possible by chemical reduction by $[\text{Eu(EGTA)}]^{2-}$, with an $E^0_{[\text{Eu(EGTA)}]^{2-}/[\text{Eu(EGTA)}]^{1-}} = -0.88 \text{ V vs SHE pH 8}$ which may support electrocatalysis at E_{red} by Co-MePy- $\alpha_3\text{C}$ and cobaloxime. Experiments with weaker chemical- and photoreductants could also be an option to probe HER at more anodic potentials by Co-MePy- $\alpha_3\text{C}$ and cobaloxime.

If the process giving rise to a wave at E_{red} is the EC-formation of $[\text{Co(III)-H(L)}]$ or $[\text{Co(I)(LH)}]$, and not electrocatalysis of HER, the *CCEE*-mechanism suggested by Dolui et al. appear to not be applicable to Co-MePy- $\alpha_3\text{C}$ as the pH-dependence of the E_{red} peak potential suggests that the mechanism begins with an *EC* step. It is not at present possible to know if the process giving rise to current at E_{cat} is corresponding to the *CCEE*-process they suggest, or previously suggested *ECEC* (mechanism A) or *ECCE* (mechanism D). Assuming that the wave at E_{red} arises from an *EC*-process, it must still be deduced if the second part of the mechanism is a *CE*- or *EC* process (i.e., if the mechanism is an *ECCE* or *ECEC* mechanism). As discussed above, the formation of one of the intermediates in the *CCEE*-mechanism suggested by Dolui et al. was shown to be energetically disfavoured.

The pH-dependence study of E_{red} indicates that the electrocatalytic behaviour of Co-MePy- $\alpha_3\text{C}$ is consistent with previously suggested mechanisms for electrocatalytic HER by cobaloximes. Further experimentation and analyses are required to further expand the knowledge of HER by Co-MePy- $\alpha_3\text{C}$, primarily the FOWA to calculate the TOF of electrocatalytic HER. This would allow the comparison of rates calculated from studies using secondary reductants, where the TOF may have been limited by the rate of electron transfer between the reductant and Co-MePy- $\alpha_3\text{C}$. This may give deeper insight into the effect of binding a redox-catalyst to a *de novo* protein scaffold, which would aid in future design of *de novo* metalloenzymes, as well as future iteration on Co-MePy- $\alpha_3\text{C}$.

4.1.1.1 Analysis of consecutive CVs of cobaloxime and Co-MePy- α_3 C

When collecting consecutive CVs of cobaloxime (Figure 30A) and Co-MePy- α_3 C (Figure 30B) some differences between the two arise. For both cobaloxime and Co-MePy- α_3 C, E_{red} and E_{cat} decreased significantly with each scan, with E_{red} decreasing more than E_{cat} . This effect is particularly apparent for Co-MePy- α_3 C (Figure 30C) where E_{red} is almost completely disappeared on the third consecutive CV.

The biggest differences are between the effects on E_{ox} . Consecutive scan of cobaloxime show no change in current or shift in peak potential of E_{ox} , whereas of Co-MePy- α_3 C E_{ox} both decreased in current and shifts to more cathodic potential for each scan (Figure 30D).

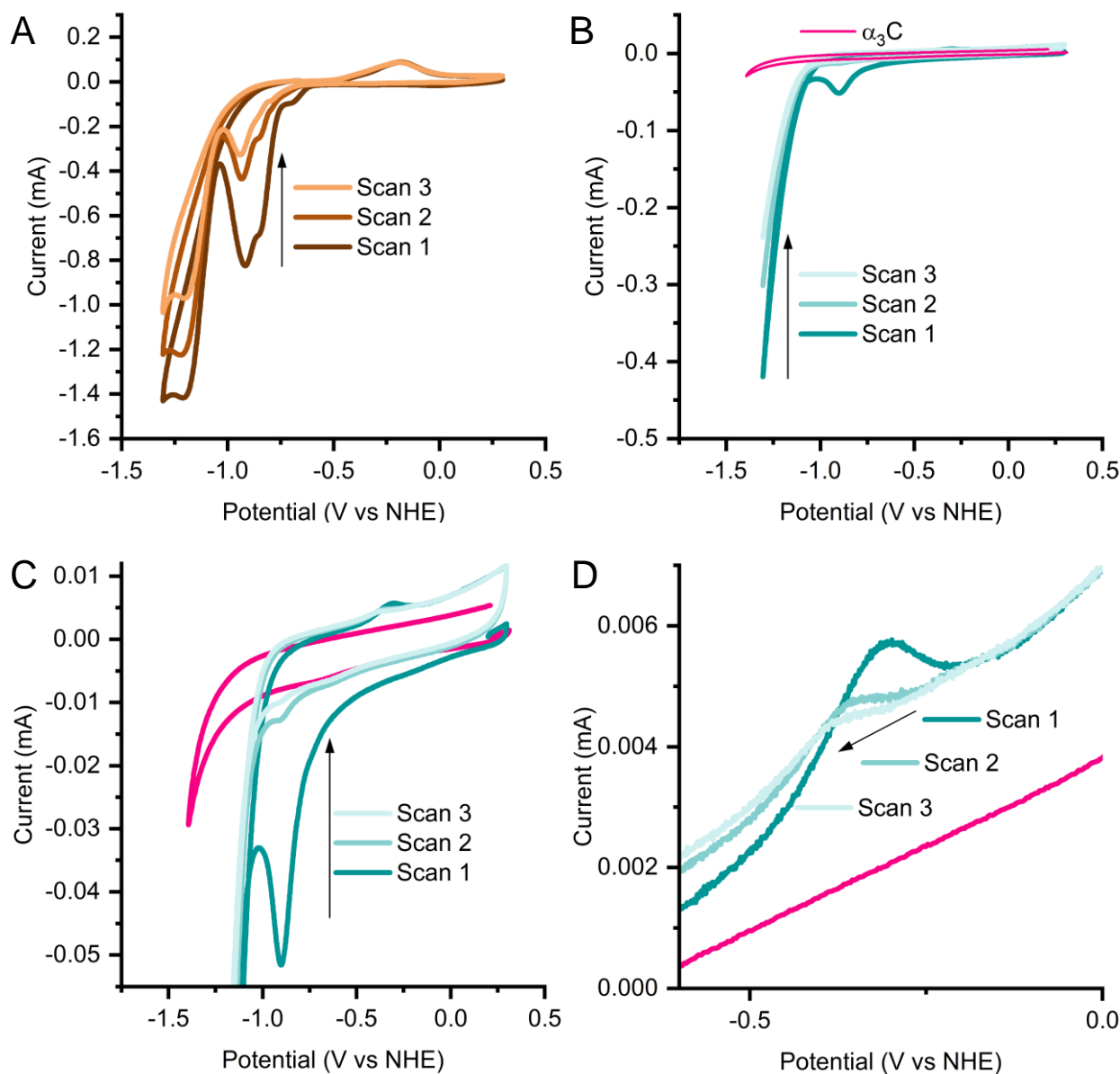


Figure 30: Three consecutive CVs of A: Cobaloxime and B: Co-MePy- α_3 C (with one scan of α_3 C shown as reference). Zoomed in views of figure B to emphasise C: E_{red} and D: E_{ox} . CVs collected at 0.25 V/s at pH 7. NB! CV of α_3 C was collected in 100 mM potassium phosphate buffer (pH 7).

As E_{cat} is swept past, the catalyst molecules in the diffusion layer are a mix of the intermediates of the electrocatalytic HER mechanism. Assuming that E_{red} corresponds to the $[\text{Co(II)}(\text{L})]$ to $[\text{Co(I)}(\text{L})]$ reduction, to see E_{red} in the consecutive scans a significant concentration of $[\text{Co(II)}(\text{L})]$ must be replenished by re-oxidation or diffusion. For Co-MePy- α_3 C the diffusion layer cannot be replenished by diffusion because all catalysts present in the sample were adsorbed to the surface of the electrode, and so all $[\text{Co(II)}(\text{L})]$ that can be reduced at E_{red} during the consecutive scans must be from what was formed either in E_{cat} or that was re-

oxidised. Because the current at E_{ox} was very small, relative to at E_{cat} and E_{red} , the species that was oxidised at that potential must have accumulated in very low concentration. If $[Co(II)(L)]$ was replenished in E_{ox} , it would be very small concentrations as the current is very small. Even if it does not replenish at E_{ox} , only small amounts of the Co-MePy- α_3C will exit the catalytic wave as $[Co(II)(L)]$. This was likely why a drastic decrease in current at E_{red} upon the consecutive scans of Co-MePy- α_3C could be observed, but not as a drastic of a decrease in E_{cat} . The mix of species present when the first E_{cat} was exited was be able to continue the electrocatalytic HER as E_{cat} was entered the second and third time.

This effect of insufficient repopulation of $[Co(II)(L)]$ was likely applicable to cobaloxime, where the apparent decrease in E_{red} but disproportional decrease in E_{cat} was observed. The decrease in E_{red} was likely not as drastic for cobaloxime as for Co-MePy- α_3C as $[Co(II)(L)]$ can be repopulated from the bulk solution for cobaloxime, but the process is likely not fast enough to yield identical currents at E_{red} in the first and the consecutive scans.

For both cobaloxime and Co-MePy- α_3C some species must accumulate that can be oxidised at their respective E_{ox} . Because their peak potentials were not identical, it was likely not the same species that was accumulated which was oxidised at E_{ox} for the two catalysts. The E_{ox} current behaviour was different between cobaloxime and Co-MePy- α_3C , for cobaloxime the current at E_{ox} remains identical through all three scans, and it decreased between them for Co-MePy- α_3C . The peak potential also shifted to more cathodic currents between the three scans for Co-MePy- α_3C .

The peak potential for reduction to $[Co(III)(L)]$ to $[Co(II)(L)]$ has been reported previously to be close to 0 V vs NHE, which is inconsistent with that current at E_{ox} should arise because of oxidation of $[Co(II)(L)]$ to $[Co(III)(L)]$ for either catalyst.(36) As discussed above, accumulation of any one intermediate that takes part in the catalytic mechanism is unlikely, which further contributes to that E_{ox} likely do not arise because of this process but rather by formation of some species that do not partake in catalysis. If the current at E_{ox} arises due to oxidation of a species formed at E_{cat} , it is expected to decrease proportionally to E_{cat} . For cobaloxime, it is clear this is not the case, as E_{ox} is constant. For Co-MePy- α_3C the current at E_{ox} decreases for each scan, but the shift in potential for each scan suggests a shift in the process that is taking place at E_{ox} for each consecutive scan.

The respective behaviours of the peak at E_{ox} for cobaloxime and Co-MePy- α_3C cannot be explained at this time using the available data. Peaks similar to E_{ox} has, to my knowledge, not been reported for cobaloximes in water. Notable examples of cobaloximes in water are the study by Dolui et al. and Wakerley and Reisner.(36,37) Dolui et al. show CVs scanned in a manner that does not reveal if a peak corresponding to E_{ox} appears, and Wakerley and Reisner do not scan to as cathodic currents as has been done here. To explore the effect of the cathodic current, a preliminary experiment scanning to different points using cobaloxime was done. This showed that E_{ox} only appears when the catalytic current is entered, and so the species that is oxidised at E_{ox} requires elevated potentials to form (Figure 31).

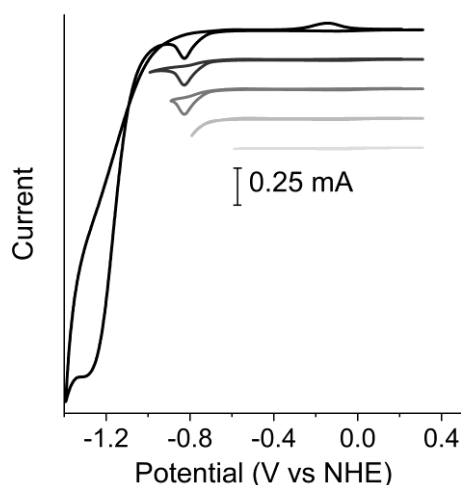


Figure 31: CVs of cobaloxime with an increasingly cathodic end potential, showing the appearance of E_{ox} only when E_{cat} has taken place. NB! These CVs were collected in 100 mM MES, 100 mM MOPS, pH 7, with **no** added KCl.

These data were collected under somewhat different conditions for the main dataset showed in Figure 29, with no KCl added to the solution. This appears to give rise to a different shape of E_{red} , and therefore the data shown in Figure 31 should be re-collected under the same conditions as the other data.

It has previously been shown that cobaloxime degrade to form cobalt nanoparticles, which necessitates the agglomeration of cobalt ions.⁽⁸⁷⁾ For samples with cobaloxime, it is possible that cobalt nanoparticles formed as a degradation process. In Co-MePy- α_3 C the cobaloxime is shielded by the protein, and so the cobalt ions cannot come together to form nanoparticles as easily. The quantity of cobaloxime in the protein films versus in the cobaloxime solution is also much lower, which is likely to further inhibit the formation of nanoparticles. If the wave at E_{ox} for cobaloxime corresponds to the oxidation of cobalt nanoparticles, it may be suspected that the peak should grow with each consecutive scan. It could however be possible that the nanoparticles deposit on the surface of the electrode as they form, and only a certain thickness of such a film could be oxidised each scan. This could account for the fact that the current at E_{ox} is identical at each consecutive scan. To gain further insight to the degradation process of cobaloxime during the experiment a surface analysing method would be necessary to measure if anything has accumulated. A simpler experiment to investigate deposition on the surface is to perform a rinse test after the collection of a CV. Then all remaining analyte is rinsed away, and a CV of a new, blank solution is gathered with the rinsed electrode. If something was deposited on the electrode that give rise to an oxidation at E_{ox} , it would appear also after the rinse.

To summarise, examining consecutive CVs of cobaloxime and Co-MePy- α_3 C, the behaviour of E_{ox} of both catalysts indicates that some form of catalyst degradation takes place for both catalysts. It is possible that cobaloxime degrades by forming cobalt nanoparticles, which may deposit on the surface of the electrode. Due to steric effects of the protein in Co-MePy- α_3 C coupled with that it is adsorbed to the electrode, nanoparticle formation by Co-MePy- α_3 C is less likely. Because the current of E_{ox} by Co-MePy- α_3 C is relatively smaller than that of cobaloxime it is likely that the potential degradation process for Co-MePy- α_3 C occurs with lower frequency.

4.2 Summary and outlook

By studying the pH-dependence of the peak potential for the wave at E_{red} it was possible to deduce that the process that gives rise to a wave at E_{red} involves one proton per electron. The process is likely the reduction of $[\text{Co(II)(L)}]$ to $[\text{Co(I)L}]$ coupled to the protonation forming $[\text{Co(III)-H(L)}]$ or $[\text{Co(I)(LH)}]$, but from the data presented here, it cannot be deduced which protonated intermediate may form. The analysis of the pH-dependence of the E_{red} process indicates that the overall mechanism for electrocatalytic HER by Co-MePy- α_3 C is likely starting with an *EC*-step, which is consistent with previously suggested mechanisms. It is currently not known if an *ECEC* mechanism or *ECCE* mechanism is the dominant one, but the *ECEC* mechanism has been suggested several times in past literature and can be used as a starting point for future interpretation of a FOWA to calculate TOFs for electrocatalytic HER by Co-MePy- α_3 C and cobaloxime. A previous study of electrocatalysis of HER by cobaloxime in water suggested that E_{red} arose because of a separate HER mechanism, and that a *CCEE*-mechanism was the dominant process giving rise to E_{cat} . This has not been excluded by the present analysis of the data presented in this chapter and further experimentation to quantify the evolved H_2 in the headspace would be necessary to draw further conclusions regarding this.

From the data discussed in this chapter it is indicated that cobaloxime and Co-MePy- α_3 C go through some kind of degradation process through the electrocatalysis, giving rise to a species that may be oxidised, although at different potentials for the two catalysts. This suggests that the potential degradation product is different for cobaloxime and Co-MePy- α_3 C. The relative current of E_{ox} (compared to E_{red}) is smaller for Co-MePy- α_3 C than cobaloxime, further indicating that potential catalyst degradation is lessened in Co-MePy- α_3 C. Exploring this further may be interesting, as it could indicate that the known degradation of cobaloxime into cobalt nanoparticles is inhibited by the protein, which for now is preliminary speculation.

Other facets of the voltammetry of Co-MePy- α_3 C and cobaloxime is of interest for further study in this project that has not been discussed in depth in this chapter, for example the difference in shape of the E_{red} wave upon addition of KCl, and clearer elucidation of the $[\text{Co(III)(L)}]$ to $[\text{Co(II)(L)}]$ reduction for both catalysts.

5 Summary and outlook

Transition metals are abundant in nature as structural and functional components of proteins and enzymes. They partake in catalysis in all types of enzymes, where they work in synergy with the protein scaffold to give rise to the excellent catalytic functions seen across nature. Because metals together with protein scaffolds give rise to such a wide variety of catalysis, research interest in the construction of artificial metalloenzymes has grown the last 30 years. Today specific, and completely non-natural catalysis has been shown to be catalysed by artificial metalloenzymes.

As humanity is facing a climate crisis, harvesting and storing sustainable energy are key problems to solve. Storing electricity in batteries is commonplace but comes with issues relating to extraction of raw materials and storage space of said batteries. Instead, utilising fuels such as H₂ may be a future method for energy storage. Today, production of H₂ is mainly performed with unsustainable methods, either using fossil feedstock, releasing CO₂, or using precious metals which the Earth's crust does not contain enough of to quench our thirst for energy. Developing and improving sustainable catalysts for H₂ evolution is an essential research problem to prioritise in the green energy transition.

This thesis has described methods for design, production and characterisation of an artificial metalloenzyme for hydrogen evolution. The design, production and characterisation of the *de novo* metalloenzyme Co-MePy- α_3 C has been described here. Co-MePy- α_3 C is based on the catalyst cobaloxime and the *de novo* protein α_3 C, and the studies of Co-MePy- α_3 C gave insight into how a *de novo* protein and catalyst can be combined, and some of the challenges that may be faced in such a process.

The following questions were the focus of this thesis:

1. Will the resulting protein-catalyst conjugate be catalytically active? And if yes, how has the HER catalysis been altered by incorporation into the protein?
2. Does binding of the catalyst to the protein change the protein structure?
3. By what mechanism does electrocatalytic HER take place in the *de novo* metalloenzyme and does it differ from homogenous catalysis?
4. What role can a *de novo* protein scaffold play in the design of ArMs, and how is it different from using a natural protein? What are the advantages and limitations?

The results discussed in this thesis show that Co-MePy- α_3 C is catalytically active for HER, and it produced slightly less hydrogen than cobaloxime itself (ca 80%), with reduced rates (ca 40%). This was attributed to the burial of the catalyst in the protein scaffold, which does not contain any amino acid residues that may partake in proton – or electron transfer to the active site. Future studies to improve the activity can include incorporating proton- and electron relaying amino acids, or to position the catalyst to be more solvent exposed. Both strategies would allow a higher access to reducing equivalents and protons, potentially increasing the rates of catalysis and amount of H₂ produced by Co-MePy- α_3 C. The data presented in this thesis indicate that Co-MePy- α_3 C may be stable for a longer time than cobaloxime, enabling prolonged hydrogen evolution. This is preliminary analysis of the data, and additional longevity studies are required to draw further conclusions.

The protein secondary folding in Co-MePy- α_3 C was found to be less helical compared to that of unmodified α_3 C, but the helical features of Co-MePy- α_3 C was as stable as those in α_3 C. That indicates that although partial unfolding may occur as a result of binding cobaloxime, the general secondary structure remains folded just as well as in unmodified α_3 C.

The mechanism of electrocatalytic HER could not be fully understood with the data available at the time of writing of this thesis, but preliminary analysis suggests that an *ECEC*-type mechanism takes place, which is consistent with previously published mechanistic studies of electrocatalytic HER by cobaloxime. This knowledge can help steer future studies, for example in how to apply and evaluate a FOWA to the

voltammetry-data collected with Co-MePy- α_3 C, which is planned as a next step in this study. FOWA is used to calculate electrocatalytic rates, which is a valuable addition to the study of Co-MePy- α_3 C. Electrocatalysis eliminates the use of photosensitisers and chemical reductants, which may impact the rates of catalysis, allowing for a clearer understanding of the impact of the protein on cobaloxime-catalysed HER.

In this thesis it has been shown that using a *de novo* protein as the scaffold for an artificial metalloenzyme can be practical. *De novo* proteins can be engineered to be structurally stable at many different conditions and to be able to unfold and refold to allow for internal chemical modification, and can be designed to only include one modifiable site giving control over the final location of the incorporated catalyst.

Future studies planned for Co-MePy- α_3 C primarily concern the analysis of its electrocatalysis, where especially a FOWA is of interest. However, several other facets of the electrocatalytic behaviour of Co-MePy- α_3 C remain interesting, for example the potential of using a protein to inhibit catalyst degradation by disfavours cobalt nanoparticle formation. Further analysis of the mechanism of HER by Co-MePy- α_3 C may also be of interest, especially comparing it to other studies performed in aqueous solvent.

Populärvetenskaplig sammanfattning

I en värld där temperaturen snabbt stiger på grund av ansvarslös användning av energi och naturresurser för att främja okontrollerad ekonomisk tillväxt behövs nya tekniker baserade på hållbar utvinning av naturresurser för att producera och lagra energi. Människor har sedan länge producerat energi på ett koldioxid-effektivt sätt med hjälp av vind, vatten och sol, och under de senaste åren har produktionen av solenergi ökat snabbt. Det största problemet med dessa energikällor är att de endast är tillgängliga för energiproduktion vid vissa tidpunkter och kanske inte när vi behöver dem. Solenergi kan till exempel endast utnyttjas under dagtid, vilket i Sverige är få timmar på vintern, men det största energibehovet finns på kvällen. Detta problem kan lösas genom att hitta sätt att lagra energi på ett effektivt och hållbart sätt, till exempel med hjälp av batterier, vattenkraftverk och svänghjul. Dessa kräver dock stora mängder material och utrymme. Batterier som kan anslutas till privata solpaneler finns på marknaden och är den vanligaste lösningen för privat bruk, men tyvärr är det i för närvarande i Sverige lönsamt att sälja överskottsenergin till elnätet än att lagra den för eget bruk.

En lovande metod för energilagring är vätgas, där förnybar energi kan lagras i den kemiska bindningen mellan två väteatomer. När mer energi behövs i form av elektricitet kan den kemiska bindningen brytas, och energin kan tas tillbaka som elektricitet in i elnätet. För närvarande är den enda koldioxidneutrala metoden för vätgasproduktion elektrolys där platina behövs vilket är en sällsynt metall på vår planet och det finns inte tillräckligt med platina i vår jordskorpa för att tillgodose hela planetens behov av väte. Därför måste vi uppfinna nya och hållbara sätt att producera väte för lagring av energi som framställts med sol, vind och vatten.

För att kunna skapa dessa nya metoder för bränsleproduktion måste vi både skaffa oss kunskap om de kemiska komponenter som behövs för att skapa en ny vätgasproducerande molekyl samt utforma dessa nya vätgasproducerande molekyler. Molekyler som kan producera andra molekyler genom att skapa eller bryta kemiska bindningar kallas katalysatorer, så i detta fall kallas molekylen som producerar vätgas för en vätgasutvecklande katalysator. Denna avhandling fokuserar främst på att utveckla förståelsen för de kemiska komponenterna i en biologiskt inspirerad vätgasutvecklande katalysator som kallas för ett konstgjort metallenzym. Enzymer är baserade på proteiner, som är stora biologiska molekyler och är också kända som naturens byggstenar. De har väldefinierade strukturer och utför många kemiska funktioner, oftast mycket mer effektivt än motsvarande konstgjorda katalysatorer.

I denna avhandling visades det att det är möjligt att kombinera ett artificiellt protein med en metallbaserad, vätgasutvecklande katalysator för att skapa ett konstgjort metallenzym som kan producera vätgas. Det kan producera nästan lika mycket vätgas som den ursprungliga katalysatorn, men gör det långsammare. Detta beror troligen på att proteindelen av det konstgjorda enzymet är isolerande och gör det svårt för de komponenter som behövs för att producera vätgas att binda till katalysatorn inuti enzymet. Det visades också att det konstgjorda metallenzymet beter sig på samma sätt som katalysatorn som inte är bunden till proteinet, både inom denna studie och jämfört med andra studier, men fler experiment behövs för att förstå exakt hur det konstgjorda metallenzymet fungerar.

Popular scientific summary

In a world rapidly increasing in temperature because the irresponsible use of energy and natural resources to fuel unchecked economic growth, new technologies based on sustainable extraction of natural resources are needed to make and store energy. Humans have been producing energy in a carbon efficient way for some time using wind, water and sun, and in recent years the production of solar energy has rapidly grown. The main issue is that all these energy sources is that they are only available for energy production at certain times and might not be when we need it. For example, solar energy is only available in daytime, which in Sweden can be very few hours in winter, but most energy used in homes is needed in evening and at night. This issue can be overcome by finding ways to store energy efficiently and sustainably, for example using batteries, water dams and flywheels, all which require large amounts of materials and space. Batteries to connect to private solar panels are available on the market and is the most feasible solution for an in-home solution. Unfortunately, in Sweden it's currently more economically viable to sell the excess energy to the grid, rather than storing it for yourself.

A promising method of energy storage is hydrogen gas, where renewable energy can be stored in the chemical bond between two hydrogen atoms. When more energy is needed as electricity, the chemical bond can be broken, and the energy can be taken back as electricity and put into the electrical grid. Currently, the only carbon neutral method for hydrogen gas production is by electrolysis, where platinum is needed, which is a rare resource on our planet. There is not enough platinum in our crust to fulfil the hydrogen needs for the whole planet. Because of this, we need to invent new and sustainable ways of making hydrogen for energy storage, so that it can be coupled with sustainable energy production facilities like solar panel- and wind turbine parks.

To be able to create these new methods for fuel production, we need to both gain understanding into the chemical components needed to make a new hydrogen producing molecule, as well as design these new hydrogen producing molecules. Molecules that can produce other molecules by making or breaking chemical bonds are known as catalysts, so in this case the molecule that makes hydrogen, would be a hydrogen evolving catalyst.

This thesis has been focused mainly on developing our understanding of the chemical components in biologically inspired hydrogen evolving catalyst called an artificial metalloenzyme. Enzymes are based on proteins, which are big, biological molecules and are known as the building blocks of nature. They have well-defined structures and perform many chemical functions, usually much more efficiently than human-made catalysts

. Many natural proteins incorporate metal ions to perform their designated function, very often acting as a metalloenzyme. Nature's own hydrogen evolving enzyme requires iron and nickel metal ions, and they are essential to make the protein into a catalyst. The work described in this thesis combines proteins and metals in a way that is not found in nature for two reasons: to understand how a protein may affect how well a hydrogen evolving catalyst works, and to attempt to create a completely artificial metalloenzyme.

In this thesis it was shown that it is possible to combine an artificial protein with a metal-based hydrogen evolving catalyst to make an artificial metalloenzyme that can make hydrogen. It can produce nearly as much hydrogen as the starting catalyst but does so slower. This is most likely because the protein part of the artificial enzyme act as an insulator and makes it difficult for the components that are needed to make hydrogen to bind to the catalyst inside the enzyme. It was also shown that that the artificial metalloenzyme behaves similarly to the catalyst that is not bound to the protein, both within this study, and when compared to other studies but more experiments are needed to understand exactly how the artificial metalloenzyme functions.

Acknowledgements

There are many who have helped me these seven years, thank you all for your care, friendship and time. I know all of you will continue to do so until the end of my PhD and beyond, I trust that you know I will always return the favour. Special thanks go out to the following:

Starla, for taking a chance with me, for everything you have taught me and for all your time and patience.

Ann, for having been there since my first day in house seven, and for always helping me with small and large things and for encouraging me to do the hard things you know I can manage.

E och K.G. Lennanders stipendiestiftelse, for giving me the financial means to continue my PhD-studies.

Rima and Nina, for the time and care spent helping me with this thesis and for your unyielding friendship.

Co-workers past and present, for making it bearable to come to the office when I have been feeling down and always making me feel better no matter how sad I am, and for being excellent friends both in and out of work.

My friends outside of work, the English Bookshop Feelgood-group, Västgöta nationskör and Östgöta nation, for giving me somewhere to go and have a good time and not think about my PhD.

My parents for encouraging me to be a scientist for as long as I can remember and for always supporting me.

Stefan and Tijmen, my constant support team, for never saying no to any small or big thing I want help with and for never making that feel like an inconvenience, and for loving me as much as I love you.

References

1. Bertini I et al. 2006. Biological inorganic chemistry: structure and reactivity. 1st edn. Sausalito, California, USA: University Science Books;
2. Ferreira KN et al. 2004. Architecture of the Photosynthetic Oxygen-Evolving Center. *Science*. 303(5665):1831–8.
3. Hodgkin DC et al. 1956. Structure of Vitamin B12. *Nature*. 178(4524):64–6.
4. Lancaster KM et al. 2011. X-ray Emission Spectroscopy Evidences a Central Carbon in the Nitrogenase Iron-Molybdenum Cofactor. *Science*. 334(6058):974–7.
5. Beinert H et al. 1997. Iron-Sulfur Clusters: Nature’s Modular, Multipurpose Structures. *Science*. 277(5326):653–9.
6. Chan MK et al. 1995. Structure of a Hyperthermophilic Tungstopterin Enzyme, Aldehyde Ferredoxin Oxidoreductase. *Science*. 267(5203):1463–9.
7. Stančín H et al. 2020. A review on alternative fuels in future energy system. *Renew Sustain Energy Rev*. 128:109927.
8. Shih AJ et al. 2022. Water electrolysis. *Nat Rev Methods Primer*. 2(1):84.
9. Muron M et al. Clean Hydrogen Monitor 2022 [Internet].
10. Espitalier-Noël M et al. Clean Hydrogen Monitor 2024. Hydrogen Europe;
11. 2021. Abundance of Elements in the Earth’s Crust and in the Sea. Boca Raton, FL: Taylor & Francis; (Rumble JR, editor. CRC Handbook of Chemistry and Physics; vol. 102 (Internet Version 2021)).
12. Pourbaix M 1974. Atlas of Electrochemical Equilibria in Aqueous Solutions. Houston, Texas: NACE International;
13. Zhang B et al. 2019. Artificial photosynthesis: opportunities and challenges of molecular catalysts. *Chem Soc Rev*. 48(7):2216–64.
14. Lu Y et al. 2019. O₂ sensitivity and H₂ production activity of hydrogenases—A review. *Biotechnol Bioeng*. 116(11):3124–35.
15. McDonald AG et al. 2023. Enzyme nomenclature and classification: the state of the art. *FEBS J*. 290(9):2214–31.
16. Alfano M et al. 2020. Structure, function, and biosynthesis of nickel-dependent enzymes. *Protein Sci*. 29(5):1071–89.
17. Kobayashi M et al. 1999. Cobalt proteins. *Eur J Biochem*. 261(1):1–9.
18. Qiu S et al. 2020. Learning from nature: Understanding hydrogenase enzyme using computational approach. *WIREs Comput Mol Sci*. 10(1):e1422.
19. Feng X et al. 2022. Structure and electron transfer pathways of an electron-bifurcating NiFe-hydrogenase. *Sci Adv*. 8(8):eabm7546.
20. Tai H et al. 2021. Proton Transfer Mechanisms in Bimetallic Hydrogenases. *Acc Chem Res*. 54(1):232–41.

21. Berggren G et al. 2013. Biomimetic assembly and activation of [FeFe]-hydrogenases. *Nature*. 499(7456):66–9.
22. Simmons TR et al. 2014. Mimicking hydrogenases: From biomimetics to artificial enzymes. *Coord Chem Rev*. 270–271:127–50.
23. Banerjee R et al. 2003. The Many Faces of Vitamin B12: Catalysis by Cobalamin-Dependent Enzymes1. *Annu Rev Biochem*. 72(Volume 72, 2003):209–47.
24. Whipple GH et al. 1926. Iii. muscle hemoglobin as a source of bile pigment. *Am J Physiol-Leg Content*. 78(3):675–82.
25. Minot GR et al. 1926. Treatment of Pernicious Anemia bay a Special Diet. *J Am Med Assoc*. 87(7):470–6.
26. Hodgkin DC et al. 1955. Structure of Vitamin B12: The Crystal Structure of the Hexacarboxylic Acid derived from B12 and the Molecular Structure of the Vitamin. *Nature*. 176(4477):325–8.
27. Rickes EL et al. 1948. Crystalline Vitamin B12. *Science*. 107(2781):396–7.
28. Woodward RB 1973. The total synthesis of vitamin B12. *Pure Appl Chem*. 33(1):145–78.
29. Martens JH et al. 2002. Microbial production of vitamin B12. *Appl Microbiol Biotechnol*. 58(3):275–85.
30. Schrauzer GN 1976. New Developments in the Field of Vitamin B12: Reactions of the Cobalt Atom in Corrins and in Vitamin B12 Model Compounds. *Angew Chem Int Ed Engl*. 15(7):417–26.
31. Connolly P et al. 1986. Cobalt-catalyzed evolution of molecular hydrogen. *Inorg Chem*. 25(16):5.
32. Sobczyńska-Malefora A et al. 2021. Vitamin B12 status in health and disease: a critical review. Diagnosis of deficiency and insufficiency – clinical and laboratory pitfalls. *Crit Rev Clin Lab Sci*. 58(6):399–429.
33. Bakac A et al. 1984. Unimolecular and bimolecular homolytic reactions of organochromium and organocobalt complexes. Kinetics and equilibria. *J Am Chem Soc*. 106(18):5197–202.
34. Lazarides T et al. 2009. Making Hydrogen from Water Using a Homogeneous System Without Noble Metals. *J Am Chem Soc*. 131(26):9192–4.
35. Schrauzer GN et al. 1966. Alkylcobaloximes and Their Relation to Alkylcobalamins. *J Am Chem Soc*. 88(16):3738–43.
36. Dolui D et al. 2019. Enzyme-Inspired Synthetic Proton Relays Generate Fast and Acid-Stable Cobalt-Based H₂ Production Electrocatalysts. *ACS Catal*. 9(11):10115–25.
37. Wakerley DW et al. 2014. Development and understanding of cobaloxime activity through electrochemical molecular catalyst screening. *Phys Chem Chem Phys*. 16(12):5739–46.
38. Du P et al. 2009. Visible Light-Driven Hydrogen Production from Aqueous Protons Catalyzed by Molecular Cobaloxime Catalysts. *Inorg Chem*. 48(11):4952–62.
39. Bacchi M et al. 2014. Cobaloxime-Based Artificial Hydrogenases. *Inorg Chem*. 53(15):8071–82.
40. Bacchi M et al. 2016. Artificial Hydrogenases Based on Cobaloximes and Heme Oxygenase. *Chempluschem*. 81(10):1083–9.
41. Roy S et al. 2019. Electrocatalytic Hydrogen Evolution from a Cobaloxime-Based Metal-Organic Framework Thin Film. *J Am Chem Soc*. 141(40):15942–50.
42. Gottschling K et al. 2020. Rational Design of Covalent Cobaloxime–Covalent Organic Framework Hybrids for Enhanced Photocatalytic Hydrogen Evolution. *J Am Chem Soc*. 142(28):12146–56.
43. Reuillard B et al. 2016. A Poly(cobaloxime)/Carbon Nanotube Electrode: Freestanding Buckypaper with Polymer-Enhanced H₂-Evolution Performance. *Angew Chem Int Ed*. 55(12):3952–7.

44. Tommos C et al. 1999. *De Novo* Proteins as Models of Radical Enzymes. *Biochemistry*. 38(29):9495–507.
45. Cox N et al. 2020. Current Understanding of the Mechanism of Water Oxidation in Photosystem II and Its Relation to XFEL Data. *Annu Rev Biochem*. 89(Volume 89, 2020):795–820.
46. Kang G et al. 2020. Structure of a trapped radical transfer pathway within a ribonucleotide reductase holo-complex. *Science*. 368(6489):424–7.
47. Lovejoy B et al. 1993. Crystal Structure of a Synthetic Triple-Stranded α -Helical Bundle. *Science*. 259(5099):1288–93.
48. Johansson JS et al. 1998. A Native-Like Three- α -Helix Bundle Protein from Structure-Based Redesign: A Novel Maquette Scaffold. *J Am Chem Soc*. 120(16):3881–6.
49. O’Neil KT et al. 1990. A Thermodynamic Scale for the Helix-Forming Tendencies of the Commonly Occurring Amino Acids. *Science*. 250(4981):646–51.
50. Betz S et al. 1997. Design of two-stranded and three-stranded coiled-coil peptides. *Philos Trans R Soc Lond B Biol Sci*. 348(1323):81–8.
51. McLachlan AD et al. 1975. Tropomyosin coiled-coil interactions: Evidence for an unstaggered structure. *J Mol Biol*. 98(2):293–304.
52. Sodek J et al. 1972. Amino-Acid Sequence of Rabbit Skeletal Tropomyosin and Its Coiled-Coil Structure. *Proc Natl Acad Sci*. 69(12):3800–4.
53. Tommos C et al. 2013. Reversible Phenol Oxidation and Reduction in the Structurally Well-Defined 2-Mercapto-phenol- α 3C Protein. *Biochemistry*. 52(8):1409–18.
54. Schwizer F et al. 2018. Artificial Metalloenzymes: Reaction Scope and Optimization Strategies. *Chem Rev*. 118(1):142–231.
55. Davis HJ et al. 2019. Artificial Metalloenzymes: Challenges and Opportunities. *ACS Cent Sci*. 5(7):1120–36.
56. Drienovská I et al. 2014. Novel artificial metalloenzymes by in vivo incorporation of metal-binding unnatural amino acids. *Chem Sci*. 6(1):770–6.
57. Lin YW 2024. Functional metalloenzymes based on myoglobin and neuroglobin that exploit covalent interactions. *J Inorg Biochem*. 257:112595.
58. Michael Green N 1990. [5] Avidin and streptavidin. In: Wilchek M, Bayer EA, editors. *Methods in Enzymology*. Academic Press; p. 51–67. (Avidin-Biotin Technology; vol. 184).
59. Wilson ME et al. 1978. Conversion of a protein to a homogeneous asymmetric hydrogenation catalyst by site-specific modification with a diphosphinerhodium(I) moiety. *J Am Chem Soc*. 100(1):306–7.
60. Keller SG et al. 2018. Photo-Driven Hydrogen Evolution by an Artificial Hydrogenase Utilizing the Biotin-Streptavidin Technology. *Helv Chim Acta*. 101(4):e1800036.
61. Monnard FW et al. 2013. Human carbonic anhydrase II as host protein for the creation of artificial metalloenzymes: the asymmetric transfer hydrogenation of imines. *Chem Sci*. 4(8):3269–74.
62. Srivastava P et al. 2015. Engineering a dirhodium artificial metalloenzyme for selective olefin cyclopropanation. *Nat Commun*. 6(1):7789.
63. Davies RR et al. 1997. A Semisynthetic Metalloenzyme Based on a Protein Cavity That Catalyzes the Enantioselective Hydrolysis of Ester and Amide Substrates. *J Am Chem Soc*. 119(48):11643–52.
64. Tommos C et al. 1998. Radical Maquettes as Models of Radical Enzymes. In: Garab G, editor. *Photosynthesis: Mechanisms and Effects: Volume I–V: Proceedings of the XIth International Congress on Photosynthesis, Budapest, Hungary, August 17–22, 1998*. Dordrecht: Springer Netherlands; p. 4221–4.

65. Dai QH et al. 2002. Structure of a de Novo Designed Protein Model of Radical Enzymes. *J Am Chem Soc.* 124(37):10952–3.
66. Moreira DC 2022. RGBBradford: Accurate measurement of protein concentration using a smartphone camera and the blue to green intensity ratio. *Anal Biochem.* 655:114839.
67. Bradford MM. A Rapid and Sensitive Method for the Quantitation of Microgram Quantities of Protein Utilizing the Principle of Protein-Dye Binding.
68. Smith PK US4839295A, 1989. Measurement of protein using bicinchoninic acid [Internet].
69. Gómez E et al. 1992. Simultaneous spectrophotometric determination of metal ions with 4-(pyridyl-2-azo)resorcinol (PAR). *Fresenius J Anal Chem.* 342(4):318–21.
70. Kocyla A et al. 2015. Molar absorption coefficients and stability constants of metal complexes of 4-(2-pyridylazo)resorcinol (PAR): Revisiting common chelating probe for the study of metalloproteins. *J Inorg Biochem.* 152:82–92.
71. Säbel CE et al. 2009. A direct spectrophotometric method for the simultaneous determination of zinc and cobalt in metalloproteins using 4-(2-pyridylazo)resorcinol. *Anal Biochem.* 391(1):74–6.
72. Brustolon M et al. 2009. Electron Paramagnetic Resonance: A Practitioners Toolkit [Internet]. Newark, United States: John Wiley & Sons, Incorporated;
73. 2020. IEEE Standard Letter Designations for Radar-Frequency Bands. *IEEE Std 521-2019 Revis IEEE Std 521-2002.* :1–15.
74. Spencer SEF et al. 2021. Bayesian inference assessment of protein secondary structure analysis using circular dichroism data – how much structural information is contained in protein circular dichroism spectra? *Anal Methods.* 13(3):359–68.
75. Miles AJ et al. 2015. Chapter 6 - Circular Dichroism Spectroscopy for Protein Characterization: Biopharmaceutical Applications. In: Houde DJ, Berkowitz SA, editors. *Biophysical Characterization of Proteins in Developing Biopharmaceuticals.* Amsterdam: Elsevier; p. 109–37.
76. Santoro MM et al. 1988. Unfolding free energy changes determined by the linear extrapolation method. 1. Unfolding of phenylmethanesulfonyl .alpha.-chymotrypsin using different denaturants. *Biochemistry.* 27(21):8063–8.
77. Graham DJ 2018. Standard Operating Procedures for Cyclic Voltammetry. 1st edn.
78. Tsierkezos NG 2007. Cyclic Voltammetric Studies of Ferrocene in Nonaqueous Solvents in the Temperature Range from 248.15 to 298.15 K. *J Solut Chem.* 36(3):289–302.
79. Bard AJ 2001. Electrochemical methods: fundamentals and applications. 2. ed. New York: Wiley; xxi+833.
80. Hu X et al. 2005. Electrocatalytic hydrogen evolution by cobalt difluoroboryl-diglyoximate complexes. *Chem Commun.* (37):4723–5.
81. Elgrishi N et al. 2018. A Practical Beginner's Guide to Cyclic Voltammetry. *J Chem Educ.* 95(2):197–206.
82. H₂ Sensor for Hydrogen Research. Unisense. Retrieved on 2025-10-09 from <https://unisense.com/products/h2-sensor/>
83. Berglund S et al. 2024. Hydrogen production by a fully *de novo* enzyme. *Dalton Trans.* 53(31):12905–16.
84. Trogler WC et al. 1974. Cis and trans effects on the proton magnetic resonance spectra of cobaloximes. *Inorg Chem.* 13(7):1564–70.
85. Schrauzer GN 1968. Bis(dimethylglyoximate)cobalt complexes. McGraw-Hill Book Company, Inc.; (Jolly WL, editor. *Inorganic Syntheses*; vol. XI).

86. Berg JM et al. 2012. *Biochemistry*. 7. ed., International ed. Basingstoke: Palgrave Macmillan;
87. Kaeffer N et al. 2016. The Dark Side of Molecular Catalysis: Diimine–Dioxime Cobalt Complexes Are Not the Actual Hydrogen Evolution Electrocatalyst in Acidic Aqueous Solutions. *ACS Catal.* 6(6):3727–37.
88. Vincent KA et al. 2003. Instantaneous, stoichiometric generation of powerfully reducing states of protein active sites using Eu(II) and polyaminocarboxylate ligands. *Chem Commun.* (20):2590.
89. Nilsen-Moe A et al. 2020. Proton-Coupled Electron Transfer from Tyrosine in the Interior of a *de novo* Protein: Mechanisms and Primary Proton Acceptor. *J Am Chem Soc.* 142(26):11550–9.
90. Matsui T et al. 2005. Roles of Distal Asp in Heme Oxygenase from *Corynebacterium diphtheriae*, HmuO: A Water-Driven Oxygen Activation Mechanism. *J Biol Chem.* 280(4):2981–9.
91. Lehr M et al. 2020. A Paramagnetic NMR Spectroscopy Toolbox for the Characterisation of Paramagnetic/Spin-Crossover Coordination Complexes and Metal–Organic Cages. *Angew Chem Int Ed.* 59(43):19344–51.
92. Costentin C et al. 2012. Turnover Numbers, Turnover Frequencies, and Overpotential in Molecular Catalysis of Electrochemical Reactions. Cyclic Voltammetry and Preparative-Scale Electrolysis. *J Am Chem Soc.* 134(27):11235–42.
93. Wang VCC et al. 2019. Interpreting the Electrocatalytic Voltammetry of Homogeneous Catalysts by the Foot of the Wave Analysis and Its Wider Implications. *ACS Catal.*
94. Rountree ES et al. 2016. Linear Free Energy Relationships in the Hydrogen Evolution Reaction: Kinetic Analysis of a Cobaloxime Catalyst. *ACS Catal.* 6(5):3326–35.
95. Baffert C et al. 2007. Cobaloximes as Functional Models for Hydrogenases. 2. Proton Electroreduction Catalyzed by Difluoroborylbis(dimethylglyoximato)cobalt(II) Complexes in Organic Media. *Inorg Chem.* 46(5):1817–24.
96. Bhattacharjee A et al. 2013. A Computational Study of the Mechanism of Hydrogen Evolution by Cobalt(Diimine-Dioxime) Catalysts. *Chem – Eur J.* 19(45):15166–74.

Appendix 1

The pH-dependence of the potential is a linear relationship derived from the Nernst equation (equation A1):

$$E = E_0 - \frac{RT}{nF} \ln \left(\frac{[X^-]}{[X]} \right) \quad (\text{A1})$$

Which for the electrochemically reversible process X^-/X relates the concentrations of a reduced ($[X^-]$) and oxidised ($[X]$) species with the potential (E) and the standard equilibrium potential for the X^-/X -couple (E_0), where R is the universal gas constant ($8.3145 \text{ J K}^{-1} \text{ mol}^{-1}$), T is the temperature in $^\circ\text{K}$, n is the number of electrons passed in the process and F is the Faraday constant ($96\,485 \text{ C/mol e}^-$). (79)

Then, because $\ln(x) = 2.303 \log(x)$, the Nernst equation can also be expressed with a base 10 logarithm:

$$E = E_0 - \frac{2.303RT}{nF} \log \left(\frac{[X^-]}{[X]} \right)$$

Which at 25°C is:

$$\begin{aligned} E &= E_0 - \frac{2.303 \times 8.3145 \times 298.15}{n \times 96485} \log \left(\frac{[X^-]}{[X]} \right) = \\ &= E_0 - \frac{0.0591}{n} \log \left(\frac{[X^-]}{[X]} \right) \end{aligned}$$

For $2H^+ + 2e^- \leftrightarrow H_2$ it is:

$$E = E_0 - \frac{0.0591}{2} \log \left(\frac{P_{H_2}}{[H^+]^2} \right)$$

The superscript 2 on $[H^+]$ represents the two protons involved in the process. P_{H_2} is the H_2 partial pressure in atmosphere, and under normal conditions (1 atm and 25°C):

$$\begin{aligned} E &= E_0 - \frac{0.0591}{2} \log \left(\frac{1}{[H^+]^2} \right) = \\ &= E = E_0 + \frac{0.0591}{2} \log([H^+]^2) = \\ &= E = E_0 + \frac{0.0591}{2} 2 \log([H^+]) = \\ &= E = E_0 + 0.0591 \log([H^+]) \end{aligned}$$

The pH is the negative logarithm of the proton concentration, finally yielding the linear relationship between potential and pH:

$$E = E_0 + 0.0591(-\log([H^+])) =$$
$$E = E_0 - 0.0591 \text{ pH} \quad (\text{A2})$$

This equation can also be generalised to equation A3:

$$E = E_0 - \frac{0.0591m}{n} \text{ pH} \quad (\text{A3})$$

From equation A3 we can see that if we plot the potential E vs the pH, we will obtain a line with a slope of ca -59 mV/pH for a one proton/one electron process ($m/n = 1$). Likewise, for a one proton/two electron process ($m = 1, n = 2$) the slope will be ca -29.5 mV/pH ; and for a two protons/one electron process ($m = 2, n = 1$) it will be ca 118 mV/pH .

The derivation of equation 2 is done with hydrogen evolution in mind, where we imagine the equilibrium reaction between protons and hydrogen in the presence of a platinum group metal (an NHE), which has the E_0 of 0 V, but it is applicable for other processes too. The fundamental process the equation describes is the reduction of a proton, therefore regardless of what the protonated product is E will always rely on $\log ([H]/[H^+])$ which can be simplified to pH, just as described above.

Appendix 2

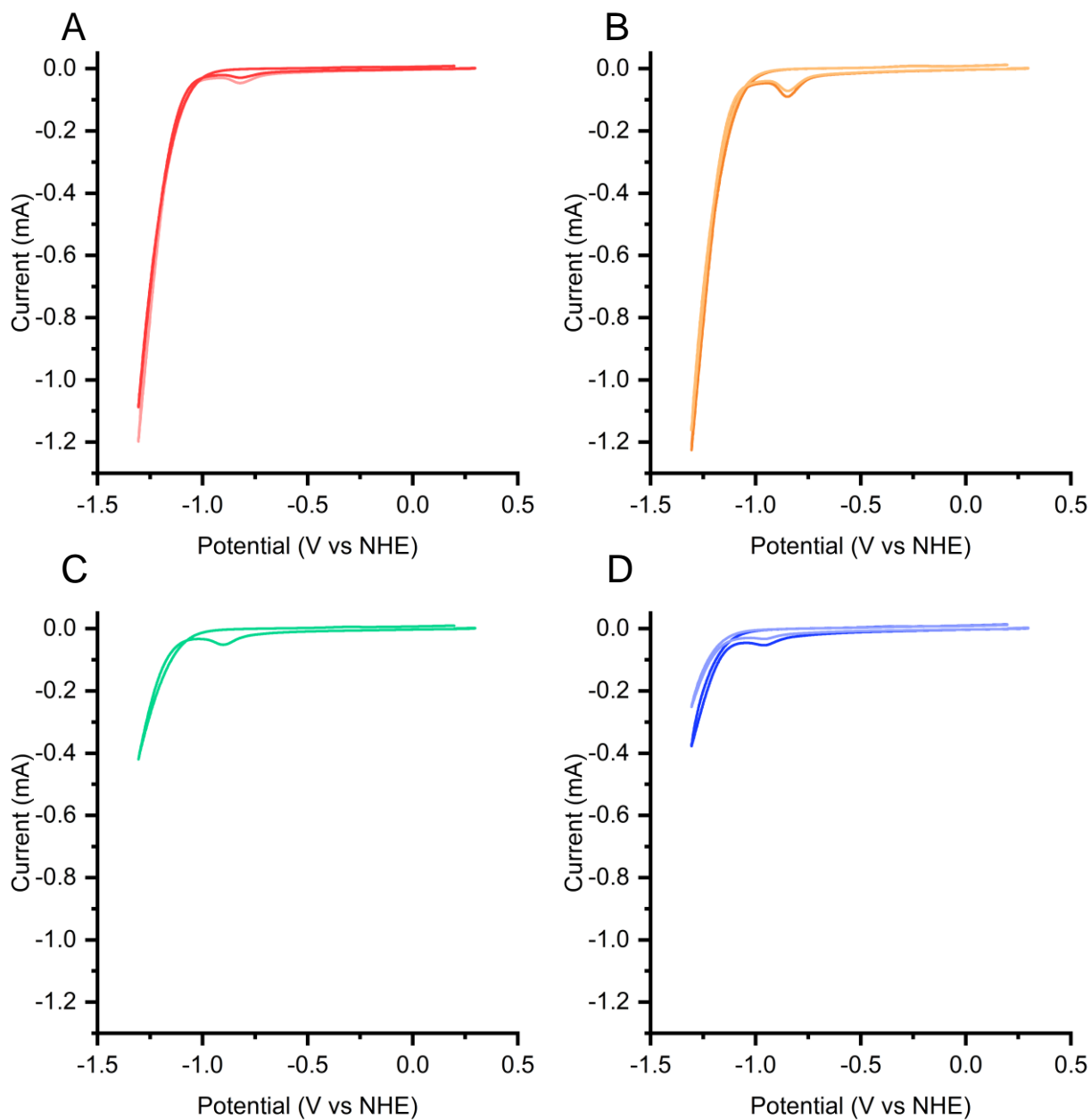


Figure A1: CVs of Co-MePy- α_3 C at pH 5.5 (A, 2 repeats), 6 (B, 2 repeats), 7 (C, 1 repeat) and 7.9 (D, 2 repeats).

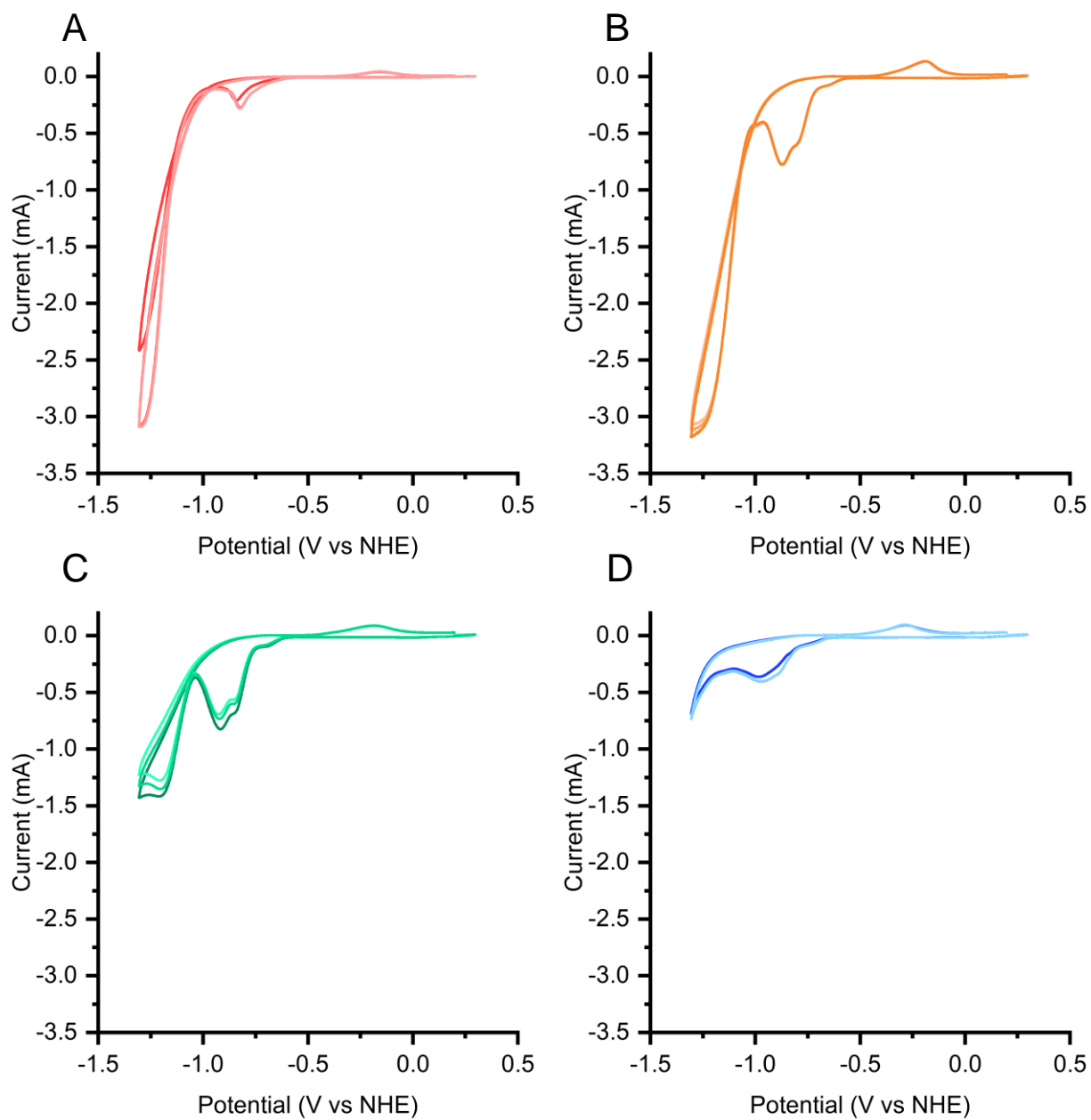


Figure A2: Triplicate CVs of cobaloxime at pH 5.5 (A), 6 (B), 7 (C) and 7.9 (D).

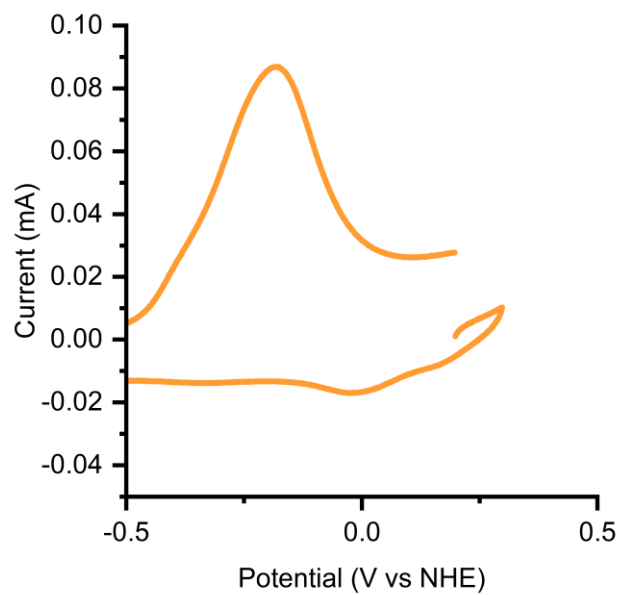


Figure A3: Zoomed in view of CV of cobaloxime at pH 7, emphasising the broad cathodic peak at -0.020 V vs NHE corresponding to what has previously been assigned as the reduction of Co[III] to Co[II].